Carbon-Dioxide Storage in the Subsurface: A Fully Coupled Analysis of Transport Phenomena and Solid Deformation

Von der Fakultät Bau- und Umweltingenieurwissenschaften
der Universität Stuttgart zur Erlangung der Würde
eines Doktor-Ingenieurs (Dr.-Ing.)
genehmigte Abhandlung

Vorgelegt von

Irina Komarova, M. Sc.

aus

Sankt-Petersburg, Russland

Hauptberichter: Prof. Dr.-Ing. Wolfgang Ehlers

1. Mitberichter: Prof. Dr.-Ing. Rainer Helmig

2. Mitberichter: Prof. Dr. Ir. Hans Bruining

Tag der mündlichen Prüfung: 16. Juli 2012

Institut für Mechanik (Bauwesen) der Universität Stuttgart
Lehrstuhl für Kontinuumsmechanik
Prof. Dr.-Ing. W. Ehlers
2012

Report No. II-24
Institut für Mechanik (Bauwesen)
Lehrstuhl für Kontinuumsmechanik
Universität Stuttgart, Germany, 2012

Editor:
Prof. Dr.-Ing. W. Ehlers

© Irina Komarova
Institut für Mechanik (Bauwesen)
Lehrstuhl für Kontinuumsmechanik
Universität Stuttgart
Pfaffenwaldring 7
70569 Stuttgart, Germany

Printed by F.U.T.Müllerbader GmbH - Filderstadt, Germany, 2012

ISBN 3-937399-23-2
(D 93 - Dissertation, Universität Stuttgart)

Acknowledgements

First of all, I would like to thank my supervisor, Professor Wolfgang Ehlers, for his guidance throughout my entire doctoral work at the Institute of Applied Mechanics, University of Stuttgart. I am especially grateful to him for providing me with an opportunity to work at a research institute with bright and highly skilled group of people, for sharing his ideas in our scientific discussions, which strongly contributed to the development of this thesis.

I would also like to acknowledge the contribution of Professor Rainer Helmig, the first co-chair of my examination and a founder of the NUPUS international research group, within which this work was performed. His remarks and feedback were essential for the improvement of this thesis. I would also like to thank Professor Hans Bruining, the second co-chair in my promotion procedure, for his corrections, advice and our interesting discussions during my stay at the University of Delft.

Special thanks go to all my colleagues at the Institute of Applied Mechanics for their help, encouragement and friendly working atmosphere that they created during the time I spent at the Institute. In particular, to Okan Avci and Kai Häberle for the great help in the final stages of working on this thesis, to Arzu Avci and Yousef Heider for their friendly support and company during many evenings and weekends spent at the Institute, and to Christine Klee for her warm friendship. I am also thankful to the members of the NUPUS research group for sharing their ideas and creating a fun atmosphere at various seminars, workshops and "NUPUS-lunches". Furthermore, many thanks go to my former colleagues from the Institute of Engineering Mechanics of the University of Innsbruck and Max-Plank-Institute for Plasma Physics in Munich.

I would like to thank my friends from all over the world: my faithful friends of many years from Russia, and my new friends from Germany, Chile, Italy, Canada, Austria and England, who I met during my stay in Europe. Their warmth and support throughout all these years mean a lot to me. They truly helped make my stay in Stuttgart during the years of doctoral research work a pleasant and fun experience.

And last, but definitely not least, I would like to thank my family, my parents Teresa and Victor, and my brother Oleg, for their love, support and for being the people that I can always hold on to.

I would not manage without all of you. Thank you so very much.

Stuttgart, July 2012 Irina Komarova

The dictionary is the only place where success comes before work.

Vince Lombardi

Never, never, never give up.

Winston Churchill

Contents

Deutsche Zusammenfassung

Motivation

Kohlendioxid (CO_2) spielt eine wesentliche Rolle bei der Unterstützung von Leben auf der Erde. Es wird von Pflanzen für die Photosynthese genutzt und ist ein wichtiger Teil des globalen Kohlenstoffkreislaufs. Im überkritischen Aggregatzustand wird CO_2 in industriellen Anwendungen, wie der Stromerzeugung, der Produktion von Biokraftstoffen, Einfriervorgängen und vielen anderen Verfahren verwendet. Des Weiteren gehört CO_2 zu den Gasen, den sogenannten Treibhausgasen, die zum Treibhauseffekt beitragen. Die CO_2-Konzentration in der Atmosphäre erhöht sich jedes Jahr, was heute von vielen Wissenschaftlern und Ingenieuren als eine der Hauptursachen der globalen Erwärmung zugeschrieben wird. Um den Anstieg der globalen Durchschnittstemperatur zu vermindern, sollte die Konzentration von Treibhausgasen in der Atmosphäre herabgesetzt werden. In diesem Zusammenhang ist die Reduktion der CO_2-Konzentration besonders relevant, da ihre Emissionen deutlich höher sind im Vergleich zu anderen Treibhausgasen.

Es ist eine Reihe von Möglichkeiten vorhanden, um die CO_2-Freisetzung in die Atmosphäre zu verringern. Optional können alternative Energiequellen wie Wind- und Wasserkraft verwendet werden, die kein CO_2 produzieren. Ein weiterer Anhaltspunkt zur Verringerung der CO_2-Emission könnte die Verbesserung der Energieeffizienz bereits bestehender Technologien sein, vgl. Bielinski [11]. Eine weitere wichtige Strategie, die Gegenstand der vorliegenden Untersuchung ist, ist die Speicherung von CO_2 in geologischen Formationen über einen längeren Zeitabschnitt von hundert bis tausend Jahren, siehe Bachu [4], Metz *et al.* [73], Baines & Worden [6].

Im Allgemeinen besteht der geologische Speicherungsprozess von CO_2 aus mehreren charakteristischen Schritten: das Abfangen von CO_2 aus Quellen, der Transport, die Injektion und die Lagerung. Die vorliegende Arbeit konzentriert sich auf die Modellierung des Sequestrierungsvorgangs, im Einzelnen auf die Injektion und Speicherung. Insbesondere die Wirkung von injiziertem CO_2 auf die Verformung von Festkörpern sowie die Auswirkungen des CO_2-Phasenübergangs auf die weitere Ausbreitung innerhalb eines Reservoirs sind Gegenstand des Interesses.

Zielsetzung und Vorgehensweise

Im Rahmen der CO_2-Speicherungsproblematik wird angenommen, dass die geologische Speicherung von Kohlendioxid eine vielversprechende Technologie zur Reduktion von atmosphärischen CO_2 Emissionen ist. Derzeit laufen weltweit verschiedene Industrieprojekte, um unterschiedliche Mengen von CO_2 zu speichern. Von Projekten wie am Sleipner Ölfeld in Norwegen, Weyburn in Kanada und in Salah in Algerien wird erwartet, insgesamt mehr als 1 $MtCO_2$/Jahr zu speichern, vgl. Metz *et al.* [73]. Die geologische Speicherung von CO_2 als Treibhausgas wurde erstmals in den 1970er Jahren vorgeschlagen, aber bis in die frühen 1990er Jahre wurde in diesem Bereich kein bedeutender Forschungsfortschritt erzielt. Ein ausgereiftes Injektionsverfahren von CO_2 wurde zum ersten Mal in Texas (USA) in den frühen 1970er Jahren vorgestellt und erfolgreich als Teil eines „Enhanced Oil Recovery"-Projekts angewendet. Zusätzliche nützliche Erfahrungen wurden aus dem Alberta Basin in Kanada und den USA zur Verfügung gestellt. Das weltweit erste großtechnisch realisierte Speicherungsprojekt wurde im Sleipner-Gasfeld in der Nordsee im Jahr 1996 initiiert. Des Weiteren gibt es mehrere Pilotprojekte in Deutschland, die die Injektion von CO_2 in einem salinen Aquifer in Ketzin und das Abfangen von CO_2 aus der Kohleverbrennung im Kraftwerk Schwarze Pumpe vorschlagen. Für weitere Informationen wird der Leser unter anderem auf die Forschungsarbeiten von van der Meer [72], Pruess & García [86], Gunter *et al.* [55], Baines & Worden [6] verwiesen.

Es existieren verschiedene Arten von geologischen Formationen, die für die CO_2 Endlagerung zur Verfügung stehen. Im Rahmen dieser Arbeit werden Reservoire, unter anderem in tiefen salinen Aquiferen, betrachtet. Die Vorteile dieser Lagerung im Vergleich zu anderen sind die relativ hohe Leistungsfähigkeit und die weltweite Verfügbarkeit. Die CO_2-Verteilung über einen Aquifer hängt von vielen verschiedenen Faktoren ab, unter anderem von der Interaktion zwischen dem injizierten CO_2 und den festen Partikeln im Aquifer, der Heterogenität in verschiedenen Skalen und der Schwerkraft. Die CO_2-Injektion in einen Aquifer ist ein sehr komplizierter Vorgang und bedarf einer eingehenden Untersuchung. In diesem Zusammenhang wurde eine Reihe von Studien durchgeführt, um diesen Mechanismus zu verstehen und die Erkenntnisse über das CO_2-Verhalten während und nach der Injektion in einen Aquifer zu erweitern. Die vorliegende wissenschaftliche Arbeit ist der Erarbeitung des theoretischen Hintergrunds und der numerischen Methode zur Untersuchung der CO_2-Sequestrierung in einem Aquifer und der Beschreibung mehrerer charakteristischer Prozesse gewidmet.

Forscher und Ingenieure betrachten die Verteilung von CO_2 in einem Reservoir oft unter Vernachlässigung der thermischen, chemischen und mechanischen Kopplung der Prozesse. Diese Effekte können eine bedeutende Rolle in der CO_2-Speicherung spielen und sind sehr komplex zu beschreiben. Die Besonderheit dieser wissenschaftlichen Arbeit liegt darin, dass neben der Untersuchung der Prozesse im Rahmen der Fluiddynamik und der Mehrphasenströmungen die mechanischen Effekte ebenfalls berücksichtigt werden. Insbesondere die Deformation von Festkörpern im Grundwasserleiter und der „cap-rock"-Schicht sowie die Phasenumwandlung von überkritischem CO_2 werden hier untersucht.

Um diese Prozesse zu beschreiben, wird ein mehrphasiges Modell in einer kontinuumsmechanischen Betrachtungsweise im Rahmen der fundierten Theorie Poröser Medien (TPM) verwendet. Die der TPM zugrunde liegenden Mischungstheorie wird durch das Konzept der Volumenanteile erweitert, siehe Truesdell & Toupin [102], de Boer [14], Bowen [18], Ehlers [34, 36, 37]. Die Eigenschaften der einzelnen Bestandteile von Mehrphasenmaterialen werden durch die konstitutiven Gleichungen beschrieben, welche anhand der Auswertung der Entropieungleichung gewonnen werden. Die restlichen Konstitutivgleichungen können basierend auf thermodynamischen Grundlagen sowie auf den Gesetzmäßigkeiten der Mechanik, Chemie, Elektrizität und anderen Bereichen abhängig von den Anforderungen des eigentlichen Problems definiert werden. Weiterführende Informationen über die historische Entwicklung der TPM findet der Leser in de Boer [14] und in weiteren Veröffentlichungen.

Es wurden bereits diverse Mehrphasenmodelle für unterschiedlichste Anwendungen entwickelt. Ein Dreiphasenmodell mit elasto-viskoplastischem Festkörperskelett, materiell inkompressibler Flüssigkeit und materiell kompressiblem Gas wurde in den Arbeiten von Blome [12] und Ehlers *et al.* [46] diskutiert. Dieses Modell wurde von Graf [53] einschließlich nicht-isothermen Eigenschaften für jede Phase und dem Massenaustauschprozess zwischen den Fluidphasen erweitert. Ghadiani [51] untersuchte in seiner Arbeit ein Zweiphasenmodell, bei dem jede Phase durch ihre jeweilige Temperatur geregelt wird. Darüber hinaus wurde von Acartürk [2] ein Modell, welches die mechanischen, chemischen und elektrischen Eigenschaften von geladenen hydratisierten porösen Materialien kombiniert, entwickelt. Weiterhin erweiterte Karajan [60] ein Zweiphasenmodell, um das komplexe Verhalten der Bandscheibe in Bezug auf ihre strukturellen, mechanischen und elektro-chemischen Komponenten zu beschreiben. Bezüglich der detaillierten Betrachtung des Verhaltens eines Festkörperskeletts innerhalb der elasto-plastischen Theorie mittels der Modellierung von Verhärtungs- und Erweichungseffekten wird der interessierte Leser an Müllerschön [75], Scholz [92] und Ehlers & Avci [42] verwiesen.

Die numerische Abhandlung eines Mehrphasenmodells mit elasto-viskoplastischem Festkörperskelett wird in Arbeiten von Ellsiepen [48] und Ammann [3] diskutiert. Darin werden verschiedene Raum- und Zeit-adaptive Verfahren unter Verwendung von parallelen Lösungsstrategien mit Anwendungen auf verschiedenen praktischen Beispielen untersucht. Es gibt zahlreiche weitere Publikationen, die sich auf die Beschreibung des komplexen Verhaltens von porösen Materialien unter Verwendung der TPM fokussieren, vgl. Helmig [57], Wieners *et al.* [103], Ehlers & Acartürk [40], Ehlers [38], Ehlers *et al.* [41].

Das in der vorliegenden Arbeit entwickelte Mehrphasenmodell stellt das Verhalten des gekoppelten Fluid-Festköper-Systems innerhalb der Anwendung der CO_2-Lagerungsproblematik dar. Insbesondere werden drei- und vierphasige Modelle für die Modellierung von CO_2-Injektionen dargestellt, wobei der Massenaustauschprozess zwischen den CO_2-Phasen im Detail betrachtet wird. Auch thermische Effekte werden in das Modell aufgenommen. Im Vergleich zu bisher entwickelten Modellen, bei denen zur Beschreibung des Verhaltens von Gasphasen das ideale Gasgesetz verwendet wurde, nimmt das aktuelle Modell die *Peng-Robinson*-Zustandsgleichung für die CO_2-Komponente. In dieser Arbeit werden zudem die unterschiedlichen Zustandsgleichungen, der Massenübergangprozess und das Schalter-Kriterium, das angibt, ob der Phasenübergang stattfindet, diskutiert.

Gliederung der Arbeit

Im Anschluss an die Einleitung wird in **Kapitel 2** eine allgemeine Diskussion über die CO_2-Speicherungsproblematik präsentiert. Dieses Kapitel konzentriert sich auf die Betrachtung der geologischen Möglichkeiten zur CO_2-Sequestrierung, verschiedene Rückhaltemechanismen und spezifische physikalische Eigenschaften von Kohlendioxid sowie deren Darstellung mit Hilfe des Phasendiagramms. **Kapitel 2** wird mit einer Liste von offenen Fragen und Wissenslücken auf dem Gebiet der CO_2-Sequestrierungsproblematik abgeschlossen.

Kapitel 3 behandelt den theoretischen Rahmen für diese Fragestellungen. Ausgehend von den kontinuumsmechanischen Grundlagen der TPM wird die Diskussion durch die

Einführung der kinematischen Beziehungen und Bilanzgleichungen ergänzt. Nachfolgend werden in diesem Kapitel die erforderlichen thermodynamischen Grundlagen, insbesondere das Phasendiagramm, die verschiedenen Zustandsgleichungen, die Definition der chemischen Potentiale sowie ein Phasenübergangsprozess vorgestellt.

Kapitel 4 konzentriert sich auf die konstitutive Modellierung. Die Auswertung der Entropieungleichung liefert für zwei unterschiedliche Modelle, die die idealen und kritischen Szenarien der CO_2-Injektion darstellen, die konstitutiven Beziehungen. Anschließend werden die charakteristischen Konstitutivgleichungen für die festen und flüssigen Bestandteile des Mehrphasenmodells formuliert. Hierbei wird die Verformung des Festkörperskeletts anhand eines linear-elastischen Gesetzes beschrieben. Das Verhalten von CO_2 wird durch die *Peng-Robinson*-Zustandsgleichung beschrieben, welche die entsprechenden Formen der *Helmholtz*-Energien und Entropien für die CO_2-Phasen berücksichtigt. Der Massenaustauschprozess wird durch eine zusätzliche konstitutive Beziehung für den Massenproduktionsanteil hergeleitet, siehe **Kapitel 5**. Hierin wird ebenfalls das entsprechende Schalter-Kriterium für den Massenaustauschprozess diskutiert.

Die numerische Umsetzung der entwickelten theoretischen Modelle wird in **Kapitel 6** vorgestellt. Darin werden die schwache Formulierung der Erhaltungsgleichungen sowie die Diskretisierung des räumlichen und zeitlichen Gebiets erläutert. Mehrere entsprechende numerische Beispiele finden sich in **Kapitel 7**.

Schließlich werden die wichtigsten Aspekte der Arbeit und Ideen für eine weitere Forschung in **Kapitel 8** zusammengefasst dargestellt.

List of Figures

List of Acronyms

CCS	Carbon-Dioxide Capture and Storage
GHG	Greenhouse Gases
EOR	Enhanced Oil Recovery
EGR	Enhanced Gas Recovery
CBM	Coal Bed Methane
TPM	Theory of Porous Media
TM	Theory of Mixture
REV	Representative Elementary Volume
EOS	Equation of State
PDE	Partial Differential Equation
IBVP	Initial Boundary-Value Problem
FEM	Finite-Element Method
FE	Finite Element
DOF	Degree of Freedom
PANDAS	Porous Media Adaptive Nonlinear Finite Element Solver based on Differential Algebraic Systems

Nomenclature

Symbol	Unit	Description
$\mathbf{A}_\alpha$	[−]	*Almansi*an solid strain tensor
$\mathbf{b}, \mathbf{b}_\alpha$	[m/s^2]	mass specific body force vector of φ and φ^α
$\mathbf{B}_\alpha$	[−]	left *Cauchy-Green* deformation tensor
$\mathcal{B}, \partial\mathcal{B}$		aggregate body and boundary of the aggregate body
C_V^α	[J/(K kg)]	specific heat of φ^α
$\mathbf{C}_\alpha$	[−]	right *Cauchy-Green* deformation tensor
d		differential operator
$\mathrm{d}m^\alpha$	[kg]	local mass element of φ^α
$\mathrm{d}v^\alpha$	[m^3]	local volume element of φ^α
$\mathrm{d}v$	[m^3]	volume element of φ in the actual configuration
dV_α	[m^3]	volume element of φ^α in the reference configuration
$\mathrm{d}\mathbf{a}$	[m^2]	oriented actual area element
$\mathrm{d}\mathbf{k}^\alpha$	[N]	surface force of φ^α
$\mathrm{d}\mathbf{x}$	[m]	actual line element
$\mathrm{d}\mathbf{A}_\alpha$	[m^2]	oriented reference area element
$\mathrm{d}\mathbf{X}_\alpha$	[m]	reference line element
$\mathbf{d}_\alpha$	[m/s]	diffusion velocity of φ^α
D		dimension in space
$\mathbf{D}_\alpha$	[1/s]	symmetric part of $\mathbf{L}_\alpha$
$\mathcal{D}$		dissipative inequality
$\hat{e}^\alpha$	[J/(m^3 s)]	volume-specific total energy production of φ^α
$\mathbf{e}_1, \mathbf{e}_2, \mathbf{e}_3$		positive oriented orthonormal triad of vectors
$\mathbf{E}_\alpha$	[−]	contravariant *Green-Lagrange*an solid strain tensor
$\boldsymbol{f}$		generalised force vector
$\boldsymbol{F}$		vector of the residuum

$\mathbf{F}_\alpha, \mathbf{F}_\alpha^{-1}$	[−]	material and inverse material deformation gradient
$\mathbf{F}_{S_m}, \mathbf{F}_{S_\theta}$	[−]	mechanical and thermal part of the deformation gradient $\mathbf{F}_S$
$\mathbf{g}$	[m/s^2]	constant gravitation vector
$\mathcal{G}_{(\cdot)}$		abstract function vectors containing the weak forms
$\hat{\mathbf{h}}^\alpha$	[N/m^2]	volume-specific total angular momentum production of φ^α
$H^1(\Omega)$		*Sobolev* function space
$\mathbf{H}^\alpha$	[W/(K m)]	heat conduction tensor
$\mathbf{I}$	[−]	identity tensor
J_α	[−]	*Jacobi*an determinant
k_{ij}	[−]	empirical interaction parameter
$k^\varepsilon_{\theta\beta}$	[W/(K m^2)]	heat exchange coefficients
k^W_r	[W/(K m^2)]	relative permeability factor
K^S_{0S}	[m^2]	intrinsic permeability in the reference configuration
$\boldsymbol{k}$		generalised stiffness vector
$\mathbf{K}^\beta$	[m/s]	*Darcy* permeability tensor
$\mathbf{K}^S$	[m^2]	intrinsic permeability tensor
$\mathbf{L}_\alpha$	[1/s]	spatial solid velocity gradient
m	[−]	*van Genuchten* parameter
$\hat{\mathbf{m}}^\alpha$	[N/m^2]	volume-specific direct angular momentum production of φ^α
M_{CO_2}	[kg/mol]	molar mass of CO_2
$\boldsymbol{M}$		generalised mass matrix
n	[−]	*van Genuchten* parameter
n^α	[−]	volume fraction of φ^α
n^F	[−]	porosity
$\mathbf{n}$		outward-oriented unit surface normal vector
N_e, N_n		number of elements and nodes
p^C	[Pa]	capillary pressure
p_d	[N/m^2]	*Brooks & Corey* parameter
$\hat{\mathbf{p}}^\alpha, \hat{\mathbf{p}}^\alpha_E$	[N/m^3]	volume-specific direct and extra momentum production of φ^α
P^α		material points

$\mathbf{P}^\alpha$	[$\mathrm{N/m^2}$]	first *Piola-Kirchhoff* stress tensor
$\bar{q}$	[m/s]	volume efflux of φ^F over the boundary Γ_q
$\mathbf{q}, \mathbf{q}^\alpha$	[$\mathrm{J/(m^2\ s)}$]	heat influx vectors of φ and φ^α
r, r^α	[J/(kg s)]	mass-specific external heat supplies of φ and φ^α
R	[J/(mol K)]	universal gas constant
$\mathcal{R}$		set of response functions
$s^\beta, s^\beta_{eff}, s^\beta_{res}$	[−]	saturation function, effective and residual saturation functions
$\hat{\mathbf{s}}^\alpha$	[$\mathrm{N/m^3}$]	volume-specific total momentum production of φ^α
$\mathbf{S}^\alpha$	[$\mathrm{N/m^2}$]	second *Piola-Kirchhoff* stress tensor
$\mathcal{S}$		specific set of the constitutive variables
$\mathcal{S}_{(\cdot)}$		trial spaces of the primary variables
t, t_0	[s]	time and initial time
$\bar{\mathbf{t}}$	[$\mathrm{N/m^2}$]	external load vector acting on the boundary $\Gamma_{\mathbf{t}}$
$\mathbf{t}^\alpha$	[$\mathrm{N/m^2}$]	surface traction vector
$\mathbf{T}^\alpha$	[$\mathrm{N/m^2}$]	*Cauchy* stress tensor
$\boldsymbol{u}$		discrete vector containing the nodal degrees of freedom
$\mathbf{u}_S$	[m]	solid displacement vector
v		molar volume and specific volume
$\mathrm{V}, \mathrm{V}^\alpha$	[$\mathrm{m^3}$]	overall volume of $\mathcal{B}$ and partial volume of $\mathcal{B}^\alpha$
$\mathcal{V}$		set of fundamental process variables
$\mathbf{w}_\beta$	[m]	fluid seepage velocity vector
$\mathbf{W}_\alpha$	[1/s]	skew-symmetric part of $\mathbf{L}_\alpha$ (spin tensor)
x_i		molar fraction
$\mathbf{x}$	[m]	actual position vector
$\dot{\mathbf{x}}$	[m/s]	aggregate velocity vector
$\overset{\prime}{\mathbf{x}}_\alpha$	[m/s]	velocity vector
$\ddot{\mathbf{x}}$	[$\mathrm{m/s^2}$]	aggregate acceleration vector
$\overset{\prime\prime}{\mathbf{x}}_\alpha$	[$\mathrm{m/s^2}$]	acceleration vector
$\mathbf{X}_\alpha$	[m]	reference position vector of P^α
Z	[−]	compressibility factor

α		constituent identifier (here: $\alpha = \{S,\ F\}$)
α^S	[1/K]	linear thermal expansion coefficient of φ^S
α_ω		function of the acentric factor
β		fluid component identifier (here: $\beta = \{W,\ L,\ G\}$)
γ	[−]	*van Genuchten* parameter
γ^W	[1/K]	volumetric thermal expansion coefficient of φ^W
$\gamma^{\beta R}$	[N/m^3]	specific weight
$\Gamma_{(\cdot)}$		*Dirichlet* and *Neumann* boundaries
δ_{kl}	[−]	*Kronecker* symbol
$\varepsilon, \varepsilon^\alpha$	[J/kg]	mass-specific internal energies of φ and φ^α
$\hat{\varepsilon}^\alpha$	[J/(m^3 s)]	volume-specific direct energy production of φ^α
$\hat{\zeta}^\alpha$	[J/(K m^3 s)]	volume-specific direct entropy production of φ^α
η, η^α	[J/(K kg)]	mass-specific entropies of φ and φ^α
$\hat{\eta}, \hat{\eta}^\alpha$	[J/(K m^3 s)]	volume-specific total entropy productions of φ and φ^α
θ, θ^α	[K]	absolute *Kelvin*'s temperatures of φ and φ^α
λ	[−]	*Brooks* & *Corey* parameter
λ^S	[N/m^2]	*Lamé* constant
$\Lambda, \bar{\Lambda}, \bar{\bar{\Lambda}}, \bar{\bar{\bar{\Lambda}}}$	[N/mm^2]	*Lagrange*an multipliers representing hydraulic pressure
$\mu^{\beta R}$	[N s/m^2]	effective shear viscosity
μ^α	[J/kg]	chemical potential of φ^α
μ^S	[N/m^2]	*Lamé* constant
ξ, ξ^α	[J/kg]	*Gibbs* energies of φ and φ^α
π	[−]	material parameter for intrinsic permeability
ρ	[kg/m^3]	density of the overall aggregate φ
$\rho^\alpha,\ \rho^{\alpha R}$	[kg/m^3]	partial and effective density of φ^α
$\hat{\rho}^\alpha$	[kg/(m^3 s)]	volume-specific mass production of φ^α
σ, σ^α		scalar-valued supply terms of mechanical quantities
$\sigma_\eta, \sigma_\eta^\alpha$		volume-specific external entropy supply
$\boldsymbol{\sigma}, \boldsymbol{\sigma}^\alpha$		vector-valued supply terms of mechanical quantities

$\boldsymbol{\tau}^\alpha$	[$\mathrm{N/m^2}$]	*Kirchhoff* stress
$\mathcal{T}_{(\cdot)}$		test spaces of the primary variables
φ, φ^α		entire aggregate and constituent α
$\phi^j_{(\cdot)}$	[$-$]	shape functions in a finite element
$\boldsymbol{\phi}, \boldsymbol{\phi}^\alpha$		general vector-valued mechanical quantities
$\boldsymbol{\phi}_\eta, \boldsymbol{\phi}^\alpha_\eta$	[$\mathrm{J/(K\ m^2\ s)}$]	entropy efflux vectors
$\mathbf{\Phi}, \mathbf{\Phi}^\alpha$		general tensor-valued mechanical quantities
$\boldsymbol{\chi}_\alpha, \boldsymbol{\chi}_\alpha^{-1}$		motion and inverse motion function of the constituents φ^α
ψ, ψ^α	[$\mathrm{J/kg}$]	mass-specific *Helmholtz* free energies of φ and φ^α
Ψ, Ψ^α	[$(\cdot)/\mathrm{m^3}$]	volume-specific densities of scalar mechanical quantities
$\hat{\Psi}, \hat{\Psi}^\alpha$	[$(\cdot)/\mathrm{m^3}$]	volume-specific productions of scalar mechanical quantities
$\boldsymbol{\Psi}, \boldsymbol{\Psi}^\alpha$	[$(\cdot)/\mathrm{m^3}$]	volume-specific densities of vectorial mechanical quantities
$\hat{\boldsymbol{\Psi}}, \hat{\boldsymbol{\Psi}}^\alpha$	[$(\cdot)/\mathrm{m^3}$]	volume-specific productions of vectorial mechanical quantities
ω		acentric factor
$\Omega, \partial\Omega$		spatial domain and boundary of the aggregate body $\mathcal{B}$
Ω_e, Ω^h		one finite element and the discretised finite element mesh

Super- and Subscripts:

$(\cdot)^\alpha$	all constituents
$(\cdot)^\beta$	fluid components
$(\cdot)^S$	solid matrix
$(\cdot)^F$	overall fluid (porosity)
$(\cdot)^W$	water phase
$(\cdot)^L$	CO_2 in the supercritical phase (liquid)
$(\cdot)^G$	CO_2 in the gaseous phase (gas)
$(\cdot)^{\alpha R}$	effective (realistic) quantity of φ^α
$(\cdot)_E$	extra quantities
$(\cdot)_{E_\mathrm{mech}}$	mechanical extra quantities
$(\cdot)_\mathrm{lin}$	linearised quantities
$(\cdot)_{0\alpha}$	initial quantities of φ^α

Chapter 1: Introduction and Overview

1.1 Motivation

Carbon dioxide (CO_2) plays an essential role in supporting life on Earth. It is used by plants for the photosynthesis and is an important part of the global carbon cycle. In the supercritical state, CO_2 is used in industrial activities, such as power generation, biofuel production, refrigeration and many other applications. CO_2 is also one of the greenhouse gases (GHG). Its concentration in the atmosphere increases every year, which is attributed to one of the main causes of the global warming by many scientists and engineers today. In order to avoid the increase of the average global temperature, the concentration of GHG in the atmosphere should be reduced. In this regard, the decrease of CO_2 concentration is particularly relevant, since its emission is much higher compared to other GHG.

There are a number of ways to reduce the CO_2 release into the atmosphere. Optionally, alternative energy sources such as wind and hydro-power, which do not produce CO_2, can be used, or the energy efficiency of already existing technologies can be improved, cf. Bielinski [11]. Another important strategy, which is the subject of the current investigation, is the capture and storage of CO_2 in geological formations for a long period of time (hundreds or even thousands of years), cf. Bachu [4], Metz *et al.* [73], Baines & Worden [6].

In general, the geological sequestration process of CO_2 consists of several characteristic

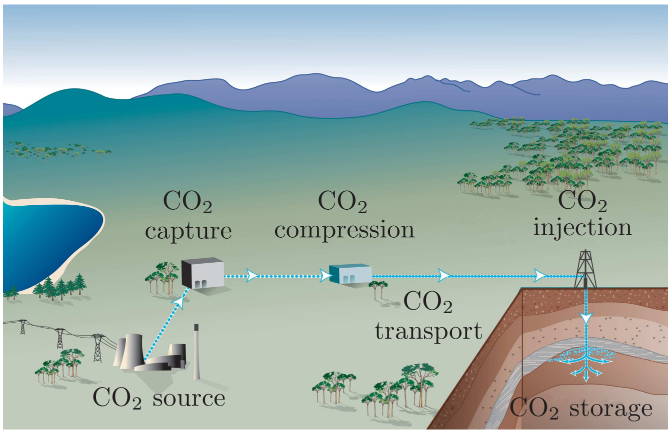

[www.co2crc.com.au]

Figure 1.1: Steps of the CO_2 sequestration process.

steps illustrated in Figure 1.1, which include capture from sources, transport, injection and storage. The present work will focus on the modelling of specific processes taking part at the end of the sequestration process, namely, injection and storage. In particular, the effect of pumped CO_2 on the deformation of the solid within a reservoir and the impact of CO_2 phase transition on its propagation within a storage formation are the subject of interest.

1.2 Scope, Aims and State of the Art

Within the scope of carbon-dioxide capture and storage (CCS) problem, the geological storage of CO_2 is assumed to be a promising technology for the reduction of atmospheric CO_2 emission from human activity. Various industrial projects all over the world are currently underway planning to store different amounts of CO_2. For example, the projects at Sleipner oilfield in Norway, Weyburn in Canada and In Salah in Algeria are expected to store more than 1 $MtCO_2$/year in total, cf. Metz *et al.* [73]. The geological storage of CO_2 as a GHG was first proposed in the 1970s, but not much research had been done until the early 1990s. The engineered injection of CO_2 was first undertaken in Texas, USA, in the early 1970s, as part of an enhanced oil recovery (EOR) project. Additional useful experience is provided from the Alberta Basin in Canada and the USA. The world's first large-scale storage project was initiated at the Sleipner Gas Field in the North Sea in 1996. There are also several pilot projects proposed in Germany: the injection of CO_2 into a saline aquifer in Ketzin and the capture of CO_2 from coal combustion at the power plant Schwarze Pumpe. For more information, the readership is referred to the research works by van der Meer [72], Pruess & García [86], Gunter *et al.* [55], Baines & Worden [6], and many others.

There are different types of geological formations suitable for CO_2 disposal. Among many others, deep saline aquifers are taken into consideration in the present contribution. The advantages of this reservoir compared to others are its relatively high capability and world-wide availability. The CO_2 distribution over the aquifer depends on many different factors, such as the interaction between the injected CO_2 and solid particles in the aquifer, the heterogeneity at different scales, gravity and many others. It can be noted that CO_2 injection into an aquifer is a very complicated mechanism and requires detailed investigation. In this regard, a number of studies have been carried out to understand and to extend the knowledge of the CO_2 behaviour during and after injection into an aquifer. The present contribution is as well dedicated to the development of a theoretical background and a numerical tool for the investigation of the CO_2 sequestration process in the aquifer focusing on several specific processes described below.

Researchers and engineers often consider the distribution of CO_2 in the reservoir neglecting the thermal, chemical and mechanical coupling of the processes. These effects can play a significant role in the CO_2 sequestration and are quite complex to describe. In this context, the distinguishing feature of this investigation is that besides studying the processes in the framework of fluid dynamics and multiphase flow, the mechanical effects are also taken into consideration. In particular, the deformation of the solid within the aquifer and the cap-rock layer as well as the phase transformation of the supercritical CO_2 are studied here.

In order to describe these processes, a multiphasic model in the continuum mechanical framework of the well-founded Theory of Porous Media (TPM) is applied. The fundamentals of the TPM, which is based on the Theory of Mixture (TM) combined with the concept of volume fractions, can be found in the works by Truesdell & Toupin [102], de Boer [14], Bowen [18], Ehlers [34, 36, 37] and others. The characteristics of the individual constituents of the multiphasic material are described by the constitutive equations obtained mainly from the evaluation of the entropy principle. The remaining constitutive settings can be defined based on thermodynamical fundamentals as well as on the knowledge of mechanics, chemistry, electricity and other fields depending on the requirements of the actual problem. Some information about the historical development of the TPM can be found in de Boer [14] and in other publications.

Many multiphasic models for various applications were developed in the past. For example, for a multiphasic material consisting of more than one pore fluid, a triphasic model with elasto-viscoplastic behaviour of the solid skeleton and a materially incompressible liquid as well as a materially compressible gas was discussed in Blome [12] and Ehlers *et al.* [46]. This model was extended by Graf [53] including non-isothermal properties for each phase and the mass interaction between the fluid phases in a specific form. Ghadiani [51] considered a biphasic model, where each phase is governed by its respective temperature. Furthermore, a model combining the mechanical, chemical and electrical properties of charged hydrated porous materials was developed by Acartürk [2]. Karajan [60] extended a biphasic model in order to describe the complex behaviour of the intervertebral disc regarding its structural, mechanical and electro-chemical components. Regarding the detailed description of the behaviour of a solid skeleton within the elasto-plastic theory with modelling of the hardening and softening effects, the interested reader is referred to Müllerschön [75], Scholz [92] and Ehlers & Avci [42].

The numerical treatment of a multiphasic model with elasto-viscoplastic behaviour of the solid skeleton can be found in works by Ellsiepen [48] and Ammann [3]. Therein, various space- and time- adaptive methods using parallel solution strategies are discussed with applications to different practical examples. There are numerous other publications dedicated to the description of the complex behaviour of porous materials using the TPM, cf. Helmig [57], Wieners *et al.* [103], Ehlers & Acartürk [40], Ehlers [38], Ehlers *et al.* [41] among many others.

The multiphasic model developed in the present contribution is capable to represent the coupled behaviour of the fluid-solid system within the application of the CO_2 storage problem. In particular, the tri- and four- phasic models are suggested here for the modelling of CO_2 injection, where the mass exchange process between the CO_2 phases is considered in detail. Also thermal effects are included into the model. Compared to previously developed models, where the ideal gas law was used to describe the behaviour of gas phases, the current model takes the *Peng-Robinson* equation of state (EOS) for the CO_2 component, cf. Peng & Robinson [81]. The details of the variety of EOS, the mass transition process and the switching criterion are discussed further in this thesis.

1.3 Outline of the Thesis

Following the introductory part, a general discussion of the CCS problem is presented in Chapter 2. This chapter focuses on the consideration of geological options for CO_2 sequestration, various trapping mechanisms and specific physical properties of CO_2 as well as their representation by means of the phase diagram. Chapter 2 is concluded by a list of open questions and gaps in knowledge in the field of the CO_2 sequestration problem.

Chapter 3 concerns the theoretical framework of the problems under investigation. Starting from the continuum-mechanical fundamentals of the TPM, the discussion is supplemented by the introduction of kinematical and balance relations. Afterwards, the required thermodynamical fundamentals, namely, the phase diagram, various EOS, the definition of chemical potentials and a phase transition process are presented in this chapter.

Chapter 4 focuses on the constitutive modelling. In order to derive constitutive relations, evaluation of the entropy inequality is presented for two different models corresponding to the ideal and critical scenarios of CO_2 injection. Then, the specific constitutive equations for the solid and fluid constituents of the multiphasic model are formulated. In particular, the deformation of the solid skeleton is modelled by a linear-elastic law. The behaviour of CO_2 is described by the *Peng-Robinson* EOS resulting in the corresponding forms of the *Helmholtz* energies and entropies for the CO_2 phases. The mass transition process is modelled by an additional constitutive relation for the mass production term, which is derived in Chapter 5. Herein, also the appropriate switching criterion for the mass transition process is discussed.

The numerical implementation of the developed theoretical models is presented in Chapter 6. Therein, the weak form of the governing equations as well as the discretisation procedure of the spatial and time domains are introduced. Several corresponding numerical examples can be found in Chapter 7.

Finally, the main aspects of the thesis and ideas for further research are summarised in Chapter 8.

Chapter 2: Carbon-Dioxide Capture and Storage

Scientists and engineers from different fields have been working on the problem of carbon dioxide capture and storage (CCS) making outstanding contribution for many years up to this day, see e. g. Bachu [4], Pruess & García [86], Metz *et al.* [73], Bradshaw *et al.* [21], Doughty & Pruess [29]. At the same time, a number of questions still remains in the CCS field. Some problems have been only partly solved and, consequently, require further investigation. Before going into details of the continuum-mechanical fundamentals and modelling of the carbon dioxide (CO_2) sequestration problem, the problem statement itself is provided in the following chapter. In particular, this chapter offers a brief introduction into the different geological options for CO_2 storage as well as a discussion of their positive and negative aspects. Moreover, the specific physical and chemical properties of CO_2 are introduced here.

2.1 Geological Options for the Carbon-Dioxide Sequestration

Nowadays, it is commonly accepted that one of the main reasons for the global warming is an increasing concentration of greenhouse gases (GHG) in the atmosphere, such as carbon dioxide (CO_2), methane (CH_4), nitrous oxide (N_2O) and others. However, according to the annual data of the emissions of GHG into the atmosphere, the portion of released CO_2 is much higher compared to other gases. For example, in 2000, the emission of CO_2 was 72% against 18% of CH_4, 9% of N_2O and 1% of other gases. This fact makes CO_2 the most important GHG for collecting and storage. One of the options to reduce the atmospheric emissions of CO_2 is its storage in geological formations. There are different types of formations suitable for CO_2 sequestration. These are, mainly, depleted oil and gas reservoirs, deep saline aquifers and coal beds, cf. Figure 2.1. Potential reservoirs appear in both onshore and offshore basins and vary in storage capacity, circumstances of the injection process, trapping mechanisms taking place in the formations after the injection and other factors. In other words, each type of formations has special properties, which are discussed below.

Type of Formations

Depleted oil and *gas reservoirs* are the primary candidates for the CO_2 sequestration process. As storage formations, they have definite advantages compared to other reservoirs. First of all, much more data and research regarding the reservoir properties are available. Simulation and modelling procedures for the fluid flow processes, which have already been

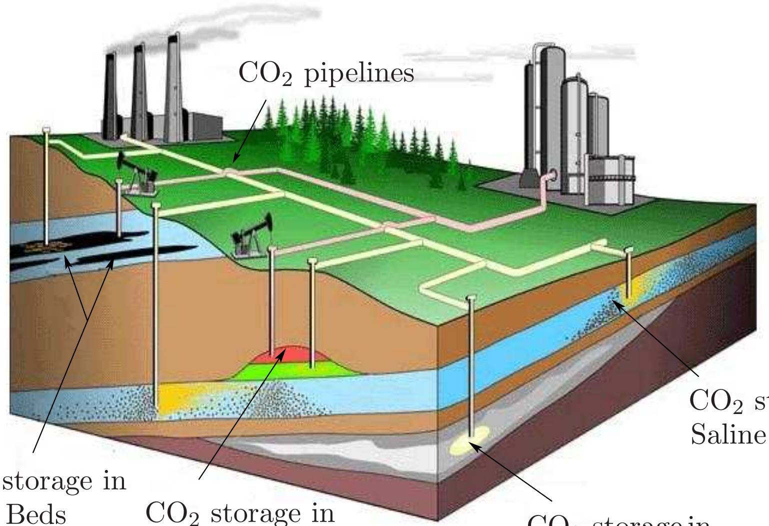

Figure 2.1: Geological storage options for CO_2, Baines & Worden [6].

developed in gas and oil industry, can also be used for prediction of CO_2 behaviour within depleted oil and gas reservoirs. Furthermore, abandoned oil and gas reservoirs are widely used in such industries as Enhanced Oil Recovery (EOR) and Enhanced Gas Recovery (EGR). CO_2 sequestration in combination with EOR or EGR is likely to be realised in the places where the cost of CO_2 storage can be reduced by producing additional oil or gas, cf. Bachu [4], Metz *et al.* [73]. However, depleted oil and gas reservoirs have also weaknesses as a storage media for CO_2. For example, they have limited geographic distribution and storage capacity, which has an average value compared to other types of the formations, cf. Table 2.1.

Reservoir type	Global capacity (Gt CO_2)
Deep saline aquifers	240 - 10000
Depleted oil and gas reservoirs	675 - 920
Unminable coal seams	3 - 270

Table 2.1: Estimated global storage capacity of different reservoirs.

The storage capacity itself can be described and evaluated in different ways including various factors and properties. There are numerous publications dedicated to the development methods for the estimation of storage capacity of a particular formation, for example, Bachu *et al.* [5], Bradshaw *et al.* [21] and Kopp *et al.* [61]. Theoretically, the storage capacity is a physical limit of how much the geological system is able to contain. Since there is no general method for estimating of the global capacity, various data can be found in literature. Table 2.1 presents the combined data from Damen *et al.* [28] and Metz *et al.* [73].

The next type of reservoirs appropriate for the CO_2 injection is the *coal bed formation*, where the permeability and adsorption properties of coal are determinant for the sequestration process. It leads to the fact that variations of these parameters during an injection process or afterwards could have a critical effect on the further pumping procedure. Therefore, the special properties for a reservoir are required. Firstly, the sequestration process has to take place at an optimal depth, because the permeability of a coal formation usually decreases with the increase in depth. Secondly, when injected CO_2 diffuses into the coal matrix, it displaces CH_4 typically adsorbed on the coal surface, and remains sequestered in coal seam. It blocks the coal pores, thus, reducing the permeability and the injectivity of coal, which is undesirable. Finally according to Bachu *et al.* [5], CO_2 storage in coal seams is a practical but not very significant option compared to the other geological media. There are many publications related to this topic, such as Larsen [65], Durucan & Shi [30]. However, the fact that CH_4 can be obtained by pumping CO_2 into coal beds is widely used in enhancing Coal Bed Methane (CBM) recovery.

Another type of geological storage formations, which is a subject of the current investigation, are *deep saline aquifers*. Currently, there is a lack of data and knowledge regarding the geology, physical and chemical processes in the aquifers. Therefore, more information about the properties and characteristics of this formation type is required. According to the definition by Bachu *et al.* [5], the deep saline aquifer is a geological formation or a layer of permeable rocks, saturated with (saline) formation water. From the point of structure, aquifers can be separated by so-called aquitard layers, which usually have extremely low porosity and permeability (e. g. shale). These nearly impermeable layers act as barriers for the injected CO_2. In other words, when CO_2 rises to the top of the reservoir after injection, it migrates further in the horizontal direction and the dense cap rock layer keeps the CO_2 in the reservoir. With time, the CO_2 dissolves into the formation water and can even take part in geochemical reactions, which leads to an effective and secure long-term CO_2 storage.

Compared to other geological reservoirs, saline aquifers have several advantages as storage formations for CO_2. Firstly, they are spread out all over the world and are readily available. Secondly, deep saline aquifers provide the largest storage capacity, followed by oil or gas reservoirs and coal seams, cf. Table 2.1. Moreover, the upper bound of capacity of the aquifers can be re-estimated and increased after an additional study of the reservoir properties.

However, the hydrology and efficiency of CO_2 storage in saline aquifers are limited and depend on many factors, including fluid properties of CO_2 (viscosity, density, solubility), geochemical properties of CO_2 (water-rock reaction with CO_2-saturated water) and geological variables (availability of pore space, low permeability of cap-rock layer) and others. More details about this topic can be found in Gunter *et al.* [55] based on van der Meer [72].

There are also other geological media, such as *salt caverns* (Figure 2.1), *oil and gas shale* and *abandoned mines*, which can locally provide an effective option for CO_2 storage, cf.

Metz *et al.* [73]. These formations could be very expensive for geological sequestration of CO_2, but in some places in the world they are the only available option for CO_2 storage.

Trapping Mechanisms

The goal of the sequestration process is the disposal of CO_2 in a subsurface for an extended period of time. For the realisation of such a long-term storage, the CO_2 has to be held back by a combination of trapping mechanisms. All trapping mechanisms could be roughly divided into two groups: physical and chemical trappings. Physical trapping, such as *structural* trapping in structural traps and *residual-gas* trapping in the pore space, occur when CO_2 as a free gas or supercritical fluid is immobilised. Chemical trapping in the form of a *solubility* trapping appears, when CO_2 is dissolved into the subsurface fluids, while *mineral* trapping occurs, when CO_2 is involved in chemical reactions with the rock matrix. Finally, during the adsorption of the CO_2 onto mineral surfaces, *adsorption* trapping can be observed.

Depending on the time scale and the type of geological formation, some trapping mechanisms are more prevalent than others. The schematic illustration in Figure 2.2 represents the dependence of storage security on the injection time and type of the trapping mechanisms.

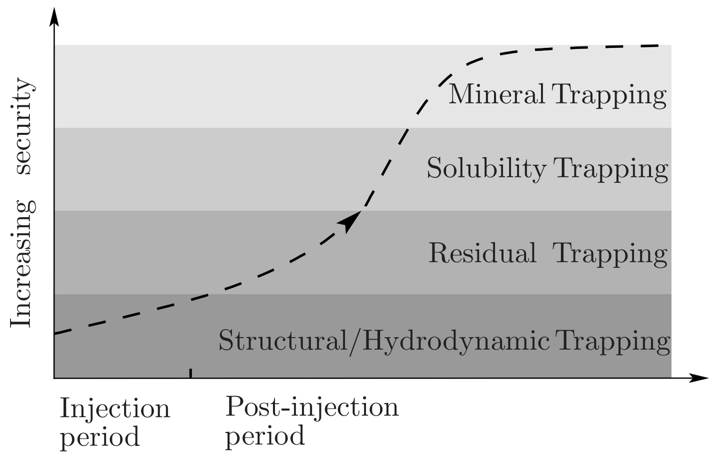

Figure 2.2: Storage security versus time scale during and after CO_2 injection.

According to Figure 2.2, *structural trapping* or *hydrodynamic trapping* plays an important role during the injection period. Since the CO_2 within an aquifer is more buoyant than water, it rises and accumulates under a dense impermeable layer (or a cap-rock), cf. Figure 2.3 a. A large amount of CO_2 can be stored in the subsurface because of the reservoir structure and, therefore, it is called structural trapping.

Residual trapping is observed when the injected CO_2 moves through the porous rock displacing water and some of CO_2 stays in the pore space in the form of disconnected (residual) droplets, which are immobile, cf. Figure 2.3 b.

Dissolution or *solubility trapping* involves the CO_2 dissolution process in the salt water (Figure 2.3 c). Since the salt water containing CO_2 is denser than the surrounding fluid, it sinks to the bottom of the formation, which makes the storage process more secure over time.

Mineral trapping is usually the chemical reaction of CO_2 with the rock matrix (Figure 2.3 d). This type of trapping can be considered as a final stage of the whole trapping process[1].

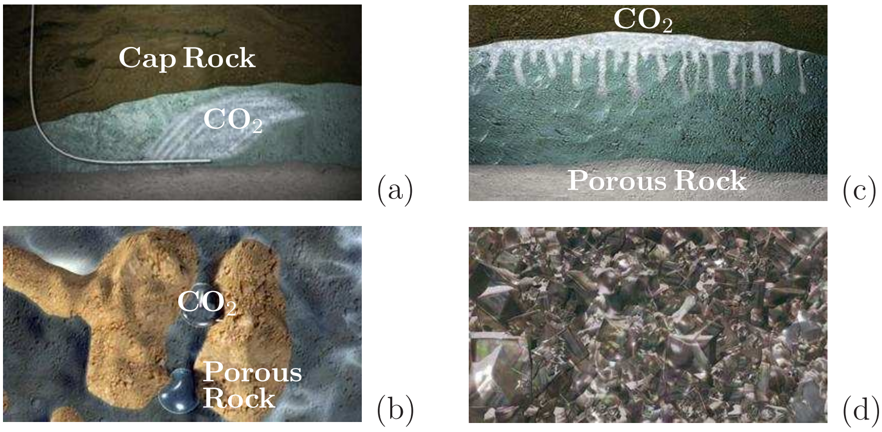

[www.co2captureproject.org]

Figure 2.3: Trapping mechanisms: (a) hydrodynamic trapping (b) residual trapping (c) solubility trapping (d) mineral trapping.

An operation of the multiple trapping mechanisms have a common goal: to make CO_2 less mobile, which increases the security and safety of CO_2 storage over the time.

2.2 Specific Physical Properties of Carbon Dioxide

CO_2 carries a significant meaning for life of natural systems, for the industry and for other aspects of human life. CO_2 can exist in different phases: solid, liquid, gaseous or even supercritical. Under the normal atmospheric conditions, at pressure $p = 1\,\text{atm}$ and temperature $\theta = 273\,\text{K}$, CO_2 is a gas with density $\rho = 1.87\,\text{kg/m}^3$. Gaseous CO_2 is used by plants for the photosynthesis, which is a key process for life on the earth. CO_2 in a solid phase is usually called “dry ice” and is used in cooling technologies, since it is colder than regular ice and leaves no moisture during phase transformations (e. g. sublimation). Moreover, CO_2 is not flammable, does not explode and is not toxic.

For a better understanding of the physical properties and the behaviour of any substance, usually the so-called phase diagram is introduced, which describes the relationship between pressure (p), specific volume (v) and temperature (θ). A definition of a phase diagram in the frame of classical thermodynamics can be found in Section 3.5.

A projection of a three-dimensional phase diagram for CO_2 on the pressure-temperature plane or, in other words, the physical CO_2 properties at a constant specific volume are

[1] CO_2 Capture Project, 2008, URL:http://www.co2captureproject.org

presented in Figure 2.4. As it can be seen from the diagram, at low temperatures and under certain pressure the aggregate state of CO_2 is solid. Further increasing the temperature, solid CO_2 can be directly sublimated into the vapour state skipping the liquid state. The p-θ area is split into two regions corresponding to a gaseous and a liquid phases by a so-called vaporisation curve. This curve rises from the triple point and ends at the critical point, where pure CO_2 has the following properties:

$$\begin{aligned} \theta_{\mathrm{cr}} &= 304.1 \quad [\mathrm{K}]\,, \\ p_{\mathrm{cr}} &= 7.38 \quad [\mathrm{MPa}]\,, \\ \rho_{\mathrm{cr}} &= 467.6 \quad [\mathrm{kg/m^3}]\,. \end{aligned} \tag{2.1}$$

Furthermore, by increasing pressure or temperature or both of them at the critical point, the region with the supercritical properties can be reached. This region is indicated by the bold dashed line on the p-θ (v = const) and ρ-θ diagrams, in Figure 2.4 and Figure 2.5, respectively.

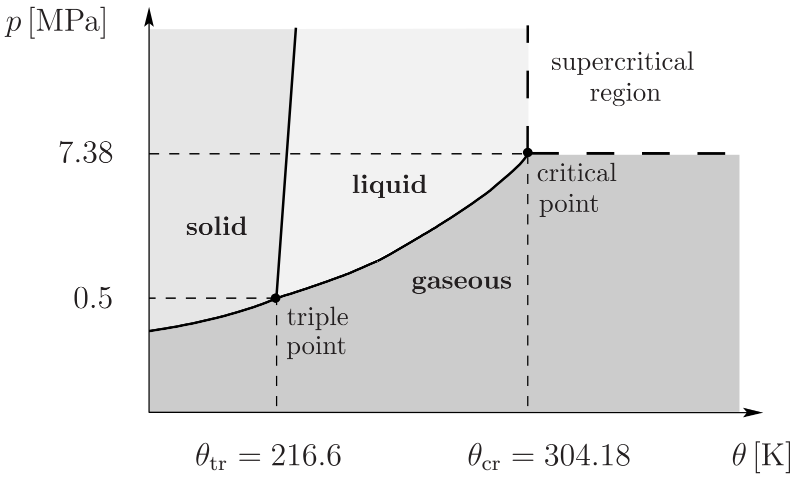

Figure 2.4: CO_2 phase diagram at v = const.

In physics, a *supercritical* state of a substance is defined as an aggregate state with properties between gas and liquid phases, because it can diffuse through solids as a gas and dissolve materials as a liquid. By changing temperature and pressure, the supercritical substance will behave more as a gas or a liquid. Often, a substance in the supercritical state is called a *supercritical fluid*. Besides other advantages, the supercritical fluid has higher mass transfer rates and low operating temperatures. Supercritical fluids are widely used in power generation, biofuel production, refrigeration and many other applications, including CCS and EOR industrial fields.

In this context, it should be noted that during pumping into the subsurface, CO_2 stays under relatively high pressure p and temperature θ and reaches the aquifer as a supercritical fluid. The density of supercritical CO_2 depends on the temperature and the pressure in the reservoir as shown in Figure 2.5. In this regard, there are several desired conditions

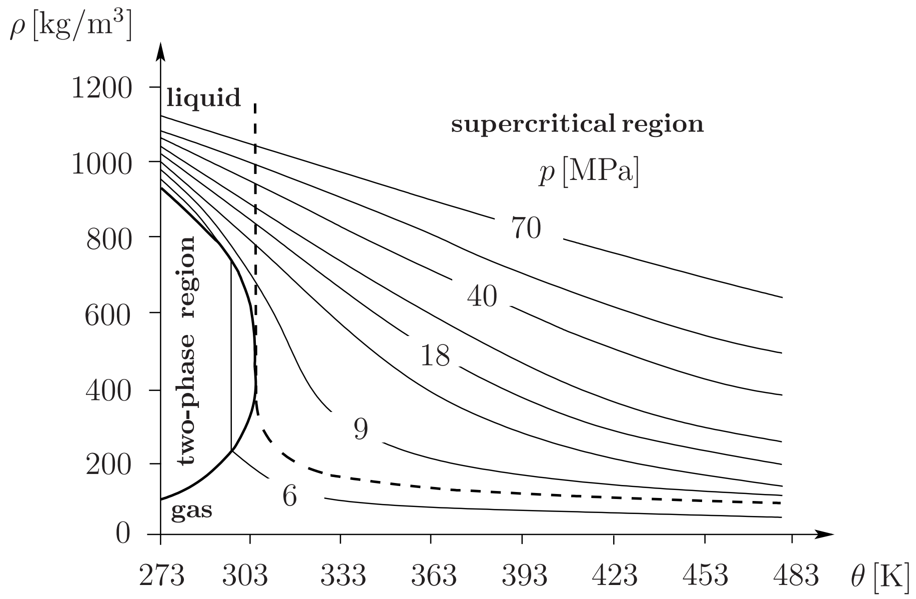

Figure 2.5: Density of CO_2 versus temperature, Baines & Worden [6].

for the reservoir properties. Firstly, it is assumed that the temperature within the reservoir is almost constant. It means that the density of CO_2 depends only on the pressure in the reservoir, which is related to the injection depth. CO_2 density as a function of the depth of a reservoir is shown in Figure 2.6. This dependence demonstrates that the deeper an injection process takes place the less space is needed for the CO_2 and, as a result, more CO_2 can be stored in a reservoir.

Secondly, it is important to have a low permeable cap-rock or a dense layer without any open faults on the upper part of a reservoir, which blocks the upwards migration of the CO_2 after injection.

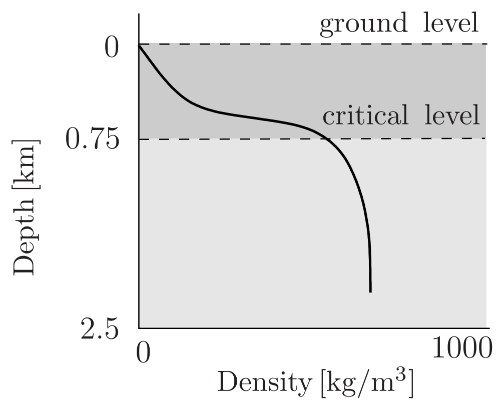

Figure 2.6: Depth of a reservoir versus CO_2 density.

From the point of the storage efficiency, it is desirable to inject CO_2 at supercritical conditions since more CO_2 can be stored per unit of an available pore volume compared to a gaseous state of CO_2, cf. Bachu [4]. However, due to the fact that the surrounding conditions within a reservoir could change, CO_2 can also change its state from the supercritical phase to liquid or gaseous phase. Thus, the problem how to describe the phase transformation process occurs. This phase change process itself is undesirable, because the occupied volume and pressure change accordingly leading to an increasing of the pressure on the cap-rock layer and, possibly, to a high deformation of the solid skeleton of the layer.

Therefore, the ideal injection depth for CO_2 storage is more than 800 m, where it is assumed that the temperature and the pressure have constant values and the CO_2 stays in the supercritical state. Nevertheless, this is an “ideal” situation, which may not always be possible in the reality. In this regard, one of the goals of the present investigation is to study the possible consequences of the injection procedure. In other words, a “critical” scenario of CO_2 injection into a reservoir where supercritical CO_2 can potentially change its phase is modelled in this work.

Moreover, pressure and temperature differences between the injection well and the aquifer can cause various problems. For example, if the pressure gradient is high, the solid rock within a stored reservoir could be highly deformed. Furthermore, the solid skeleton within a cap-rock layer also can undergo deformations, which are enough to create cracks in this layer. Due to buoyancy forces, CO_2 may leak through available pathways from a reservoir. At the same time, an escaping process is accompanied by changes in pressure and temperature, which may result in CO_2 phase transformation. This issue provides an additional motivation to study the phase change process for the supercritical CO_2 in more detail. More knowledge about the phase transition process and critical phenomena can be found, for instance, in the book by Stanley [97]. Additional information and some experimental results about an estimation of the mass-transfer rates for the CO_2-water system can be found in Farajzadeh *et al.* [49].

2.3 Gaps in Research and Remaining Questions

Although a lot of research work has been done in the area of CCS, there is still a large number of questions that needs to be answered. The current gaps in research are summarised and grouped into several categories as follows:

- improvement of available technologies for the CO_2 capture in order to decrease the costs of capturing, processing and transporting

- detailed study of the geographical relation between CO_2 sources and storage reservoirs (regional assessment)

- improvement of estimation of storage capacity; obtaining more information on storage capacity for more areas all over the world, especially, for countries with high energy consumption

- complete investigation of the particular storage mechanisms, such as long-term storage, CO_2 migration, leakage processes and others; improved understanding of the interaction between various storage mechanisms, in particular, for deep saline aquifers
- detailed study of the response of the biological systems for ocean storage; gaining experience in ecological impact of the stored CO_2
- analysis of the related environmental and safety issues
- assessment of the duration of CO_2; development of reliable methods for the estimation of the leakage rates
- several other aspects

The current investigation is focused only on some aspects from the list above. In particular, a better understanding of the deformation of the solid skeleton in a reservoir under the influence of the high pressure of the injected CO_2 is regarded as one of the main issues for investigation. Furthermore, the behaviour of geologically stored CO_2 has been incompletely studied so far. In this regard, the phase transition process between CO_2 phases is an interesting subject for research.

It is evident that besides the problems related to the CO_2 injection process mentioned above, other factors have to be taken into account, such as: economical costs, risk analysis, biological risk, transport problems, capacity estimation, physical and chemical processes taking place after injection and many others. Additional general information about the CO_2 storage problem can be found in publications by Michael *et al.* [74], Metz *et al.* [73], Bachu *et al.* [5] and by other authors. Benchmark problems and their solutions for the CO_2 injection problem are available in papers by Pruess *et al.* [87], Ebigbo *et al.* [31] and others. Some results of numerical simulations are provided in Sasaki *et al.* [91], Bielinski [11] and others, while analytical evaluation of specific aspects can be found in Nordbotten *et al.* [77].

Chapter 3:
Theoretical Fundamentals

The following chapter provides a brief introduction into the continuum-mechanical fundamentals of the Theory of Porous Media (TPM), as well as the concept of volume fractions, the kinematical relations and the governing form of balance relations. Also, an overview of the thermodynamical principles required for further constitutive modelling can be found in this chapter.

3.1 General Discussion

Each problem in fluid and solid mechanics can be considered at a micro- or a macroscale. The micromechanical consideration of a problem has the advantage of describing the motion of each individual aggregate, because within this consideration phases are separated from each other. However, it is not always possible to describe the process completely, since detailed information about the size and shape (geometry) of the particles within the considered material is often unknown at microscale. Therefore, the macromechanical consideration of the processes comes into play. Basically, the macroscale consideration is provided by a homogenisation procedure, which is defined as a statistical spread of the actual microstructural properties trough the considered domain, known as the representative elementary volume (REV), cf. Bear [8], Ehlers [37].

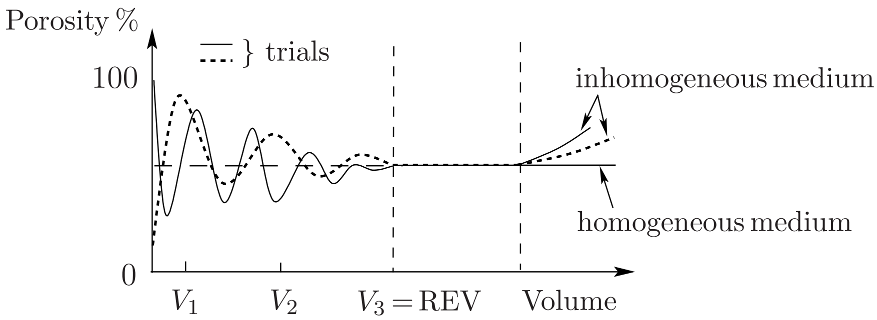

Figure 3.1: Definition of the representative elementary volume.

The size of the REV has some limits: firstly, the domain should be sufficiently large to allow performing statistical analysis and, secondly, small enough to maintain inherent heterogeneity of the considered domain. It means that the average values of macroscopic parameters must be independent of the size of the domain. As an example, an estimation of the porosity of a porous medium is illustrated in Figure 3.1. Herein, the selected volumes V_1 and V_2 are not representative since they do not reflect the real properties of the media. In contrast, the porosity of the porous medium for the volume V_3 is constant and thus provides a representative description of the material, cf. Bear [9], Helmig [57].

The description of the CO_2 injection process into an aquifer and its distribution along the reservoir can be classified as a multiphasic problem and described at the macroscale. Thus, the postulated issues including the complexity of the different formulations can be well-understood and described using the TPM, which fundamentals are explained in the next sections.

3.2 The Theory of Porous Media

Physical processes taking place within natural systems and materials, such as biological soft tissues, soils and others can be well-described by either the *Theory of Mixture*, cf. Bowen [18], Green & Naghdi [54], or the *Theory of Porous Media*, cf. Bowen [19, 20], de Boer [14], Ehlers [37] and Truesdell & Toupin [102].

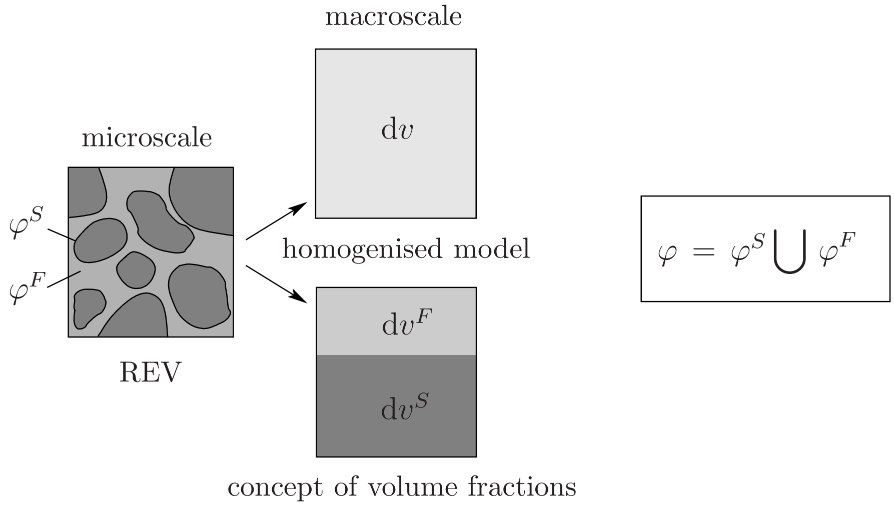

Figure 3.2: Representative elementary volume with microstructure, homogenised model and concept of volume fractions.

Basically, the modelling of miscible constituents is embedded in the Theory of Mixture (TM). However, this theory has a drawback caused by the loss of microscopic information about the system. In order to reflect the inner structure of a system, the TM is combined with the *Concept of Volume Fractions*, which forms the basis of the TPM. In contrast with the TM, the TPM represents a convenient tool for the macroscopic description of immiscible multiphasic aggregates, wherein the quantity of the individual constituents of the overall medium is characterised by their volume fractions. In particular, the TPM provides a convenient framework for the current investigation to describe the complicated behaviour of coupled fluid-solid systems such as the CO_2 sequestration problem. Within the TPM, each constituent of the overall aggregate can be described by the governing equations for a single-phase material with additional production terms representing the thermodynamical and mechanical interactions between the constituents. For more comprehensive information and details about the TPM, the readership is referred to Truesdell [100], de Boer & Ehlers [16] and Ehlers [34, 35, 37] among others.

Following the basic concept of the TPM, the properties of a multiphasic aggregate φ with individual constituents φ^α are statistically distributed over the REV, cf. Figure 3.2. This averaging procedure leads to a model of superimposed and interacting continua

$$\varphi = \bigcup_\alpha \varphi^\alpha \,, \quad \text{where} \quad \alpha \in \{S,\, F\} \quad \text{and} \quad \varphi^F = \bigcup_\beta \varphi^\beta \,. \tag{3.1}$$

Herein, S indicates the solid constituent and F is a summation over all fluid constituents β. Depending on the amount and type of the fluid constituents, β can be represented, for example, by liquid L or gas G constituents and others.

In the frame of the TPM, each immiscible phase is represented by its partial volume V^α. Then, the volume V of the overall aggregate $\mathcal{B}$ is obtained as the sum of the partial volumes of the constituents φ^α in $\mathcal{B}$

$$V = \int_{\mathcal{B}} \mathrm{d}v = \sum_\alpha V^\alpha \,, \tag{3.2}$$

where

$$V^\alpha = \int_{\mathcal{B}} \mathrm{d}v^\alpha = \int_{\mathcal{B}} n^\alpha \, \mathrm{d}v \,. \tag{3.3}$$

Herein, n^α is called *volume fraction* and is defined as a ratio between the volume element $\mathrm{d}v^\alpha$ of a constituent φ^α and the volume element $\mathrm{d}v$ of the overall aggregate φ (Figure 3.2):

$$n^\alpha = \frac{\mathrm{d}v^\alpha}{\mathrm{d}v} \,. \tag{3.4}$$

Equations (3.2) - (3.4) represent the concept of volume fractions. Furthermore, based on the assumption that there is no voids pace within the overall aggregate and examining the equations (3.2) and (3.3), the so-called saturation condition is obtained

$$\sum_\alpha n^\alpha = 1 \,. \tag{3.5}$$

Proceeding from the concept of volume fractions, two different densities can be introduced: the material (effective or realistic) density $\rho^{\alpha R}$ and the partial (global or bulk) density ρ^α. $\rho^{\alpha R}$ and ρ^α relate the local mass $\mathrm{d}m^\alpha$ to the volume elements $\mathrm{d}v^\alpha$ and $\mathrm{d}v$, respectively,

$$\rho^{\alpha R} = \frac{\mathrm{d}m^\alpha}{\mathrm{d}v^\alpha} \quad \text{and} \quad \rho^\alpha = \frac{\mathrm{d}m^\alpha}{\mathrm{d}v} \,. \tag{3.6}$$

From (3.4) and (3.6), it is determined that both densities are related to each other through the corresponding volume fraction

$$\rho^\alpha = n^\alpha \, \rho^{\alpha R} \,. \tag{3.7}$$

The partial density ρ^α can be changed either by the volume fraction n^α or the material density $\rho^{\alpha R}$. If a constituent is materially incompressible, its material density has a constant value at constant temperature ($\rho^{\alpha R}$ = const). It means that the partial density of a materially incompressible constituent can only be modified due to a deformation-driven change of the corresponding volume fraction.

For a system with more than one fluid phase, it is convenient to introduce a saturation function s^β, which describes the ratio of the pore-fluids in the pore space. s^β represents the ratio of the volume fraction of a constituent n^β to the volume fraction of the overall fluid phases n^F (porosity):

$$s^\beta = \frac{n^\beta}{n^F} \quad \text{and} \quad n^F = \sum_\beta n^\beta = 1 - n^S \,. \tag{3.8}$$

Herein, similar to condition (3.5), the restriction for the saturation function is derived as follows

$$\sum_\beta s^\beta = 1 \,. \tag{3.9}$$

3.3 Kinematical Relations

3.3.1 Motion Functions

In the framework of the TPM, the porous body $\mathcal{B}$ is defined as a manifold of material points P^α of the corresponding constituents φ^α. In the reference configuration at time t_0 material points P^α can have different coordinates $\mathbf{X}_\alpha$, while in the actual configuration at time t each partial point $\mathbf{x}$ is simultaneously occupied by points P^α of all constituents, cf. Figure 3.3.

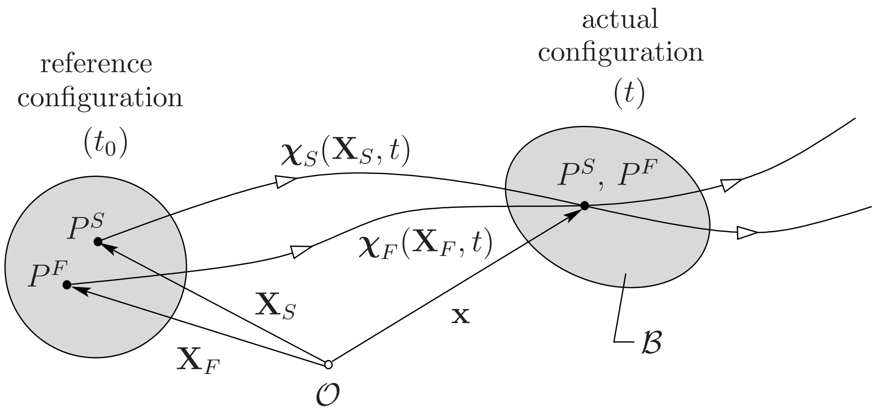

Figure 3.3: Motion of a multiphase porous material.

Kinematic relations of the constituents are described by their own motion functions $\boldsymbol{\chi}_\alpha$

$$\mathbf{x} = \boldsymbol{\chi}_\alpha\,(\mathbf{X}_\alpha, t)\,. \tag{3.10}$$

The assumption about the individuality of the motion function for each constituent requires the uniqueness of the inverse motion function based on the non-singular *Jacobi*an determinant J_α:

$$\mathbf{X}_\alpha = \boldsymbol{\chi}_\alpha^{-1}(\mathbf{x}, t) \quad \text{and} \quad J_\alpha := \det \frac{\partial \boldsymbol{\chi}_\alpha}{\partial \mathbf{X}_\alpha} \neq 0 \,. \tag{3.11}$$

This leads to the fact that each constituent has its individual velocity $\overset{\prime}{\mathbf{x}}_\alpha$ and acceleration $\overset{\prime\prime}{\mathbf{x}}_\alpha$. In a *Lagrange*an or material description, velocity and acceleration are given in terms of the reference configuration and can be written as follows

$$\overset{\prime}{\mathbf{x}}_\alpha = \frac{\partial \boldsymbol{\chi}_\alpha\,(\mathbf{X}_\alpha, t)}{\partial t} \quad \text{and} \quad \overset{\prime\prime}{\mathbf{x}}_\alpha = \frac{\partial^2 \boldsymbol{\chi}_\alpha(\mathbf{X}_\alpha, t)}{\partial t^2}\,, \tag{3.12}$$

while in an *Euler*ian or spatial description, they are expressed in terms of the actual configuration as

$$\overset{\prime}{\mathbf{x}}_\alpha = \overset{\prime}{\mathbf{x}}_\alpha\,[\,\boldsymbol{\chi}_\alpha^{-1}(\mathbf{x}, t), t\,] = \overset{\prime}{\mathbf{x}}_\alpha\;(\mathbf{x}, t) \quad \text{and} \quad \overset{\prime\prime}{\mathbf{x}}_\alpha = \overset{\prime\prime}{\mathbf{x}}_\alpha\,[\,\boldsymbol{\chi}_\alpha^{-1}(\mathbf{x}, t), t\,] = \overset{\prime\prime}{\mathbf{x}}_\alpha\;(\mathbf{x}, t)\,. \tag{3.13}$$

Herein, $(\cdot)'_\alpha$ denotes the material time derivative. The total material time derivative for an arbitrary, steady and sufficiently steady differentiable scalar function Γ or vector function $\boldsymbol{\Gamma}$ is correspondingly defined as

$$\begin{aligned} (\Gamma)'_\alpha &= \frac{\mathrm{d}_\alpha}{\mathrm{d}t}\,\Gamma(\mathbf{x}, t) = \frac{\partial \Gamma}{\partial t} + \operatorname{grad}\Gamma \cdot \overset{\prime}{\mathbf{x}}_\alpha\,, \\ (\boldsymbol{\Gamma})'_\alpha &= \frac{\mathrm{d}_\alpha}{\mathrm{d}t}\,\boldsymbol{\Gamma}(\mathbf{x}, t) = \frac{\partial \boldsymbol{\Gamma}}{\partial t} + (\operatorname{grad}\boldsymbol{\Gamma})\,\overset{\prime}{\mathbf{x}}_\alpha\,, \end{aligned} \tag{3.14}$$

where the operator "grad$\,(\cdot)$" denotes the gradient with respect to the actual position $\mathbf{x}$. In addition, the velocity of the overall aggregate, which indicates the barycentric velocity, can be introduced as

$$\dot{\mathbf{x}} = \frac{1}{\rho}\sum_\alpha \rho^\alpha\,\overset{\prime}{\mathbf{x}}_\alpha\,, \quad \text{with} \quad \rho = \sum_\alpha \rho^\alpha\,. \tag{3.15}$$

The difference between the velocity of a constituent φ^α and the barycentric velocity is interpreted as the diffusion velocity $\mathbf{d}_\alpha$:

$$\mathbf{d}_\alpha = \overset{\prime}{\mathbf{x}}_\alpha - \dot{\mathbf{x}} \quad \text{with} \quad \sum_\alpha \rho^\alpha\,\mathbf{d}_\alpha = \mathbf{0}\,. \tag{3.16}$$

The behaviour of each constituent can be mathematically described by primary variables within the modelling of coupled fluid-solid problems. Usually, the displacement vector $\mathbf{u}_S$ in the frame of the *Lagrange*an description is taken into account as a kinematic primary variable for the solid skeleton

$$\mathbf{u}_S = \mathbf{x} - \mathbf{X}_S\,. \tag{3.17}$$

For fluid phases, it is more convenient to use the seepage velocity as a primary variable, representing the velocity of the fluid phase with respect to the velocity of the solid skeleton in the frame of a modified *Euler*ian description

$$\mathbf{w}_\beta = \overset{\prime}{\mathbf{x}}_\beta - \overset{\prime}{\mathbf{x}}_S\,. \tag{3.18}$$

3.3.2 Deformation and Strain Measures

Deformation and strain measures can be introduced via the material deformation gradient $\mathbf{F}_\alpha$ and their inverse $\mathbf{F}_\alpha^{-1}$. Proceeding from the equations (3.10) and (3.11)$_1$, these gradients are defined as

$$\mathbf{F}_\alpha = \frac{\partial \mathbf{x}}{\partial \mathbf{X}_\alpha} = \mathrm{Grad}_\alpha\, \mathbf{x} \quad \text{and} \quad \mathbf{F}_\alpha^{-1} = \frac{\partial \mathbf{X}_\alpha}{\partial \mathbf{x}} = \mathrm{grad}\, \mathbf{X}_\alpha\,. \tag{3.19}$$

Therein, the operator "$\mathrm{Grad}_\alpha\,(\cdot)$" represents the gradients with respect to the reference position

$$\mathrm{Grad}_\alpha\,(\cdot) = \frac{\partial (\cdot)}{\partial \mathbf{X}_\alpha}. \tag{3.20}$$

In this regard, the deformation gradient of the solid skeleton $\mathbf{F}_S$ can be expressed in terms of the displacement vector $\mathbf{u}_S$, which leads to

$$\mathbf{F}_S = \frac{\partial \mathbf{x}}{\partial \mathbf{X}_S} = \mathrm{Grad}_S\, \mathbf{x} = \mathbf{I} + \mathrm{Grad}_S\, \mathbf{u}_S\,. \tag{3.21}$$

Due to the fact that the uniqueness of the inverse motion function (3.11) requires a non-zero *Jacobi*an J_α and the deformation gradient equals to the identity tensor $\mathbf{I}$ (or $\det \mathbf{F}_\alpha(t_0) = 1$) in the undeformed initial state, the domain of $\det \mathbf{F}_\alpha$ is restricted to positive values

$$\det \mathbf{F}_\alpha = J_\alpha > 0\,. \tag{3.22}$$

Furthermore, it is possible to derive the following relations, describing the transformation of line, area and volume elements from the reference configuration ($\mathrm{d}\mathbf{X}_\alpha$, $\mathrm{d}\mathbf{A}_\alpha$, $\mathrm{d}V_\alpha$) to the actual configuration ($\mathrm{d}\mathbf{x}$, $\mathrm{d}\mathbf{a}$, $\mathrm{d}v$) via the deformation gradient

$$\begin{aligned} \mathrm{d}\mathbf{x} &= \mathbf{F}_\alpha\, \mathrm{d}\mathbf{X}_\alpha\,, \\ \mathrm{d}\mathbf{a} &= \det \mathbf{F}_\alpha\, \mathbf{F}_\alpha^{T-1}\, \mathrm{d}\mathbf{A}_\alpha\,, \\ \mathrm{d}v &= \det \mathbf{F}_\alpha\, \mathrm{d}V_\alpha\,. \end{aligned} \tag{3.23}$$

This type of transformation is called *push-forward* transformation, while the inverse transformation, from the actual to the reference configuration, is named *pull-back* transformation. The basic operations of the tensor calculus can be found in Appendix A as well as in de Boer [13], Ehlers [34, 39], Truesdell & Noll [101] and Zhilin [104].

Furthermore, different deformation tensors could be defined via the deformation gradients. Using the relations given in (3.23), one derives

$$\begin{aligned} \mathrm{d}\mathbf{x}\cdot\mathrm{d}\mathbf{x} &= \mathbf{F}_\alpha\,\mathrm{d}\mathbf{X}_\alpha\cdot\mathbf{F}_\alpha\,\mathrm{d}\mathbf{X}_\alpha = \mathrm{d}\mathbf{X}_\alpha\cdot(\mathbf{F}_\alpha^T\,\mathbf{F}_\alpha)\,\mathrm{d}\mathbf{X}_\alpha = \mathrm{d}\mathbf{X}_\alpha\cdot\mathbf{C}_\alpha\,\mathrm{d}\mathbf{X}_\alpha\,, \\ \mathrm{d}\mathbf{X}_\alpha\cdot\mathrm{d}\mathbf{X}_\alpha &= \mathbf{F}_\alpha^{-1}\,\mathrm{d}\mathbf{x}\cdot\mathbf{F}_\alpha^{-1}\,\mathrm{d}\mathbf{x} = \mathrm{d}\mathbf{x}\cdot(\mathbf{F}_\alpha^{T-1}\,\mathbf{F}_\alpha^{-1})\,\mathrm{d}\mathbf{x} = \mathrm{d}\mathbf{x}\cdot\mathbf{B}_\alpha^{-1}\,\mathrm{d}\mathbf{x}\,. \end{aligned} \tag{3.24}$$

Herein, $\mathbf{C}_\alpha = \mathbf{F}_\alpha^T\,\mathbf{F}_\alpha$ is the right *Cauchy-Green* deformation tensor representing a deformation measure of the reference configuration, while $\mathbf{B}_\alpha = \mathbf{F}_\alpha\,\mathbf{F}_\alpha^T$ is the left *Cauchy-Green* deformation tensor representing a deformation measure of the actual configuration.

The strain measures are obtained by the difference of squares of the line elements at the current and reference configuration

$$\mathrm{d}\mathbf{x}\cdot\mathrm{d}\mathbf{x} - \mathrm{d}\mathbf{X}_\alpha\cdot\mathrm{d}\mathbf{X}_\alpha = \mathrm{d}\mathbf{X}_\alpha\cdot(\mathbf{C}_\alpha - \mathbf{I})\,\mathrm{d}\mathbf{X}_\alpha = \mathrm{d}\mathbf{X}_\alpha\cdot(\mathbf{I} - \mathbf{B}_\alpha^{-1})\,\mathrm{d}\mathbf{X}_\alpha\,. \tag{3.25}$$

Herein,

$$\mathbf{E}_\alpha = \tfrac{1}{2}(\mathbf{C}_\alpha - \mathbf{I}) \quad \text{and} \quad \mathbf{A}_\alpha = \tfrac{1}{2}(\mathbf{I} - \mathbf{B}_\alpha^{-1})\,, \tag{3.26}$$

where $\mathbf{E}_\alpha$ is the *Green-Lagrange*an strain tensor, $\mathbf{A}_\alpha$ is the *Almansi*an strain tensor.

3.3.3 Deformation and Strain Rates

In order to formulate the deformation and strain rates, the material time derivative of the deformation gradient (3.19) is introduced based on the *Lagrange*an description

$$(\mathbf{F}_\alpha)'_\alpha = \frac{\mathrm{d}_\alpha}{\mathrm{d}t}\mathbf{F}_\alpha = \frac{\partial\,\overset{\prime}{\mathbf{x}}_\alpha\,(\mathbf{X}_\alpha, t)}{\partial\mathbf{X}_\alpha} = \mathrm{Grad}_\alpha\;\overset{\prime}{\mathbf{x}}_\alpha\;. \tag{3.27}$$

On the other hand, based on the *Euler*ian description, the derivative is

$$(\mathbf{F}_\alpha)'_\alpha = \mathbf{L}_\alpha\,\mathbf{F}_\alpha\,, \tag{3.28}$$

where $\mathbf{L}_\alpha$ is known as the spatial velocity gradient of the constituent φ^α. From (3.28), one finds that

$$\mathbf{L}_\alpha = (\mathbf{F}_\alpha)'_\alpha\,\mathbf{F}_\alpha^{-1} = \mathrm{grad}\;\overset{\prime}{\mathbf{x}}_\alpha \quad \text{and} \quad \mathbf{L}_\alpha\cdot\mathbf{I} = \mathrm{div}\;\overset{\prime}{\mathbf{x}}_\alpha\;. \tag{3.29}$$

Furthermore, $\mathbf{L}_\alpha$ can be decomposed into a symmetric part $\mathbf{D}_\alpha$ named *deformation velocity* and a skew-symmetric part $\mathbf{W}_\alpha$ named *spin* or *vorticity* tensor, yielding

$$\mathbf{L}_\alpha = \mathbf{D}_\alpha + \mathbf{W}_\alpha\,, \tag{3.30}$$

where

$$\begin{aligned}\mathbf{D}_\alpha &= \tfrac{1}{2}(\mathbf{L}_\alpha + \mathbf{L}_\alpha^T)\,,\\ \mathbf{W}_\alpha &= \tfrac{1}{2}(\mathbf{L}_\alpha - \mathbf{L}_\alpha^T)\,.\end{aligned} \tag{3.31}$$

In addition, the *Green-Lagrange*an stain rate can be derived from the *Green-Lagrange*an strain tensor $\mathbf{E}_\alpha$:

$$(\mathbf{E}_\alpha)'_\alpha = \tfrac{1}{2}(\mathbf{C}_\alpha)'_\alpha = \mathbf{F}_\alpha^T\,\mathbf{D}_\alpha\,\mathbf{F}_\alpha\,. \tag{3.32}$$

3.3.4 Stress Measures

In order to complete the description of the rates and measures, the stress measures should be introduced.

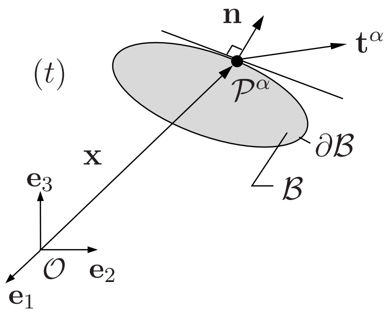

Figure 3.4: Illustration of stress measures.

Figure 3.4 shows body $\mathcal{B}$ at the current configuration t consisting of the constituents φ^α. The forces acting from the vicinity on the surface $\partial\mathcal{B}$, are captured by the surface traction vector $\mathbf{t}^\alpha(\mathbf{x}, \mathbf{n}, t)$. Following *Cauchy*'s theorem, $\mathbf{t}^\alpha(\mathbf{x}, \mathbf{n}, t)$ can be represented via

$$\mathbf{t}^\alpha(\mathbf{x}, \mathbf{n}, t) \;=\; \mathbf{T}^\alpha(\mathbf{x}, t)\, \mathbf{n}\,. \tag{3.33}$$

Therein, $\mathbf{T}^\alpha$ is the partial *Cauchy* tensor and $\mathbf{n}$ is the outward oriented unit normal vector of the surface $\partial\mathcal{B}$.

Other stress tensors could be introduced by use of the representation of the surface force $\mathrm{d}\mathbf{k}^\alpha$ via tensor $\mathbf{T}^\alpha$ and the oriented area element $\mathrm{d}\mathbf{a}$:

$$\mathrm{d}\mathbf{k}^\alpha \;=\; \mathbf{t}^\alpha\,\mathrm{d}a \;=\; \mathbf{T}^\alpha\,\mathbf{n}\,\mathrm{d}a \;=\; \mathbf{T}^\alpha\,\mathrm{d}\mathbf{a}\,. \tag{3.34}$$

Transferring the area element $\mathrm{d}\mathbf{a}$ to a weighted area element $\mathrm{d}\bar{\mathbf{a}}_\alpha = \det\mathbf{F}_\alpha^{-1}\mathrm{d}\mathbf{a}_\alpha$ leads to the *Kirchhoff* stress tensor $\boldsymbol{\tau}^\alpha$ such as

$$\mathrm{d}\mathbf{k}^\alpha \;=\; \det\mathbf{F}_\alpha\,\mathbf{T}^\alpha\,\mathrm{d}\bar{\mathbf{a}}_\alpha \;=:\; \boldsymbol{\tau}^\alpha\,\mathrm{d}\bar{\mathbf{a}}_\alpha\,. \tag{3.35}$$

Thus, using the transformation rules (3.23) and reformulating the surface force $\mathrm{d}\mathbf{k}^\alpha$ through the area element at the reference configuration $\mathrm{d}\mathbf{A}_\alpha$, the first *Piola-Kirchhoff* tensor $\mathbf{P}^\alpha$ is derived:

$$\mathrm{d}\mathbf{k}^\alpha \;=\; \det\mathbf{F}_\alpha\,\mathbf{T}^\alpha\,\mathbf{F}_\alpha^{T-1}\,\mathrm{d}\mathbf{A}_\alpha \;=:\; \mathbf{P}^\alpha\,\mathrm{d}\mathbf{A}_\alpha\,. \tag{3.36}$$

In addition, the second *Piola-Kirchhoff* tensor $\mathbf{S}^\alpha$ can be introduced by

$$\mathbf{S}^\alpha \;=\; \mathbf{F}_\alpha^{-1}\,\mathbf{P}^\alpha\,. \tag{3.37}$$

Proceeding from (3.35)-(3.37), the relations between the *Kirchhoff* tensor and both *Piola-Kirchhoff* tensors are given by

$$\begin{aligned} \mathbf{P}^\alpha &= \boldsymbol{\tau}^\alpha\,\mathbf{F}_\alpha^{T-1}\,, \\ \mathbf{S}^\alpha &= \mathbf{F}_\alpha^{-1}\,\boldsymbol{\tau}^\alpha\,\mathbf{F}_\alpha^{T-1}\,. \end{aligned} \tag{3.38}$$

It should be noted that in case of a geometrically linear theory, where $\mathbf{F}_\alpha \approx \mathbf{I}$, the stress tensors introduced above are approximately the same and can be given by one stress tensor $\boldsymbol{\sigma}^\alpha$:

$$\mathbf{T}^\alpha \;\approx\; \boldsymbol{\tau}^\alpha \;\approx\; \mathbf{P}^\alpha \;\approx\; \mathbf{S}^\alpha \;\approx:\; \boldsymbol{\sigma}^\alpha\,. \tag{3.39}$$

3.4 Balance Relations

In continuum mechanics, the evolution of any physical system can be analysed using the conservation laws for the mechanical and thermodynamical properties, such as, mass, momentum, momentum of momentum (m.o.m), energy and entropy.

In frame of the TPM, modelling of multiphasic materials follows *Truesdell*'s "metaphysical principles", cf. Truesdell [100]:

1. All properties of the mixture must be mathematical consequences of properties of the constituents.
2. So as to describe the motion of a constituent, we may in imagination isolate it from the rest of the mixture, provided we allow properly for the actions of the other constituents upon it.
3. The motion of the mixture is governed by the same equations as is a single body.

In other words, these principles mean that each constituent within the multiphasic material has to be described by individual balance relations. However, since the constituents of the multiphasic material can exchange their properties with each other, the balance relations originally taken for the single-phase material, have to be extended by so-called production terms, which describe the interaction between different constituents. Finally, the balance relations for the overall aggregate are obtained by summing over all balance relations for the individual constituents.

The next sections give a brief introduction to the general and specific forms of the balance relations based on Ehlers [37]. The corresponding unknown variables from these relations are discussed in Section 4, which represents the constitutive modelling procedure. A more comprehensive description of this topic can be found, for example, in de Boer & Ehlers [16], Ehlers [34, 38] or Marle [70].

3.4.1 Balance Relations for the Overall Aggregate

Balance relations for the mechanical (mass, momentum, m.o.m.) and thermodynamical (energy, entropy) quantities can be embedded into a general structure denoted as *master balance relation*. Proceeding from the results of classical continuum mechanics of single-phase material, the master balance relations for the overall aggregate $\mathcal{B}$ in the global form read

$$\begin{aligned} \frac{\mathrm{d}}{\mathrm{d}t}\int_{\mathcal{B}} \Psi \,\mathrm{d}v &= \int_{\partial\mathcal{B}} (\boldsymbol{\phi}\cdot\mathbf{n})\,\mathrm{d}a + \int_{\mathcal{B}} \sigma\,\mathrm{d}v + \int_{\mathcal{B}} \hat{\Psi}\,\mathrm{d}v\,, \\ \frac{\mathrm{d}}{\mathrm{d}t}\int_{\mathcal{B}} \boldsymbol{\Psi} \,\mathrm{d}v &= \int_{\partial\mathcal{B}} (\boldsymbol{\Phi}\,\mathbf{n})\,\mathrm{d}a + \int_{\mathcal{B}} \boldsymbol{\sigma}\,\mathrm{d}v + \int_{\mathcal{B}} \hat{\boldsymbol{\Psi}}\,\mathrm{d}v\,. \end{aligned} \tag{3.40}$$

Herein, Ψ and $\boldsymbol{\Psi}$ are volume-specific scalar- and vector-valued mechanical quantities respectively, which have to be balanced. The terms $(\boldsymbol{\phi}\cdot\mathbf{n})$ and $(\boldsymbol{\Phi}\,\mathbf{n})$ are the effluxes of the respective mechanical quantity at the body surface $\partial\mathcal{B}$. The symbols σ and $\boldsymbol{\sigma}$ are the supply terms of the mechanical quantities resulting from a distance. The remaining terms $\hat{\Psi}$ and $\hat{\mathbf{\Psi}}$ are the production terms of the mechanical quantities coming from the possible couplings of body $\mathcal{B}$ with its surrounding.

The global structure of the balance relations (3.40) yields the corresponding local forms by applying the time derivative for the actual volume element $\mathrm{d}v$ on the left-hand side of (3.40) and using the *Gauss* integral theorem for the surface integral on the right-hand side of (3.40). The local form of the balance relations reads

$$\begin{aligned} \dot{\Psi} + \Psi \operatorname{div} \dot{\mathbf{x}} &= \operatorname{div} \boldsymbol{\phi} + \sigma + \hat{\Psi} \\ \dot{\mathbf{\Psi}} + \mathbf{\Psi} \operatorname{div} \dot{\mathbf{x}} &= \operatorname{div} \mathbf{\Phi} + \boldsymbol{\sigma} + \hat{\mathbf{\Psi}}\,. \end{aligned} \tag{3.41}$$

The balance relations for mass, momentum, m.o.m., energy and entropy could be obtained using the corresponding physical quantities from Table 3.1.

	Ψ, $\mathbf{\Psi}$	$\boldsymbol{\phi}$, $\mathbf{\Phi}$	σ, $\boldsymbol{\sigma}$	$\hat{\Psi}$, $\hat{\mathbf{\Psi}}$
mass	ρ	$\mathbf{0}$	0	0
momentum	$\rho\,\dot{\mathbf{x}}$	$\mathbf{T}$	$\rho\,\mathbf{b}$	$\mathbf{0}$
m.o.m.	$\mathbf{x} \times (\rho\,\dot{\mathbf{x}})$	$\mathbf{x} \times \mathbf{T}$	$\mathbf{x} \times (\rho\,\mathbf{b})$	$\mathbf{0}$
energy	$\rho\,\varepsilon + \frac{1}{2}\,\dot{\mathbf{x}} \times (\rho\,\dot{\mathbf{x}})$	$\mathbf{T}^T\,\dot{\mathbf{x}} - \mathbf{q}$	$\dot{\mathbf{x}} \cdot (\rho\,\mathbf{b}) + \rho\,r$	0
entropy	$\rho\,\eta$	$\boldsymbol{\phi}_\eta$	σ_η	$\hat{\eta}$

Table 3.1: Balance relations of the overall aggregate.

Therein, ρ denotes the density of the overall aggregate, $\rho\,\dot{\mathbf{x}}$ is the momentum, whereas $\mathbf{x} \times (\rho\,\dot{\mathbf{x}})$ is the m.o.m., $\mathbf{T}$ is the *Cauchy* stress tensor and $\rho\,\mathbf{b}$ is the volume-specific body force (usually performed by gravitation). Accordingly to the energy balance equation, ε denotes the internal energy, $\mathbf{q}$ is the heat influx over the boundary and r is the external heat supply (e. g. radiation). In the entropy balance, η is the entropy, $\boldsymbol{\phi}_\eta$ is the efflux of entropy, σ_η denotes the external supply and $\hat{\eta}$ is the entropy production, which is non-negative, $\hat{\eta} \geq 0$.

By substituting the quantities from Table 3.1 into the local form of the balance relations (3.41), the specific balance relations known from continuum mechanics of single-phase materials could be derived, cf. Ehlers [36]. In order to simplify the forms of the balance relations, the so-called respective "lower" balances are used. Starting from the mass balance the momentum, m.o.m., energy and entropy balances are evaluated:

$$
\begin{aligned}
\text{mass :} \quad & \dot{\rho} + \rho \operatorname{div} \dot{\mathbf{x}} &=& \; 0\,, \\
\text{momentum :} \quad & \rho\, \ddot{\mathbf{x}} &=& \; \operatorname{div} \mathbf{T} + \rho\, \mathbf{b}\,, \\
\text{m.o.m. :} \quad & \mathbf{0} &=& \; \mathbf{I} \times \mathbf{T} \quad \longrightarrow \quad \mathbf{T} = \mathbf{T}^T\,, \\
\text{energy :} \quad & \rho\, \dot{\varepsilon} &=& \; \mathbf{T} \cdot \mathbf{L} - \operatorname{div} \mathbf{q} + \rho\, r\,, \\
\text{entropy :} \quad & \rho\, \dot{\eta} &\geq& \; \operatorname{div} \boldsymbol{\phi}_\eta + \sigma_\eta\,.
\end{aligned}
\tag{3.42}
$$

It should be noted that the m.o.m. equation leads to the symmetry of the *Cauchy* stress tensor $\mathbf{T}$.

3.4.2 Balance Relations of the Constituents

Proceeding from the *Truesdell*'s metaphysical principles and the balance relations for the overall aggregate in the global form (3.40), the balances for the individual constituent φ^α can be introduced as follows

$$
\begin{aligned}
\frac{\mathrm{d}_\alpha}{\mathrm{d}t} \int_{\mathcal{B}} \Psi^\alpha \, \mathrm{d}v &= \int_{\partial\mathcal{B}} (\boldsymbol{\phi}^\alpha \cdot \mathbf{n}) \, \mathrm{d}a + \int_{\mathcal{B}} \sigma^\alpha \, \mathrm{d}v + \int_{\mathcal{B}} \hat{\Psi}^\alpha \, \mathrm{d}v\,, \\
\frac{\mathrm{d}_\alpha}{\mathrm{d}t} \int_{\mathcal{B}} \boldsymbol{\Psi}^\alpha \, \mathrm{d}v &= \int_{\partial\mathcal{B}} (\boldsymbol{\Phi}^\alpha \, \mathbf{n}) \, \mathrm{d}a + \int_{\mathcal{B}} \boldsymbol{\sigma}^\alpha \, \mathrm{d}v + \int_{\mathcal{B}} \hat{\boldsymbol{\Psi}}^\alpha \, \mathrm{d}v\,.
\end{aligned}
\tag{3.43}
$$

Herein, the terms $(\cdot)^\alpha$ have the same physical meaning as the corresponding terms $(\cdot)$ in (3.40).

The local form of the balance relations (3.43) for the individual constituents φ^α, which is derived by differentiation of the left-hand side and transformation of the surface integral on the right-hand side via *Gauss* theorem leads to

$$
\begin{aligned}
(\Psi^\alpha)'_\alpha + \Psi^\alpha \operatorname{div} \overset{\prime}{\mathbf{x}}_\alpha &= \operatorname{div} \boldsymbol{\phi}^\alpha + \sigma^\alpha + \hat{\Psi}^\alpha\,, \\
(\boldsymbol{\Psi}^\alpha)'_\alpha + \boldsymbol{\Psi}^\alpha \operatorname{div} \overset{\prime}{\mathbf{x}}_\alpha &= \operatorname{div} \boldsymbol{\Phi}^\alpha + \boldsymbol{\sigma}^\alpha + \hat{\boldsymbol{\Psi}}^\alpha\,.
\end{aligned}
\tag{3.44}
$$

Again, following *Truesdell*'s principles, the sum over the local balances for all constituents (3.44) should yield the balances of the overall aggregate (3.41). This fact leads to the constraints between the global and the local quantities

$$
\begin{aligned}
\Psi &= \sum_\alpha \Psi^\alpha , & \boldsymbol{\Psi} &= \sum_\alpha \boldsymbol{\Psi}^\alpha ; \\
\boldsymbol{\phi} \cdot \mathbf{n} &= \sum_\alpha [\, \boldsymbol{\phi}^\alpha - \Psi^\alpha \, \mathbf{d}_\alpha \,] \cdot \mathbf{n} , & \boldsymbol{\Phi} \, \mathbf{n} &= \sum_\alpha [\, \boldsymbol{\Phi}^\alpha - \boldsymbol{\Psi}^\alpha \otimes \mathbf{d}_\alpha \,] \, \mathbf{n} ; \\
\sigma &= \sum_\alpha \sigma^\alpha , & \boldsymbol{\sigma} &= \sum_\alpha \boldsymbol{\sigma}^\alpha ; \\
\hat{\Psi} &= \sum_\alpha \hat{\Psi}^\alpha , & \hat{\boldsymbol{\Psi}} &= \sum_\alpha \hat{\boldsymbol{\Psi}}^\alpha .
\end{aligned}
\tag{3.45}
$$

Similar to the balanced quantities presented in Table 3.1, the quantities for (3.44) are summarised and introduced in Table 3.2.

	Ψ^α, $\boldsymbol{\Psi}^\alpha$	$\boldsymbol{\phi}^\alpha$, $\boldsymbol{\Phi}^\alpha$	σ^α, $\boldsymbol{\sigma}^\alpha$	$\hat{\Psi}^\alpha$, $\hat{\boldsymbol{\Psi}}^\alpha$
mass	ρ^α	$\mathbf{0}$	0	$\hat{\rho}^\alpha$
momentum	$\rho^\alpha \, \overset{\prime}{\mathbf{x}}_\alpha$	$\mathbf{T}^\alpha$	$\rho^\alpha \, \mathbf{b}^\alpha$	$\hat{\mathbf{s}}^\alpha$
m.o.m.	$\mathbf{x} \times (\rho^\alpha \, \overset{\prime}{\mathbf{x}}_\alpha)$	$\mathbf{x} \times \mathbf{T}^\alpha$	$\mathbf{x} \times (\rho^\alpha \, \mathbf{b}^\alpha)$	$\hat{\mathbf{h}}^\alpha$
energy	$\rho^\alpha \, \varepsilon^\alpha + \frac{1}{2} \, \overset{\prime}{\mathbf{x}}_\alpha \times (\rho^\alpha \, \overset{\prime}{\mathbf{x}}_\alpha)$	$(\mathbf{T}^\alpha)^T \, \overset{\prime}{\mathbf{x}}_\alpha - \mathbf{q}^\alpha$	$\overset{\prime}{\mathbf{x}}_\alpha \cdot (\rho^\alpha \, \mathbf{b}^\alpha) + \rho^\alpha \, r^\alpha$	$\hat{e}^\alpha$
entropy	$\rho^\alpha \, \eta^\alpha$	$\boldsymbol{\phi}^\alpha_\eta$	σ^α_η	$\hat{\eta}^\alpha$

Table 3.2: Balance relations of the constituents.

Herein, the production terms $\hat{\Psi}^\alpha$ and $\hat{\boldsymbol{\Psi}}^\alpha$ describe the interaction between the constituents φ^α. In particular, $\hat{\rho}^\alpha$ is the mass production term, $\hat{\mathbf{s}}^\alpha$ denotes the total momentum production term and $\hat{\mathbf{h}}^\alpha$ is the total m.o.m production term. The remaining terms $\hat{e}^\alpha$ and $\hat{\eta}^\alpha$ correspondingly describe the total energy and entropy production.

The total production terms are strongly related to the direct terms $\hat{\rho}^\alpha$, $\hat{\mathbf{p}}^\alpha$, $\hat{\mathbf{m}}^\alpha$, $\hat{\varepsilon}^\alpha$, $\hat{\zeta}^\alpha$ as

$$
\begin{aligned}
\hat{\rho}^\alpha &= \hat{\rho}^\alpha , \\
\hat{\mathbf{s}}^\alpha &= \hat{\mathbf{p}}^\alpha + \hat{\rho}^\alpha \, \overset{\prime}{\mathbf{x}}_\alpha , \\
\hat{\mathbf{h}}^\alpha &= \hat{\mathbf{m}}^\alpha + \mathbf{x} \times (\hat{\mathbf{p}}^\alpha + \hat{\rho}^\alpha \, \overset{\prime}{\mathbf{x}}_\alpha) , \\
\hat{e}^\alpha &= \hat{\varepsilon}^\alpha + \hat{\mathbf{p}}^\alpha \cdot \overset{\prime}{\mathbf{x}}_\alpha + \hat{\rho}^\alpha \, (\varepsilon^\alpha + \tfrac{1}{2} \, \overset{\prime}{\mathbf{x}}_\alpha \cdot \overset{\prime}{\mathbf{x}}_\alpha) , \\
\hat{\eta}^\alpha &= \hat{\zeta}^\alpha + \hat{\rho}^\alpha \, \eta^\alpha .
\end{aligned}
\tag{3.46}
$$

It can be seen that the total momentum production term $\hat{\mathbf{s}}^\alpha$ contains the direct production term $\hat{\mathbf{p}}^\alpha$, which results from the interaction force between φ^α and other constituents within the overall medium, and the mass production term $\hat{\rho}^\alpha$. The total m.o.m. production term $\hat{\mathbf{h}}^\alpha$ is represented by the direct production term $\hat{\mathbf{m}}^\alpha$ and an additional production term of angular momentum. The direct energy production term $\hat{\varepsilon}^\alpha$ is a part of the total energy production term $\hat{e}^\alpha$, the same as $\hat{\zeta}^\alpha$ for $\hat{\eta}^\alpha$.

Moreover, there is a possibility to specify *a priori* constitutive assumptions for the constituents φ^α for the entropy efflux $\boldsymbol{\phi}^\alpha_\eta$ and the entropy supply σ^α_η via the absolute Kelvin's temperature θ^α, cf. Ehlers [34],

$$\boldsymbol{\phi}^\alpha_\eta = -\frac{1}{\theta^\alpha}, \quad \sigma^\alpha_\eta = \frac{1}{\theta^\alpha}\,\rho^\alpha\, r^\alpha\,. \tag{3.47}$$

The specific forms of the local balance relations for the constituents can be obtained by inserting the balance quantities from Table 3.2 into the local form of the balance relations (3.45) and read

$$\begin{array}{rrcl}
\text{mass :} & (\rho^\alpha)'_\alpha + \rho^\alpha \operatorname{div} \overset{\prime}{\mathbf{x}}_\alpha & = & \hat{\rho}^\alpha, \\[1ex]
\text{momentum :} & \rho^\alpha\, \overset{\prime\prime}{\mathbf{x}}_\alpha & = & \operatorname{div}\mathbf{T}^\alpha + \rho^\alpha \mathbf{b}^\alpha + \hat{\mathbf{p}}^\alpha\,, \\[1ex]
\text{m.o.m. :} & \mathbf{0} & = & \mathbf{I}\times\mathbf{T}^\alpha + \hat{\mathbf{m}}^\alpha\,, \\[1ex]
\text{energy :} & \rho^\alpha(\varepsilon^\alpha)'_\alpha & = & \mathbf{T}^\alpha\cdot\mathbf{L}_\alpha - \operatorname{div}\mathbf{q}^\alpha + \rho^\alpha\, r^\alpha + \hat{\varepsilon}^\alpha, \\[1ex]
\text{entropy :} & \rho^\alpha(\eta^\alpha)'_\alpha & = & \operatorname{div}\left(-\dfrac{1}{\theta^\alpha}\,\mathbf{q}^\alpha\right) + \dfrac{1}{\theta^\alpha}\,\rho^\alpha\, r^\alpha + \hat{\zeta}^\alpha\,.
\end{array} \tag{3.48}$$

Assuming that the sum of the relations (3.48) over the individual constituents has to result in the balance relations for the single-phase material (3.42), the following constraints are obtained for the total production terms:

$$\sum_\alpha \hat{\rho}^\alpha = 0\,, \quad \sum_\alpha \hat{\mathbf{s}}^\alpha = \mathbf{0}\,, \quad \sum_\alpha \hat{\mathbf{h}}^\alpha = 0\,, \quad \sum_\alpha \hat{e}^\alpha = 0\,, \quad \sum_\alpha \hat{\eta}^\alpha \geq 0\,. \tag{3.49}$$

The restriction $(3.49)_5$ for the entropy production term introduces the second law of thermodynamics.

Finally, considering (3.45), the relations between the quantities of the individual constituents φ^α and overall aggregate φ can be taken into account

$$
\begin{aligned}
\rho\,\mathbf{b} &= \sum_\alpha \rho^\alpha\,\mathbf{b}^\alpha\,,\\
\mathbf{T} &= \sum_\alpha (\mathbf{T}^\alpha - \rho^\alpha\,\mathbf{d}_\alpha \otimes \mathbf{d}_\alpha)\,,\\
\mathbf{q} &= \sum_\alpha [\,\mathbf{q}^\alpha - (\mathbf{T}^\alpha)^T\,\mathbf{d}_\alpha + \rho^\alpha\,\varepsilon^\alpha\,\mathbf{d}_\alpha + \tfrac{1}{2}\,\rho^\alpha\,(\mathbf{d}_\alpha\cdot\mathbf{d}_\alpha)\,\mathbf{d}_\alpha\,]\,,\\
\rho\,\varepsilon &= \sum_\alpha \rho^\alpha\,(\varepsilon^\alpha + \tfrac{1}{2}\,\mathbf{d}_\alpha\cdot\mathbf{d}_\alpha)\,,\\
\rho\,r &= \sum_\alpha \rho^\alpha\,(r^\alpha + \mathbf{b}^\alpha\cdot\mathbf{d}_\alpha)\,,\\
\rho\,\eta &= \sum_\alpha \rho^\alpha\,\eta^\alpha\,.
\end{aligned}
\tag{3.50}
$$

3.4.3 Entropy Principle

In thermodynamics, the entropy principle postulates that the entropy of an isolated system either remains constant or increases, depending on whether the process is reversible or irreversible, cf. Potter & Somerton [85]. In other words, for adiabatic systems the entropy increases until it reaches its maximum. Based on this statement, which has to be fulfilled for any thermodynamical process, the evaluation of the entropy inequality is used to obtain the thermodynamically consistent constitutive relations for the considered problem, cf. Section 4.

Based on the total entropy production term $(3.46)_5$ substituted into the entropy balance $(3.48)_5$ and restriction $(3.49)_5$, the entropy inequality can be obtained in the following form

$$
\sum_\alpha [\,\rho^\alpha\,(\eta^\alpha)'_\alpha + \hat{\rho}^\alpha\,\eta^\alpha + \operatorname{div}(\frac{1}{\theta^\alpha}\,\mathbf{q}^\alpha) - \frac{1}{\theta^\alpha}\,\rho^\alpha\,r^\alpha\,] \geq 0\,. \tag{3.51}
$$

Introducing the *Helmholtz* free energy ψ^α via *Legendre* transformation between the conjugated variables entropy η^α and temperature θ^α, cf. Appendix B,

$$
\psi^\alpha := \varepsilon^\alpha - \theta^\alpha\,\eta^\alpha\,, \tag{3.52}
$$

and by use of the energy balance $(3.48)_4$ as well as the relation $(3.46)_4$, the entropy inequality can be transformed into the *Clausius-Duhem* form

$$
\begin{aligned}
\sum_\alpha \frac{1}{\theta^\alpha}\{\,&\mathbf{T}^\alpha\cdot\mathbf{L}_\alpha - \rho^\alpha\,[\,(\psi^\alpha)'_\alpha + (\theta^\alpha)'_\alpha\,\eta^\alpha\,] - \hat{\mathbf{p}}^\alpha\cdot\overset{\prime}{\mathbf{x}}_\alpha - \\
&- \hat{\rho}^\alpha\,(\psi^\alpha + \tfrac{1}{2}\,\overset{\prime}{\mathbf{x}}_\alpha\cdot\overset{\prime}{\mathbf{x}}_\alpha) - \frac{1}{\theta^\alpha}\,\mathbf{q}^\alpha\cdot\operatorname{grad}\theta^\alpha + \hat{e}^\alpha\} \geq 0\,.
\end{aligned}
\tag{3.53}
$$

It should be noted that in the current work the temperature is assumed to be the same for all constituents $\theta^\alpha = \theta$.

3.5 Thermodynamical Fundamentals

The capture and storage of CO_2 involves a number of complex processes, such as transportation of CO_2, dissolution of CO_2 into water (H_2O) and others. Among various factors, the thermodynamic properties of a substance play an important role in the description of these processes. In this regard, the following section presents the thermodynamical fundamentals required for the current investigation. In particular, various equations of state and their graphical representation by phase diagrams, the definitions of chemical potentials and phase transition process can be found in the following.

3.5.1 Phase Diagram

In order to widen the discussion concerning the phase diagram started in Section 2.2, a more detailed analysis of the relationships between pressure (p), specific volume (v) and temperature (θ) for a pure substance is introduced here. For more comprehensive information, the interested reader is referred to Potter & Somerton [85], Abbott & van Ness [1], Gmehling & Kolbe [52] and others.

The phase diagram for water is taken into consideration as an example. In Figure 3.5, the three-dimensional $p - v - \theta$ surface and the corresponding projections $p - v$ at $\theta =$ const, $\theta - v$ at $p =$ const and $p - \theta$ at $v =$ const are shown. The regions, where only one phase exists, are labelled "solid", "liquid" and "vapour" (or gas). The remaining regions, where two phases coexist simultaneously, are assigned by "solid-liquid" ($S - L$), "solid-vapour" ($S - V$) and "liquid-vapour" ($L - V$). The lines separating the different states of aggregation are called *phase-coexistence* lines, e. g., *vaporisation-condensation*, *sublimation* and *fusion* curves.

Moreover, there are two characteristic points on the phase diagram called *triple* and *critical* point, which play an essential role for the description of the behaviour of a substance. The triple point is known as a point where all phases (solid, liquid, vapour) occur at the same time and it is the starting point for the vaporisation curve. The critical point is the final point of the vaporisation curve and the last point where liquid and vapour phases coexist in equilibrium. In case when the pressures and temperatures exceed the critical values p_{cr} and θ_{cr}, the substance becomes a *supercritical* fluid, cf. Section 2.2.

The vaporisation curve is named the *condensation* curve, if the vaporisation process goes in the opposite direction, i. e. from the critical to the triple point. The *sublimation* curve splits solid and vapour regions, whereas the *fusion* curve separates the solid region from the liquid one.

If one of these phase-coexistence curves is crossed resulting in the changes of the properties (p, θ, v), a *phase change* process occurs. It also causes changes in the internal energy, enthalpy and entropy of the system. As it was mentioned above, a description of the phase change process between CO_2 phases during the injection process is one of the subjects of the current investigation. Therefore, proper description and understanding of this process is required for appropriate modelling. In this respect, a variety of so-called equations of state, which mathematically represent the phase diagram, are discussed in Section 3.5.2.

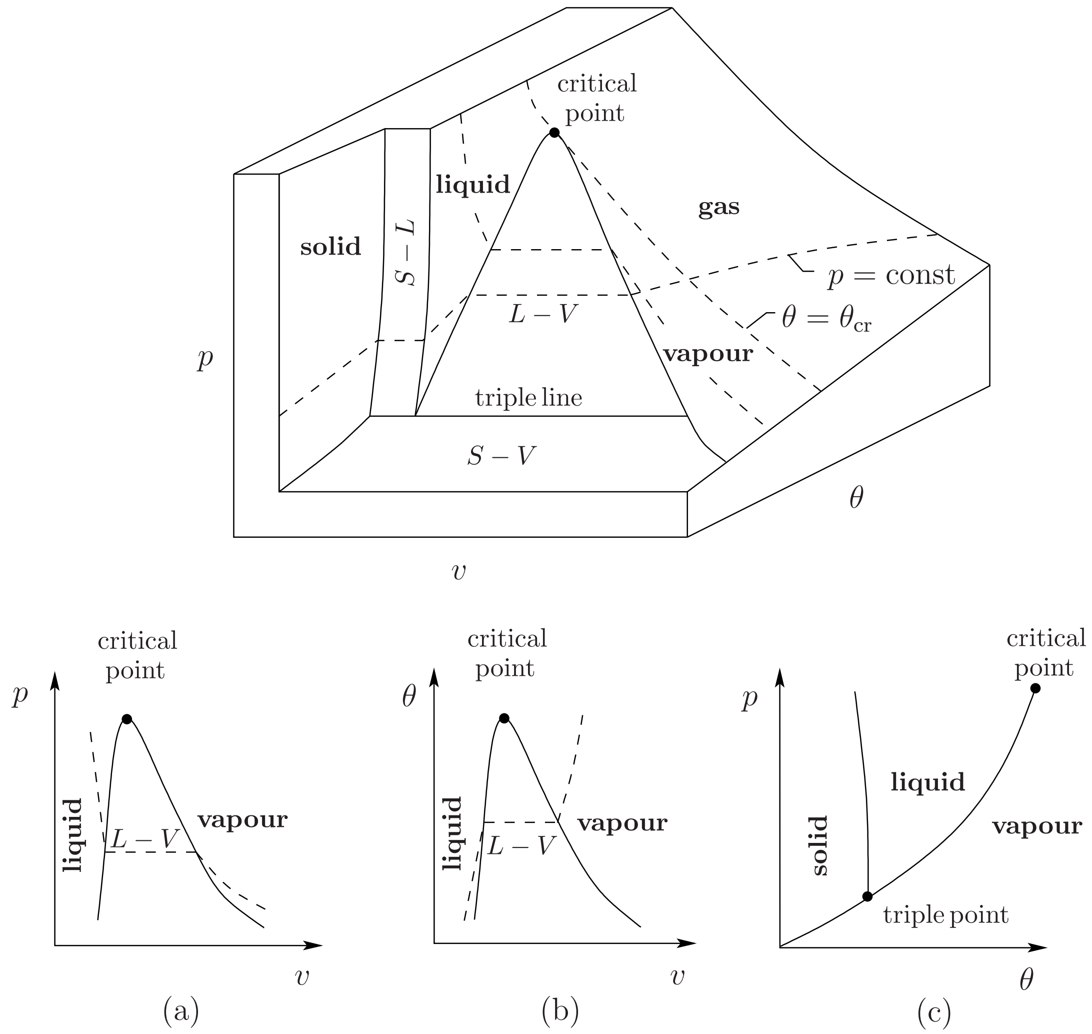

Figure 3.5: 3-d phase diagram for water, (a) $\theta = \text{const}$, (b) $p = \text{const}$, (c) $v = \text{const}$, Potter & Somerton [85].

3.5.2 Equations of State

The equations of state (EOS) are used in order to predict the thermodynamical properties and describe the behaviour of a substance. Numerous EOS developed in the past can be roughly divided into two groups: specialised equations, such as the *Span* and *Wagner* equation, and general equations, like the *van der Waals* equation. The first group consists of very detailed equations having a better accuracy, but with a very specific range of application. For example, the *Span* and *Wagner* equation is applied only for CO_2, cf. Span & Wagner [94]. The second group of the general EOS can be again divided into two classes: equations with a simple structure, such as the *Redlich-Kwong* equation, cf. Redlich & Kwong [88]:

$$p = \frac{R\,\theta}{v - b} - \frac{a}{v\,(v + b)\sqrt{\theta}}\,, \tag{3.54}$$

and equations with a complex structure, such as the *Benedict-Webb-Rubin* equation, cf. Benedict *et al.* [10]:

$$p = R\theta\rho + (B_0 R\theta - A_0 - \frac{C_0}{\theta^2})\rho^2 + (bR\theta - a)\,\rho^3 + a\alpha\rho^6 + \frac{c\rho^2}{\theta^2}\,(1 + \gamma\rho^2)\,e^{-\gamma\rho^2}\,, \quad (3.55)$$

where R is the gas constant, θ is the temperature, v is the specific volume, p is the pressure, ρ is the density and $A_0, B_0, C_0, a, b, c, \alpha, \gamma$ are constants. The equations with a complex structure, such as (3.55), will give better results, but consist of many parameters which are not always available for all substances. The complex structure of these equations makes the calculation procedure more difficult. Therefore, it is preferable to use the first type of equations with a simple structure, such as (3.54), if they produce a reasonable accuracy.

It can be noted that both types of EOS mentioned above are suitable for the description of the behaviour of real gases. In thermodynamics, in order to compare real gases to ideal gas, the compressibility factor Z is used:

$$Z = \frac{p\,v}{R\,\theta}\,. \quad (3.56)$$

For the ideal gas the compressibility factor equals to one ($Z = 1$). The closer the Z value of a real gas is to 1, the closer the physical quantities and behaviour of this real gas are to the ideal gas. Often in literature, the EOS are reformulated in terms of the Z factor.

After the general classification, a proper EOS for CO_2 should be defined. The first choice would be the standard *van der Waals* equation (1873):

$$p = \frac{R\,\theta}{v - b} - \frac{a}{v^2}\,, \quad (3.57)$$

where a, b are constants, R is the gas constant, v is the molar volume (volume of one mole of the substance) and p is the pressure. The disadvantage of using the *van der Waals* equation for CO_2 is that around the critical point this equation yields only a rough agreement with the actual curves. This motivated other researchers to improve and extend the *van der Waals* equation. Thus, *Redlich* and *Knowg* (1949) have developed equation (3.54) and later according to Li *et al.* [67] the constants a, b were modified to obtain a better accuracy for gaseous CO_2 and a mixture of CO_2 and H_2O. Another EOS was proposed by *Peng* and *Robinson* (1976), cf. Peng & Robinson [81]:

$$p = \frac{R\,\theta}{v - b} - \frac{a\,\alpha_\omega}{v^2 + 2\,b\,v - b^2}\,, \quad (3.58)$$

where v is a specific volume, R is the gas constant, a, b are constants depending on the critical pressure p_{cr} and temperature θ_{cr}:

$$\begin{aligned} a &= \frac{0.45724\,R^2\,\theta_{\mathrm{cr}}^2}{p_{\mathrm{cr}}}\,, \\ b &= \frac{0.007780\,R\,\theta_{\mathrm{cr}}}{p_{\mathrm{cr}}}\,, \end{aligned} \quad (3.59)$$

and constant α_ω is a function of the acentric factor ω:

$$\begin{aligned}
\alpha_\omega &= [1 + (0.37464 + 1.54226\,\omega - 0.26992\,\omega^2)\,(1 - \sqrt{\theta_\mathrm{r}})]^2\,, \\
\omega &= -\log_{10}(p_\mathrm{r}^\mathrm{sat}) - 1\,, \\
\theta_\mathrm{r} &= \theta/\theta_\mathrm{cr}\,, \\
p_\mathrm{r}^\mathrm{sat} &= p/p_\mathrm{cr}\,|_{\theta_\mathrm{r}}\,.
\end{aligned} \tag{3.60}$$

In reality, it is often impossible to observe the behaviour of a pure substance, because different parts of a substance (e. g., species, molecules, phases) can interact between with each other. Thus, a mixture of different constituents should be taken into consideration, e. g., a mixture of CO_2 and H_2O. In this case, the EOS has to be modified in order to describe mixtures. For example, the *Peng-Robinson* equation for a mixture of species has a form

$$p = \frac{R\,\theta}{v - b_m} - \frac{a_m\,\alpha_\omega}{v^2 + 2\,b_m\,v - {b_m}^2}\,, \tag{3.61}$$

where a_m is the attractive parameter and b_m is the repulsive parameter of the mixture. These parameters are expressed as functions of the concentration of the different components in the mixture through the mixing rules. Several different mixing rules can be found in literature, for example, in Poling *et al.* [83], Barragán-Aroche & Bazúa-Rueda [7]. For instance, following a simple conventional mixing rule for the i and j components, the coefficients are defined as

$$a_m = \sum x_i\,x_j\,a_{ij}(\theta)\,, \quad b_m = \sum x_i\,b_i\,, \tag{3.62}$$

where x_i represents a molar fraction and

$$\begin{aligned}
a_{ii}(\theta) &= 0.4572236\,(R\,\theta_{\mathrm{cr}_i})^2\,[1 + c_i\,(1 - \sqrt{\theta_{\mathrm{r}_i}})]^2\,/\,p_{\mathrm{cr}_i}\,, \\
a_{ij} &= \sqrt{a_{ii}\,a_{ij}}\,(1 - k_{ij})\,, \\
b_i &= 0.077796\,R\,\theta_{\mathrm{cr}_i}\,/\,p_{\mathrm{cr}_i}\,,
\end{aligned} \tag{3.63}$$

with

$$\begin{aligned}
c_i &= 0.37464 + 1.54226\,\omega_i - 0.26992\,\omega_i^2\,, \\
\theta_{r_i} &= \theta/\theta_{\mathrm{cr}_i}\,.
\end{aligned} \tag{3.64}$$

Herein, ω_i is the acentric factor for species i, k_{ij} is an empirical interaction parameter, which describes the attraction forces between the pairs of non-similar molecules and should be defined by regressing experimental data for each mixture separately, cf. Harstad *et al.* [56], Poling *et al.* [83] and Li & Yan [68].

Based on the fact that in the present investigation the behaviour of pure CO_2 at the supercritical state is under consideration, there is no need to use any mixing rules here.

However, it is possible to extend the model in the future in order to examine a mixture of CO_2 with other components, such as H_2O. For example, a description of the thermodynamical model for the CO_2-water mixture can be found in Eftekhari *et al.* [32] among others.

But still, the most detailed and exact EOS for CO_2 nowadays is the *Span* and *Wagner* equation proposed in the last century and improved in Span *et al.* [95]. The disadvantage of this equation is its very complicated form with a lot of parameters. Therefore, in the current investigation in order to simplify the modelling procedure, the *Peng-Robinson* equation (3.58) is taken into account.

Within the present contribution there is no need to go deeper into the topic about the variety and accuracy of EOS. However, the question about the choice of EOS is a very complex subject of research and has been discussed in depth in the literature by Lewis & Randall [66], Sterner & Pitzer [99], McPherson *et al.* [71], Pappa *et al.* [80] and by many others.

3.5.3 Chemical Potentials and Phase Transition

The chemical potential is an important characteristic of a substance in thermodynamics. In particular, conditions for the phase equilibrium and phase transition process can be properly defined with aid of the chemical potentials. In classical chemical thermodynamics, chemical potential μ for a pure substance is defined as the change of *Gibbs* free energy ξ per change of moles n of a substance at constant temperature θ and pressure p, cf. Ott & Boerio-Goates [78], Abbott & van Ness [1]:

$$\mu = \left(\frac{\mathrm{d}\xi}{\mathrm{d}n}\right)_{\theta,p} . \tag{3.65}$$

A pure substance can contain several phases, which under certain pressure and temperature coexist in equilibrium. Based on the definition given in (3.65), the criterion for a phase equilibrium can be defined. Namely, if two phases of a substance, for example, liquid L and gas G, are at equilibrium, the total *Gibbs* energy for this substance remains constant yielding

$$\mathrm{d}\xi = \mathrm{d}\xi^L + \mathrm{d}\xi^G = 0 . \tag{3.66}$$

Using definition (3.65), the relation (3.66) leads to

$$\mu^L \,\mathrm{d}n^L + \mu^G \,\mathrm{d}n^G = 0 . \tag{3.67}$$

Resulting from the assumption that the system is closed, which means

$$\mathrm{d}n^L = -\,\mathrm{d}n^G , \tag{3.68}$$

(3.67) is reformulated as

$$(\mu^L - \mu^G)\,\mathrm{d}n^G = 0 . \tag{3.69}$$

This leads to the conclusion that two phases are at equilibrium if the chemical potentials of both phases are equal

$$\mu^L = \mu^G . \tag{3.70}$$

Also the opposite statement is valid: if $\mu^L \lessgtr \mu^G$, the phases are not in equilibrium.

Going further, conditions for the phase transition process in terms of the chemical potentials can be defined. It is known that the phase transition occurs at constant pressure and temperature whenever on of the curves (line of equilibrium with $\mu^L = \mu^G$ in Figure 3.6) on phase diagram is crossed, cf. Abbott & van Ness [1]. Crossing of these equilibrium lines results into the changes of the thermodynamical properties except the *Gibbs* energy, which is in agreement with a definition of equilibrium in (3.66).

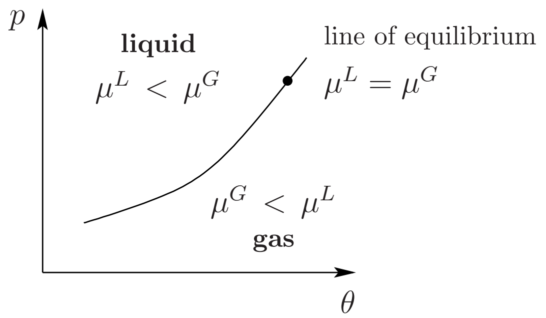

Figure 3.6: Specific region of the phase diagram.

It is also known that the chemical potential drives the flow of mass during the phase transition process, cf. Ott & Boerio-Goates [78]. A direction of the phase transition process between two phases of a pure substance is defined from the phase with a higher chemical potential to the phase with lower potential. For a better understanding a correlation between the phase transition and the chemical potentials, additionally to Figure 3.6, the relation between the chemical potentials and a temperature at a fixed pressure value is shown in Figure 3.7. Therein, θ^{eq} is a temperature at the equilibrium, μ^L and μ^G are the chemical potentials of L and G phases.

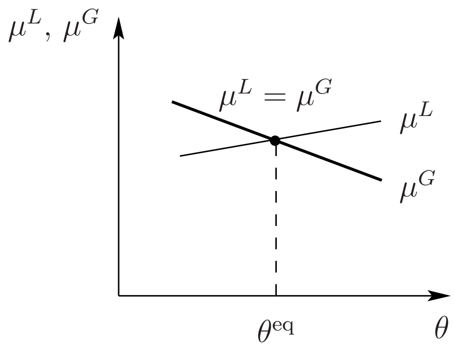

Figure 3.7: Chemical potentials μ^L, μ^G versus temperature θ.

Comparing a dependence of the chemical potentials on the temperature in Figure 3.7 and a region of the phase diagram in Figure 3.6, some relations between μ^L, μ^G, θ and p for the phase change process can be observed. Each point on the line of equilibrium ($\mu^L = \mu^G$) in Figure 3.6 at certain pressure p and temperature θ corresponds to the point of $\theta = \theta^{\mathrm{eq}}$

in Figure 3.7 plotted for the same pressure value p. Moreover, the "liquid" ("gas") region in Figure 3.6, where $\mu^L < \mu^G$ ($\mu^L > \mu^G$), corresponds to the area with $\theta < \theta^{\text{eq}}$ ($\theta > \theta^{\text{eq}}$) in Figure 3.7. In this regard, two types of the phase transition processes with respect to the relation between chemical potentials can be distinguished: a spontaneous phase transition process, if $\mu^L \lesseqgtr \mu^G$, and the phase transition at the so-called coexistence area, where $\mu^L = \mu^G$. The coexistence area is the area, where two phases are in the thermodynamical equilibrium (line of equilibrium in Figure 3.6). The phase transition process in the coexistence area is possible only if some heating is applied to the system or removed from the system. The spontaneous phase transition process takes place when $\mu^L \lesseqgtr \mu^G$ and is not required an additional heating.

In order to be clear about the relation between the phase transition and chemical potentials, a water boiling process is explained here in detail based on Figure 3.7 and Figure 3.6. Boiling, or in other words a water vaporisation, means the phase transition between water (L) and vapour (G). Using the notation from Figure 3.7, the chemical potential μ^L is assigned to the water and μ^G to the vapour. The beginning of the boiling process is referred to the region, where $\theta < \theta^{\text{eq}}$ and $\mu^L < \mu^G$. Further, applying a heating to the system, the process approaches to the equilibrium point $\theta = \theta^{\text{eq}}$. Once the boiling temperature of 100^oC, which is also an equilibrium temperature, under constant atmospheric pressure is reached, the phase transition process starts. The temperature of water stays so long constant until there is no more water left for the vaporisation, which corresponds to the point on the line of equilibrium in Figure 3.6 and also to the point θ^{eq} in Figure 3.7. Afterwards, the temperature can be further increased, which relates to the area with $\theta > \theta^{\text{eq}}$ in Figure 3.7.

In the present contribution, the chemical potential of a CO_2 component existing in two different phases, supercritical L and gaseous G, is defined via different variables than in (3.65). Namely, the relation between the *Helmholtz* energy ψ^β, pressure p^β and specific volume ν^β with $\beta \in \{L, G\}$ gives the chemical potential and reads

$$\mu^\beta = \psi^\beta + p^\beta \nu^\beta . \tag{3.71}$$

All statements discussed above are valid and used further for the definition an appropriate switching criterion for the phase transition process. In detail, this question is discussed in Section 5.2.1.

Chapter 4: Constitutive Modelling

In this chapter, the constitutive modelling procedure for the different formulations of the CO_2 injection problem regarding the number of phases and components within the multiphasic model is considered. To describe the difference between the approaches, the definition of *phase* and *component* of a media should be given. A *phase* is a homogeneous region in a system or, in other words, a quantity of matter which has the same chemical structure everywhere in a system, cf. Potter & Somerton [85]. In general, a substance may exist in solid, liquid, gaseous or even in supercritical phase. It is assumed that in a multiphasic system the phases are separated by sharp interfaces, otherwise if the phases are considered as a whole, it is called *mixture*. A *component* can be defined as an independent substance, for instance, a chemical element or molecular substance, cf. Helmig [57]. In the current work, all balance and constitutive relations are introduced for each phase separately.

4.1 Alternative Modelling Approaches

Two approaches are chosen to model the problem of CO_2 injection into an aquifer: a three-phases-three-components and a four-phases-three-components model. Both models consist of three identical components, i. e. solid, water and CO_2, and two identical phases, namely, a solid phase, represented by the rock within the porous medium, and a liquid phase, represented by the water in the aquifer. The difference between the formulations is given by the description of the CO_2 component. In the frame of the first formulation, CO_2 occurs only in the supercritical state without any phase transition, while the second formulation includes phase transition with the possibility for the CO_2 to be divided into gaseous and supercritical phases. In this context, the following notations for the phases are chosen: solid is denoted by S, liquid (water) by W, supercritical CO_2 by L and gaseous CO_2 by G. Moreover, within the current work, it is assumed that the first modelling approach corresponds to the *ideal* scenario of the CO_2 injection (model I), whereas the second approach represents the *critical* scenario (model II). Schematically, these scenarios are illustrated in Figure 4.1.

Before going into details about the modelling procedure, some general simplifications are performed. It is assumed that both models consist of a materially incompressible solid skeleton (rock) with $\rho^{SR} = \text{const}$, a materially incompressible liquid phase (water) with $\rho^{WR} = \text{const}$ and a materially compressible CO_2 in any phase, $\rho^{LR}, \rho^{GR} \neq \text{const}$. In the frame of the first formulation (model I), there is no mass exchange between the constituents ($\hat{\rho}^\alpha = 0$), whereas for the model II: $\hat{\rho}^L \neq 0$, $\hat{\rho}^G \neq 0$. Moreover, all processes have a quasi-static behaviour, which means that $\overset{\prime\prime}{\mathbf{x}}_\alpha \equiv 0$; the body forces for all constituents

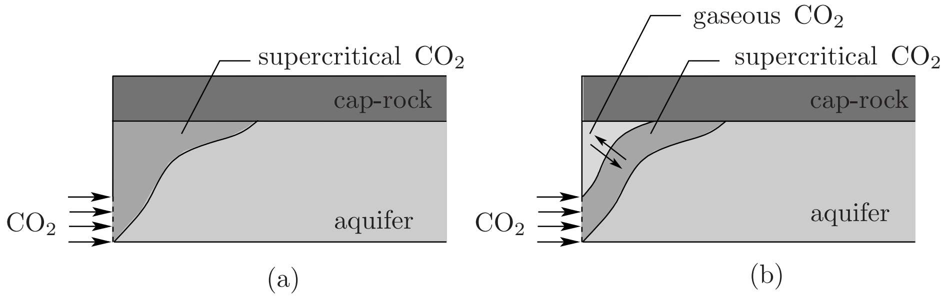

Figure 4.1: Alternative modelling approaches: (a) ideal scenario, (b) critical scenario.

are reduced to gravitation $\mathbf{b}^\alpha = \mathbf{g}$; there are no external fluxes $r^\alpha = 0$ into the system and all constituents have the same temperature $\theta^\alpha = \theta$.

To summarise, the model I corresponding to the ideal scenario is a model with three-phases-three-components $\alpha \in \{S,\, W,\, G\}$, where there are no mass production terms ($\hat{\rho}^S = 0,\ \hat{\rho}^W = 0,\ \hat{\rho}^G = 0$) and the primary variables are $\mathbf{u}_S,\ p^{WR},\ p^{LR},\ \theta$. The model II representing the critical scenario is the model with four-phases-three-components $\alpha \in \{S,\, W,\, G,\, L\}$, which includes the mass production terms for the CO_2 phases ($\hat{\rho}^S = 0$, $\hat{\rho}^W = 0,\ \hat{\rho}^L = -\hat{\rho}^G$) and the primary variables are $\mathbf{u}_S,\ p^{WR},\ p^{LR},\ p^{GR},\ \theta$.

According to the balance equations presented in (3.48), the system of the governing balance relations for model I with respect to the primary variables leads to the momentum balance for the overall aggregate $(4.1)_1$, the mass balances for water $(4.1)_2$ and the supercritical CO_2 $(4.1)_3$ and, finally, the energy balance for the overall aggregate $(4.1)_4$, $\alpha \in \{S, W, L\}$:

$$
\begin{aligned}
\mathbf{0} &= \sum_\alpha \{\operatorname{div} \mathbf{T}^\alpha + \rho^\alpha \mathbf{g} + \hat{\mathbf{p}}^\alpha\}\,,\\
(\rho^W)'_W + \rho^W \operatorname{div} \overset{\prime}{\mathbf{x}}_W &= 0\,,\\
(\rho^L)'_L + \rho^L \operatorname{div} \overset{\prime}{\mathbf{x}}_L &= 0\,,\\
\sum_\alpha \rho^\alpha (\varepsilon^\alpha)'_\alpha &= \sum_\alpha \{\mathbf{T}^\alpha \cdot \mathbf{L}_\alpha - \operatorname{div} \mathbf{q}^\alpha + \hat{\varepsilon}^\alpha\}\,.
\end{aligned}
\tag{4.1}
$$

The total momentum and energy production terms are defined by (3.49) and in this particular case read

$$
\begin{aligned}
\sum_\alpha \hat{\mathbf{s}}^\alpha &= \sum_\alpha \hat{\mathbf{p}}^\alpha = 0\,,\\
\sum_\alpha \hat{e}^\alpha &= \sum_\alpha \{\hat{\varepsilon}^\alpha + \hat{\mathbf{p}}^\alpha \cdot \overset{\prime}{\mathbf{x}}_\alpha\} = 0\,.
\end{aligned}
\tag{4.2}
$$

The system of the governing balance relations for model II with $\alpha \in \{S, W, L, G\}$ consists of the momentum balance for the overall aggregate $(4.3)_1$, the mass balances for water $(4.3)_2$, the supercritical CO_2 $(4.3)_3$ and the gaseous CO_2 $(4.3)_4$ and the energy balance for the overall aggregate $(4.3)_5$:

$$
\begin{aligned}
\mathbf{0} &= \sum_\alpha \{\operatorname{div} \mathbf{T}^\alpha + \rho^\alpha \mathbf{g} + \hat{\mathbf{p}}^\alpha\}\,, \\
(\rho^W)'_W + \rho^W \operatorname{div} \overset{\prime}{\mathbf{x}}_W &= 0\,, \\
(\rho^L)'_L + \rho^L \operatorname{div} \overset{\prime}{\mathbf{x}}_L &= \hat{\rho}^L\,, \\
(\rho^G)'_G + \rho^G \operatorname{div} \overset{\prime}{\mathbf{x}}_G &= \hat{\rho}^G\,, \\
\sum_\alpha \rho^\alpha (\varepsilon^\alpha)'_\alpha &= \sum_\alpha \{\mathbf{T}^\alpha \cdot \mathbf{L}_\alpha - \operatorname{div} \mathbf{q}^\alpha + \hat{\varepsilon}^\alpha\}\,.
\end{aligned}
\tag{4.3}
$$

In this case, the total mass, momentum and energy production terms yield

$$
\begin{aligned}
\sum_\alpha \hat{\rho}^\alpha &= \hat{\rho}^G + \hat{\rho}^L = 0, \\
\sum_\alpha \hat{\mathbf{s}}^\alpha &= \sum_\alpha \{\hat{\mathbf{p}}^\alpha + \hat{\rho}^\alpha \overset{\prime}{\mathbf{x}}_\alpha\} = 0, \\
\sum_\alpha \hat{e}^\alpha &= \sum_\alpha \{\hat{\varepsilon}^\alpha + \hat{\mathbf{p}}^\alpha \cdot \overset{\prime}{\mathbf{x}}_\alpha + \hat{\rho}^\alpha (\varepsilon^\alpha + \tfrac{1}{2} \overset{\prime}{\mathbf{x}}_\alpha \cdot \overset{\prime}{\mathbf{x}}_\alpha)\} = 0.
\end{aligned}
\tag{4.4}
$$

Except the primary variables, which are obtained by solving the system of the governing balance equations (4.1) and (4.3), there are also other unknowns named constitutive variables, which have to be defined by constitutive relations. Before performing this task, the constitutive variables themselves are identified in Section 4.2.

4.2 Identification of the Constitutive Variables

In general, all constitutive variables could be split into several categories, which are restricted here to two sets of fundamental $\mathcal{V}$ and response $\mathcal{R}$ constitutive variables. Wherein, each variable from the response set $\mathcal{R}$ is defined as a function of the variables from the fundamental set $\mathcal{V}$.

According to Ehlers [34], the fundamental set of constitutive variables for the general case, where the multiphasic system consists of a single solid skeleton percolated by several fluids, reads

$$
\begin{aligned}
\mathcal{V}(\mathbf{x}, t) = \{\theta^\alpha, \operatorname{grad}\theta^\alpha,\ & n^\alpha, \operatorname{grad} n^\alpha, \rho^{\alpha R}, \operatorname{grad}\rho^{\alpha R}, \\
& \mathbf{F}_\alpha, \operatorname{Grad}_\alpha \mathbf{F}_\alpha, \overset{\prime}{\mathbf{x}}_\alpha, \operatorname{Grad}_\alpha \overset{\prime}{\mathbf{x}}_\alpha, \mathbf{X}_\alpha\}\,.
\end{aligned}
\tag{4.5}
$$

This set of variables includes the temperature θ^α describing the thermal state of the constituents φ^α. The volume fraction n^α, real density $\rho^{\alpha R}$ and deformation gradient $\mathbf{F}^\alpha$ as well as their gradients define the deformation of the constituents. The remaining variables, $\overset{\prime}{\mathbf{x}}_\alpha$ and $\operatorname{Grad}_\alpha \overset{\prime}{\mathbf{x}}_\alpha$, are used in order to describe the viscosity effect and $\mathbf{X}_\alpha$ is needed to describe possible inhomogeneities of the individual constituents. The fundamental set $\mathcal{V}$

can be also extended, in case it is necessary to describe some particular behaviour of the system, for example visco-elastic behaviour of the solid skeleton.

Based on the fundamental set of the constitutive variables and the relations for the *Helmholtz* energy $\psi^\alpha = \varepsilon^\alpha - \theta^\alpha \eta^\alpha$ and the density $\rho^\alpha = n^\alpha \rho^{\alpha R}$, the unknown response set of the constitutive variables $\mathcal{R}$ can be defined as

$$\mathcal{R}\,[\mathcal{V}\,(\mathbf{x},\,t)] = \{\mathbf{T}^\alpha,\,\mathbf{q}^\alpha,\,\psi^\alpha,\eta^\alpha,\,\hat{\mathbf{p}}^\alpha,\,\hat{\varepsilon}^\alpha,\,\hat{\rho}^\alpha\}\,. \tag{4.6}$$

Using the effective quantities of the constituents, which are discussed in detail in Section 4.3 and Graf [53], the set of constitutive variables $\mathcal{V}$ can be reduced to specific set $\mathcal{S}$ of variables:

$$\mathcal{S} \;=\; \{\theta^\alpha,\,\mathrm{grad}\,\theta^\alpha,\,s^\beta,\,\mathrm{grad}\,s^\beta,\,\rho^{\beta R},\,\mathrm{grad}\,\rho^{\beta R},\,\mathbf{F}_S,\,\mathrm{Grad}_S\,\mathbf{F}_S\,,\mathbf{w}_\beta\,\}. \tag{4.7}$$

Further, according to the works by Truesdell & Noll [101], Ehlers [34, 37], based on the *principles of determinism*, *local action*, *equipresence*, *frame indifference* and *dissipation*, the functions defined in the response set $\mathcal{R}$ can depend on the variables given in $\mathcal{S}$: $\mathcal{R} = \mathcal{R}[\mathcal{S}]$. Moreover, this specific set of the constitutive variables in (4.7) can be reduced to a minimum number of variables for each response function separately depending on the material behaviour.

4.3 Evaluation of the Entropy Inequality

The evaluation of the entropy inequality in order to obtain the constitutive equations was first applied by Coleman & Noll [27] to single-phasic materials. Here, the entropy inequality is separately evaluated for both considered models, model I (ideal scenario) and model II (critical scenario). Firstly, model I is represented, where no mass transfer is included into the modelling, and CO_2 exists only in one state. Secondly, the entropy inequality for model II is introduced, where CO_2 can occur in two different phases and the phase transition process between these phases is considered. Moreover, since model II includes three fluid phases, there are several possibilities to perform the capillary pressure-saturation relation between these phases, cf. Class [25]. Here, it is assumed that there are two capillary pressures: between water and supercritical CO_2 and between supercritical and gaseous phases of CO_2. The definition of the capillary pressure itself and the capillary pressure-saturation relations are given in Section 4.5.

4.3.1 Model I: Ideal Scenario

Taking into account that the mass production terms are zero ($\hat{\rho}^\alpha = 0$), the entropy inequality (3.53) is reformulated as

$$\begin{aligned}\sum_\alpha \frac{1}{\theta^\alpha}\,\{\,\mathbf{T}^\alpha\cdot\mathbf{L}_\alpha \,-\, \rho^\alpha\,[\,(\psi^\alpha)'_\alpha \,+\, (\theta^\alpha)'_\alpha\,\eta^\alpha\,] \,-\, \hat{\mathbf{p}}^\alpha\cdot\overset{\prime}{\mathbf{x}}_\alpha \,-\\ -\,\frac{1}{\theta^\alpha}\,\mathbf{q}^\alpha\cdot\mathrm{grad}\,\theta^\alpha \,+\, \hat{e}^\alpha\} \,\geq\, 0\,,\end{aligned} \tag{4.8}$$

where $\alpha \in \{S, W, L\}$. Multiplying (4.8) by $\theta^\alpha = \theta$ and inserting the constraints (4.2), the entropy inequality leads to

$$\sum_\alpha \{ \mathbf{T}^\alpha \cdot \mathbf{L}_\alpha - \rho^\alpha \, [\, (\psi^\alpha)'_\alpha + \theta'_\alpha \, \eta^\alpha \,] - \frac{1}{\theta} \, \mathbf{q}^\alpha \cdot \operatorname{grad} \theta + \hat{\varepsilon}^\alpha \} \geq 0 \, . \tag{4.9}$$

As a further constraint, the saturation condition (3.5) has to be fulfilled. For this reason, the time derivative of the saturation constraint with respect to the solid skeleton is taken and yields

$$(n^S)'_S + (n^W)'_S + (n^L)'_S = 0 \, . \tag{4.10}$$

Therein, the derivatives of the individual volume fractions are obtained from the corresponding mass balances in the following form:

$$\begin{aligned}
(n^S)'_S &= \frac{1}{\rho^{SR}} \, (- n^S \, (\rho^{SR})'_S - n^S \, \rho^{SR} \operatorname{div} \overset{\prime}{\mathbf{x}}_S) \, , \\
(n^W)'_S &= \frac{1}{\rho^{WR}} \, (- n^W \, (\rho^{WR})'_W - n^W \, \rho^{WR} \operatorname{div} \overset{\prime}{\mathbf{x}}_W) - \operatorname{grad} n^W \cdot \mathbf{w}_W \, , \\
(n^L)'_S &= \frac{1}{\rho^{LR}} \, (- n^L \, (\rho^{LR})'_L - n^L \, \rho^{LR} \operatorname{div} \overset{\prime}{\mathbf{x}}_L) - \operatorname{grad} n^L \cdot \mathbf{w}_L \, .
\end{aligned} \tag{4.11}$$

The effective densities of the solid skeleton ρ^{SR} and water ρ^{WR} depend only on the temperature θ, because of their predetermination as materially incompressible constituents, whereas the effective density ρ^{LR} of CO_2 depends on the temperature θ and the pressure p^{LR}:

$$\begin{aligned}
\rho^{SR} &= \rho^{SR}(\theta) & \longrightarrow \quad (\rho^{SR})'_S &= \frac{\mathrm{d}\rho^{SR}}{\mathrm{d}\theta} \, \theta'_S \, , \\
\rho^{WR} &= \rho^{WR}(\theta) & \longrightarrow \quad (\rho^{WR})'_W &= \frac{\mathrm{d}\rho^{WR}}{\mathrm{d}\theta} \, \theta'_W \, , \\
\rho^{LR} &= \rho^{LR}(\theta, \, p^{LR}) & \longrightarrow \quad (\rho^{LR})'_L &= \frac{\partial\rho^{LR}}{\partial\theta} \, \theta'_L + \frac{\partial\rho^{LR}}{\partial p^{LR}} \, (p^{LR})'_L \, .
\end{aligned} \tag{4.12}$$

Relations (4.11), (4.12) are inserted into the saturation condition (4.10). Then, this condition is weighted by the *Lagrange*an multiplier Λ and added to the entropy inequality (4.9), which finally leads to the form

$$\begin{aligned}
& (\mathbf{T}^S + \Lambda \, n^S \, \mathbf{I}) \cdot \mathbf{L}_S + \theta'_S \, (-\rho^S \, \eta^S + \Lambda \, \frac{n^S}{\rho^{SR}} \, \frac{\mathrm{d}\rho^{SR}}{\mathrm{d}\theta}) - \rho^S \, (\psi^S)'_S + \\
& + (\mathbf{T}^W + \Lambda \, n^W \, \mathbf{I}) \cdot \mathbf{L}_W + \theta'_W \, (-\rho^W \, \eta^W + \Lambda \, \frac{n^W}{\rho^{WR}} \, \frac{\mathrm{d}\rho^{WR}}{\mathrm{d}\theta}) - \rho^W \, (\psi^W)'_W + \\
& + (\mathbf{T}^L + \Lambda \, n^L \, \mathbf{I}) \cdot \mathbf{L}_L + \theta'_L \, (-\rho^L \, \eta^L) - \rho^L \, (\psi^L)'_L + \Lambda \, \frac{n^L}{\rho^{LR}} \, (\rho^{LR})'_L + \\
& + \Lambda \operatorname{grad} n^W \cdot \mathbf{w}_W + \Lambda \operatorname{grad} n^L \cdot \mathbf{w}_L - \frac{1}{\theta} \, \mathbf{q} \cdot \operatorname{grad}\theta + \hat{\varepsilon}^S + \hat{\varepsilon}^W + \hat{\varepsilon}^L \geq 0 \, .
\end{aligned} \tag{4.13}$$

Therein, $\mathbf{q}$ denotes the heat influx for the overall aggregate. It is obtained by a summation of the heat fluxes over the individual constituents and reads

$$\mathbf{q} = \mathbf{q}^S + \mathbf{q}^W + \mathbf{q}^L . \tag{4.14}$$

The energy production terms for the fluid constituents $\hat{\varepsilon}^W$, $\hat{\varepsilon}^L$ describe the energy exchange between the constituents in case of different temperatures of the constituents. According to Graf [53] and Ghadiani [51], they can be defined as

$$\begin{aligned} \hat{\varepsilon}^W &= k^{\varepsilon}_{\theta W}\,(\theta^S - \theta^W) \;+\; k^{\varepsilon}_{\theta W}\,(\theta^L - \theta^W)\,, \\ \hat{\varepsilon}^L &= k^{\varepsilon}_{\theta L}\,(\theta^S - \theta^L) \;+\; k^{\varepsilon}_{\theta L}\,(\theta^W - \theta^L)\,, \end{aligned} \tag{4.15}$$

where $k^{\varepsilon}_{\theta W}$ and $k^{\varepsilon}_{\theta L}$ are the heat exchange coefficients. However, in the current investigation, $\hat{\varepsilon}^W$, $\hat{\varepsilon}^L$ disappear, because the temperatures of the constituents are the same in (4.15), the energy production $\hat{\varepsilon}^S$ for the solid constituent is derived from (4.2) via the momentum production terms and reads

$$\hat{\varepsilon}^S = -\,\hat{\mathbf{p}}^W \cdot \mathbf{w}_W - \hat{\mathbf{p}}^L \cdot \mathbf{w}_L . \tag{4.16}$$

Going further, the free *Helmholtz* energies ψ^α have to be specified. Proceeding from the principle of constituent separation, cf. Ehlers [33], postulating that ψ^α depends only on the variables from the set (4.7) of the corresponding constituent φ^α, the free energies lead to

$$\begin{aligned} \psi^S &= \psi^S(\theta,\,\mathbf{F}_S) &\longrightarrow\quad (\psi^S)'_S &= \frac{\partial \psi^S}{\partial \theta}\,\theta'_S + \frac{\partial \psi^S}{\partial \mathbf{F}_S}\,\mathbf{F}_S^T \cdot \mathbf{L}_S\,, \\ \psi^W &= \psi^W(\theta,\,s^W) &\longrightarrow\quad (\psi^W)'_W &= \frac{\partial \psi^W}{\partial \theta}\,\theta'_W + \frac{\partial \psi^W}{\partial s^W}\,(s^W)'_W\,, \\ \psi^L &= \psi^L(\theta,\,\rho^{LR}) &\longrightarrow\quad (\psi^L)'_L &= \frac{\partial \psi^L}{\partial \theta}\,\theta'_L + \frac{\partial \psi^L}{\partial \rho^{LR}}\,(\rho^{LR})'_L\,. \end{aligned} \tag{4.17}$$

The exact form of the *Helmholtz* energies will be discussed in Section 4.4 and Section 4.5. The term $(s^W)'_W$, which is needed to derive $(\psi^W)'_W$, is obtained from the definition of the saturation function

$$(s^W)'_W = \frac{1}{n^F}\,[\,(n^W)'_W - s^W\,(n^F)'_W\,]\,, \tag{4.18}$$

where $(n^W)'_W$ and $(n^F)'_W$ are evaluated using the mass balances. Thus,

$$\begin{aligned} (s^W)'_W = -\frac{1}{n^F}\Big[&\frac{n^W}{\rho^{WR}}\frac{\mathrm{d}\rho^{WR}}{\mathrm{d}\theta}\,\theta'_W + n^W\,\mathbf{L}_W\cdot\mathbf{I} + s^W\,\frac{n^S}{\rho^{SR}}\frac{\mathrm{d}\rho^{SR}}{\mathrm{d}\theta}\,\theta'_S + \\ &+ s^W\,n^S\,\mathbf{L}_S\cdot\mathbf{I} + s^W\,\mathrm{grad}\,n^F\cdot\mathbf{w}_W\Big]\,. \end{aligned} \tag{4.19}$$

Incorporating the free energies from (4.17) with use of (4.19), the entropy inequality transforms into

$$
\begin{aligned}
&(\underbrace{\mathbf{T}^S + \Lambda\, n^S\, \mathbf{I}}_{\mathbf{T}^S_E} + n^S\,(s^W)^2\,\rho^{WR}\,\frac{\partial\psi^W}{\partial s^W}\,\mathbf{I} - \rho^S\,\frac{\partial\psi^S}{\partial\mathbf{F}_S}\,\mathbf{F}^T_S\,)\cdot\mathbf{L}_S + \\
&+ (\,\underbrace{\mathbf{T}^W + \Lambda\, n^W\,\mathbf{I}}_{\mathbf{T}^W_E} + n^W\,s^W\,\rho^{WR}\,\frac{\partial\psi^W}{\partial s^W}\,\mathbf{I}\,)\cdot\mathbf{L}_W + (\,\underbrace{\mathbf{T}^L + \Lambda\, n^L\,\mathbf{I}}_{\mathbf{T}^L_E})\cdot\mathbf{L}_L - \\
&- \rho^S\,\theta'_S\,(\,\underbrace{\eta^S - \Lambda\,\frac{1}{(\rho^{SR})^2}\,\frac{\mathrm{d}\rho^{SR}}{\mathrm{d}\theta}}_{\eta^S_E} - \frac{(s^W)^2\rho^{WR}}{(\rho^{SR})^2}\,\frac{\mathrm{d}\rho^{SR}}{\mathrm{d}\theta}\,\frac{\partial\psi^W}{\partial s^W} + \frac{\partial\psi^S}{\partial\theta}) - \\
&- \rho^W\,\theta'_W\,(\,\underbrace{\eta^W - \Lambda\,\frac{1}{(\rho^{WR})^2}\,\frac{\mathrm{d}\rho^{WR}}{\mathrm{d}\theta}}_{\eta^W_E} - \frac{s^W}{\rho^{WR}}\,\frac{\mathrm{d}\rho^{WR}}{\mathrm{d}\theta}\,\frac{\partial\psi^W}{\partial s^W} + \frac{\partial\psi^W}{\partial\theta}) - \\
&- \rho^L\,\theta'_L\,(\,\eta^L + \frac{\partial\psi^L}{\partial\theta}) + (\rho^{LR})'_L\,(\Lambda\,\frac{n^L}{\rho^{LR}} - \rho^L\,\frac{\partial\psi^L}{\partial\rho^{LR}}) - \\
&- (\,\underbrace{\hat{p}^W - \Lambda\,\mathrm{grad}\,n^W}_{\hat{p}^W_E} - (s^W)^2\,\rho^{WR}\,\frac{\partial\psi^W}{\partial s^W}\,\mathrm{grad}\,n^F)\cdot\mathbf{w}_W - \\
&- (\underbrace{\hat{p}^L - \Lambda\,\mathrm{grad}\,n^L}_{\hat{p}^L_E})\cdot\mathbf{w}_L - \frac{1}{\theta}\,\mathbf{q}\cdot\mathrm{grad}\theta \ \geq\ 0\,.
\end{aligned}
\tag{4.20}
$$

Herein, $\mathbf{T}^\alpha_E$ with $\alpha \in \{S,\, W,\, L\}$ account for the so-called extra stresses, η^S_E, η^W_E represent the extra entropies and $\hat{p}^\beta_E$ with $\beta \in \{W,\, L\}$ are the extra momentum production terms:

$$
\begin{aligned}
\mathbf{T}^\alpha_E &= \mathbf{T}^\alpha + \Lambda\, n^\alpha\,\mathbf{I}\,,\\
\eta^S_E &= \eta^S - \Lambda\,\frac{1}{(\rho^{SR})^2}\,\frac{\mathrm{d}\rho^{SR}}{\mathrm{d}\theta}\,,\\
\eta^W_E &= \eta^W - \Lambda\,\frac{1}{(\rho^{WR})^2}\,\frac{\mathrm{d}\rho^{WR}}{\mathrm{d}\theta}\,,\\
\hat{p}^\beta_E &= \hat{p}^\beta - \Lambda\,\mathrm{grad}\,n^\beta\,.
\end{aligned}
\tag{4.21}
$$

According to the principles of evaluation of the entropy inequality presented in Ehlers [34], the expressions in front of the free parameters $\mathbf{L}_S$, θ'_α, $(\rho^{LR})'_L$ with arbitrary values, have to vanish in order to fulfil the inequality. This leads to the following constraints for the mechanical extra stress $\mathbf{T}^S_{E\,\mathrm{mech}}$, cf. Graf [53],

$$
\mathbf{T}^S_{E\,\mathrm{mech}} = \mathbf{T}^S_E + n^S\,(s^W)^2\,\rho^{WR}\,\frac{\partial\psi^W}{\partial s^W} = \rho^S\,\frac{\partial\psi^S}{\partial\mathbf{F}_S}\,\mathbf{F}^T_S\,, \tag{4.22}
$$

and for the mechanical extra entropies $\eta^S_{E\,\mathrm{mech}}$, $\eta^W_{E\,\mathrm{mech}}$ and η^L:

$$\begin{aligned}
\eta^S_{E\,\mathrm{mech}} &= \eta^S_E - \frac{(s^W)^2\,\rho^{WR}}{(\rho^{SR})^2}\,\frac{\mathrm{d}\rho^{SR}}{\mathrm{d}\theta}\,\frac{\partial\psi^W}{\partial s^W} &&= -\frac{\partial\psi^S}{\partial\theta}\,,\\
\eta^W_{E\,\mathrm{mech}} &= \eta^W_E - \frac{s^W}{\rho^{WR}}\,\frac{\mathrm{d}\rho^{WR}}{\mathrm{d}\theta}\,\frac{\partial\psi^W}{\partial s^W} &&= -\frac{\partial\psi^W}{\partial\theta}\,,\\
\eta^L &= -\frac{\partial\psi^L}{\partial\theta}\,.
\end{aligned} \tag{4.23}$$

The *Lagrange*an multiplier Λ is obtained from the coefficient in front of $(\rho^{LR})'_L$ in (4.20) and can be interpreted as the pressure of the corresponding fluid phase:

$$\Lambda = (\rho^{LR})^2\,\frac{\partial\psi^L}{\partial\rho^{LR}} = p^{LR}. \tag{4.24}$$

The remaining terms from the entropy inequality are collected in the dissipation inequality $\mathcal{D}$:

$$\mathcal{D} = -\,\hat{p}^W_{E\,\mathrm{mech}}\cdot\mathbf{w}_W - \hat{p}^L_E\cdot\mathbf{w}_L - \frac{1}{\theta}\,\mathbf{q}\cdot\mathrm{grad}\,\theta \geq 0\,. \tag{4.25}$$

Herein, the extra momentum production terms of the fluid constituents are

$$\begin{aligned}
\hat{p}^W_{E\,\mathrm{mech}} &= \hat{p}^W - \Lambda\,\mathrm{grad}\,n^W - (s^W)^2\,\rho^{WR}\,\frac{\partial\psi^W}{\partial s^W}\,\mathrm{grad}\,n^F\,,\\
\hat{p}^L_E &= \hat{p}^L - \Lambda\,\mathrm{grad}\,n^L\,.
\end{aligned} \tag{4.26}$$

The appropriate constitutive assumptions have to be introduced for $\hat{p}^W_{E\,\mathrm{mech}}$, $\hat{p}^L_E$ and $\mathbf{q}$ in order to fulfil the dissipation inequality $\mathcal{D}$ such that it has a positive value. In this context, following the argumentation in Acartürk [2], Graf [53] and Markert [69], the momentum production terms for the isotropic material yield

$$\hat{p}^W_{E\,\mathrm{mech}} = -\,(n^W)^2\,\gamma^{WR}(\mathbf{K}^W_r)^{-1}\,\mathbf{w}_W \quad \text{and} \quad \hat{p}^L_E = -\,(n^L)^2\,\gamma^{LR}(\mathbf{K}^L_r)^{-1}\,\mathbf{w}_L\,, \tag{4.27}$$

with the coefficients $\mathbf{K}^\beta_r$, $\beta\in\{W,\,L\}$, in the form:

$$\mathbf{K}^\beta_r = k^\beta_r(s^\beta)\mathbf{K}^\beta(n^S)\,,\quad \mathbf{K}^\beta = \frac{\gamma^{\beta R}}{\mu^{\beta R}}\,\mathbf{K}^S\,,\quad \mathbf{K}^S = \left(\frac{1-n^S}{1-n^S_{0S}}\right)^\pi K^S_{0S}\,\mathbf{I}\,. \tag{4.28}$$

Therein, k^W_r is the relative permeability factor depending on the saturation s^β. The *Darcy* permeability $\mathbf{K}^\beta$ is introduced via the solid volume fraction n^S, the shear viscosity $\mu^{\beta R}$ of the considered pore liquid and the specific weight $\gamma^{\beta R} = \rho^{\beta R}\,\mathbf{g}$. $\mathbf{K}^S$ is the so-called intrinsic permeability, where π is a material parameter and K^S_{0S} is an intrinsic permeability in the reference configuration. For more details on this formulation, the interested reader is referred to Eipper [47] and Graf [53].

The heat influx $\mathbf{q}^\alpha$ of the individual constituent is analysed using *Fourier*'s law via the heat conduction tensor $\mathbf{H}^\alpha$:

$$\mathbf{q}^\alpha = -\mathbf{H}^\alpha\,\mathrm{grad}\,\theta\,. \tag{4.29}$$

The sum of the heat influxes over the individual constituents results in the heat influx $\mathbf{q}$ for the overall aggregate, cf. (4.14).

Proceeding from (4.20), (4.22) and (4.23), the relations for the *Cauchy* stress tensors read

$$
\begin{aligned}
\mathbf{T}^S_{E\,\mathrm{mech}} &= \mathbf{T}^S + n^S\,(\underbrace{\Lambda + (s^W)^2\,\rho^{WR}\,\frac{\partial\psi^W}{\partial s^W}}_{\bar{\Lambda}})\,\mathbf{I}\,,\\
\mathbf{T}^W_{E\,\mathrm{mech}} &= \mathbf{T}^W + n^W\,(\underbrace{\Lambda + s^W\,\rho^{WR}\,\frac{\partial\psi^W}{\partial s^W}}_{\bar{\bar{\Lambda}}})\,\mathbf{I}\,,\\
\mathbf{T}^L_E &= \mathbf{T}^L + n^L\,\Lambda\,\mathbf{I}\,.
\end{aligned}
\tag{4.30}
$$

Wherein, the variables $\bar{\Lambda}$, $\bar{\bar{\Lambda}}$ are introduced by the effective pressures p^{WR}, p^{LR} and the pore pressure p^{FR} as follows

$$
\begin{aligned}
\bar{\bar{\Lambda}} &= \Lambda + s^W\,\rho^{WR}\,\frac{\partial\psi^W}{\partial s^W} &= p^{WR}\,,\\
\bar{\Lambda} &= \Lambda + (s^W)^2\,\rho^{WR}\,\frac{\partial\psi^W}{\partial s^W} &= p^{FR}\,.
\end{aligned}
\tag{4.31}
$$

These notations are in agreement with the definition of the pore pressure p^{FR} given usually by *Dalton*'s law:

$$
p^{FR} = s^W\,p^{WR} + s^L\,p^{LR}\,. \tag{4.32}
$$

Moreover, as a consequence of (4.31) and (4.32), the classical definition of the capillary pressure p^C as a difference between the pressures of the non-wetting (CO_2) and wetting (water) phases, cf. Section 4.5,

$$
p^C = p^{LR} - p^{WR}\,, \tag{4.33}
$$

can be reformulated via the free energies and the saturations:

$$
p^C = -s^W\,\rho^{WR}\,\frac{\partial\psi^W}{\partial s^W}\,. \tag{4.34}
$$

According to the arguments discussed in Ehlers *et al.* [45] and Markert [69], the extra stress of the fluid constituents, $\mathbf{T}^W_{E\,\mathrm{mech}}$ and $\mathbf{T}^L_E$, are negligible compared to the mechanical extra momentum production term $\hat{p}^W_{E\,\mathrm{mech}}$ representing the effective drag force. Also it should be noted that by means of $\hat{p}^W_{E\,\mathrm{mech}}$, the fluid viscosity is included into the modelling. Thus, the resulting form of the stress tensors leads to

$$
\begin{aligned}
\mathbf{T}^S &= -n^S\,p^{FR}\,\mathbf{I} + \mathbf{T}^S_{E\,\mathrm{mech}}\,,\\
\mathbf{T}^W &= -n^W\,p^{WR}\,\mathbf{I}\,,\\
\mathbf{T}^L &= -n^L\,p^{LR}\,\mathbf{I}\,.
\end{aligned}
\tag{4.35}
$$

Applying the same procedure as for the stress tensors and using the terms from (4.23) and (4.20), the entropies read

$$\begin{aligned} \eta^S &= \frac{1}{(\rho^{SR})^2}\frac{\mathrm{d}\rho^{SR}}{\mathrm{d}\theta}\,p^{FR} - \frac{\partial\psi^S}{\partial\theta}\,, \\ \eta^W &= \frac{1}{(\rho^{WR})^2}\frac{\mathrm{d}\rho^{WR}}{\mathrm{d}\theta}\,p^{WR} - \frac{\partial\psi^W}{\partial\theta}\,, \\ \eta^L &= -\frac{\partial\psi^L}{\partial\theta}\,. \end{aligned} \tag{4.36}$$

The remaining constitutive relations required to close the system of equations are defined in the Section 4.4 and Section 4.5.

Finally, based on the discussed relations for the stress tensors and production terms and denoting $\rho = \sum_\alpha \rho^\alpha$, the system (4.1) of the governing equations leads to

momentum balance:

$$\operatorname{div}(\mathbf{T}^S_E - p^{FR}\,\mathbf{I}) + \rho\,\mathbf{g} = \mathbf{0}\,, \tag{4.37}$$

mass balances:

$$\begin{aligned} (\rho^W)'_S + \operatorname{div}(\rho^W\,\mathbf{w}_W) + \rho^W \operatorname{div}(\mathbf{u}_S)'_S &= 0\,, \\ (\rho^L)'_S + \operatorname{div}(\rho^L\,\mathbf{w}_L) + \rho^L \operatorname{div}(\mathbf{u}_S)'_S &= 0\,, \end{aligned} \tag{4.38}$$

energy balance:

$$\begin{aligned} &\rho^S(\varepsilon^S)'_S + \rho^W(\varepsilon^W)'_W + \rho^L(\varepsilon^L)'_L - \mathbf{T}^S_E\cdot\mathbf{L}_S + n^S\,p^{FR}\operatorname{div}(\mathbf{u}_S)'_S + \\ &+ n^W\,p^{WR}\operatorname{div}\overset{\prime}{\mathbf{x}}_W + n^L\,p^{LR}\operatorname{div}\overset{\prime}{\mathbf{x}}_L + \operatorname{div}\mathbf{q} + \hat{\mathbf{p}}^W\cdot\mathbf{w}_W + \hat{\mathbf{p}}^L\cdot\mathbf{w}_L = 0\,. \end{aligned} \tag{4.39}$$

4.3.2 Model II: Critical Scenario

For model II the entropy inequality has a form of

$$\begin{aligned} \sum_\alpha \frac{1}{\theta}\,\{\,&\mathbf{T}^\alpha\cdot\mathbf{L}_\alpha - \rho^\alpha\,[\,(\psi^\alpha)'_\alpha + \theta'_\alpha\,\eta^\alpha\,] + \\ &+ \hat{\rho}^\alpha\,(\varepsilon^\alpha - \psi^\alpha) - \frac{1}{\theta}\,\mathbf{q}^\alpha\cdot\operatorname{grad}\theta + \hat{\varepsilon}^\alpha\} \geq 0\,, \end{aligned} \tag{4.40}$$

which results from a substitution of the entropy function in the form $\eta^\alpha = (\varepsilon^\alpha - \psi^\alpha)/\theta^\alpha$ into (3.51) and using the energy balance $(4.3)_5$ with $\theta^\alpha = \theta$, $\alpha \in \{S, W, L, G\}$.

Similar to (4.10), the saturation constraint has to be fulfilled here. Thus,

$$(n^S)'_S + (n^W)'_S + (n^L)'_S + (n^G)'_S = 0\,. \tag{4.41}$$

Herein, the mass production terms are included in the derivatives of $(n^L)'_S$ and $(n^G)'_S$:

$$
\begin{aligned}
(n^S)'_S &= \frac{1}{\rho^{SR}} \, (-n^S \, (\rho^{SR})'_S - n^S \, \rho^{SR} \, \mathrm{div} \, \overset{\prime}{\mathbf{x}}_S) \, , \\
(n^W)'_S &= \frac{1}{\rho^{WR}} \, (-n^W \, (\rho^{WR})'_W - n^W \, \rho^{WR} \, \mathrm{div} \, \overset{\prime}{\mathbf{x}}_W) \quad - \quad \mathrm{grad} \, n^W \cdot \mathbf{w}_W \, , \\
(n^L)'_S &= \frac{1}{\rho^{LR}} \, (\hat{\rho}^L - n^L \, (\rho^{LR})'_L - n^L \, \rho^{LR} \, \mathrm{div} \, \overset{\prime}{\mathbf{x}}_L) \quad - \quad \mathrm{grad} \, n^L \cdot \mathbf{w}_L \, , \\
(n^G)'_S &= \frac{1}{\rho^{GR}} \, (\hat{\rho}^G - n^G \, (\rho^{GR})'_G - n^G \, \rho^{GR} \, \mathrm{div} \, \overset{\prime}{\mathbf{x}}_G) \quad - \quad \mathrm{grad} \, n^G \cdot \mathbf{w}_G \, .
\end{aligned}
\tag{4.42}
$$

The effective densities of the solid skeleton ρ^{SR}, water ρ^{WR} and supercritical CO_2 ρ^{LR} have the same form as in (4.12), whereas the effective density of the gaseous CO_2 ρ^{GR} has to be defined additionally. ρ^{GR} is defined as a function of temperature and pressure analogously to the density ρ^{LR}:

$$
\begin{aligned}
\rho^{SR} &= \rho^{SR}(\theta) & \longrightarrow \quad (\rho^{SR})'_S &= \frac{\mathrm{d}\rho^{SR}}{\mathrm{d}\theta} \, \theta'_S \, , \\
\rho^{WR} &= \rho^{WR}(\theta) & \longrightarrow \quad (\rho^{WR})'_W &= \frac{\mathrm{d}\rho^{WR}}{\mathrm{d}\theta} \, \theta'_W \, , \\
\rho^{LR} &= \rho^{LR}(\theta, \, p^{LR}) & \longrightarrow \quad (\rho^{LR})'_L &= \frac{\partial\rho^{LR}}{\partial\theta} \, \theta'_L + \frac{\partial\rho^{LR}}{\partial p^{LR}} \, (p^{LR})'_L \, , \\
\rho^{GR} &= \rho^{GR}(\theta, \, p^{GR}) & \longrightarrow \quad (\rho^{GR})'_G &= \frac{\partial\rho^{GR}}{\partial\theta} \, \theta'_G + \frac{\partial\rho^{GR}}{\partial p^{GR}} \, (p^{GR})'_G \, .
\end{aligned}
\tag{4.43}
$$

Equations (4.42) and (4.43) are inserted into (4.41). Afterwards, (4.41) is multiplied by the *Lagrangean* multiplier Λ and added to the entropy inequality yielding

$$
\begin{aligned}
&(\mathbf{T}^S + \Lambda\, n^S\,\mathbf{I}) \cdot \mathbf{L}_S + \theta'_S\,(-\rho^S\,\eta^S + \Lambda\,\frac{n^S}{\rho^{SR}}\,\frac{\mathrm{d}\rho^{SR}}{\mathrm{d}\theta}) - \rho^S\,(\psi^S)'_S + \\
&+ (\mathbf{T}^W + \Lambda\, n^W\,\mathbf{I}) \cdot \mathbf{L}_W + \theta'_W\,(-\rho^W\,\eta^W + \Lambda\,\frac{n^W}{\rho^{WR}}\,\frac{\mathrm{d}\rho^{WR}}{\mathrm{d}\theta}) - \rho^W\,(\psi^W)'_W + \\
&+ (\mathbf{T}^L + \Lambda\, n^L\,\mathbf{I}) \cdot \mathbf{L}_L + \theta'_L\,(-\rho^L\,\eta^L) - \rho^L\,(\psi^L)'_L + \Lambda\,\frac{n^L}{\rho^{LR}}\,(\rho^{LR})'_L + \\
&+ (\mathbf{T}^G + \Lambda\, n^G\,\mathbf{I}) \cdot \mathbf{L}_G + \theta'_G\,(-\rho^G\,\eta^G) - \rho^G\,(\psi^G)'_G + \Lambda\,\frac{n^G}{\rho^{GR}}\,(\rho^{GR})'_G - \\
&- \hat{\rho}^L\,(\varepsilon^L - \psi^L - \Lambda\,\frac{1}{\rho^{LR}}) - \hat{\rho}^G\,(\varepsilon^G - \psi^G - \Lambda\,\frac{1}{\rho^{GR}}) + \\
&+ \Lambda\,\mathrm{grad}\, n^W \cdot \mathbf{w}_W + \Lambda\,\mathrm{grad}\, n^L \cdot \mathbf{w}_L + \Lambda\,\mathrm{grad}\, n^G \cdot \mathbf{w}_G - \\
&- \frac{1}{\theta}\,\mathbf{q} \cdot \mathrm{grad}\theta + \hat{\varepsilon}^S + \hat{\varepsilon}^W + \hat{\varepsilon}^L + \hat{\varepsilon}^G \geq 0\,.
\end{aligned}
\tag{4.44}
$$

In comparison to the entropy inequality of model I, the mass production terms are included in (4.44).
The heat flux for the overall aggregate $\mathbf{q}$ leads to

$$
\mathbf{q} = \mathbf{q}^S + \mathbf{q}^W + \mathbf{q}^L + \mathbf{q}^G\,, \quad \text{where} \quad \mathbf{q}^\alpha = -\mathbf{H}^\alpha\,\mathrm{grad}\,\theta\,,\ \alpha \in \{S,\, W,\, L,\, G\}\,. \tag{4.45}
$$

The energy production terms for the fluid constituents $\hat{\varepsilon}^W$, $\hat{\varepsilon}^L$, $\hat{\varepsilon}^G$ vanish: $\hat{\varepsilon}^W \approx 0$, $\hat{\varepsilon}^L \approx 0$, $\hat{\varepsilon}^G \approx 0$, since in the present model all constituents have the same temperature. The energy production term for the solid constituent $\hat{\varepsilon}^S$ is derived from $(4.4)_3$ via momentum and mass production terms ($\hat{\rho}^L = -\hat{\rho}^G$) as follows

$$
\begin{aligned}
\hat{\varepsilon}^S = &-\hat{p}^W \cdot \mathbf{w}_W - \hat{p}^L \cdot \mathbf{w}_L - \hat{p}^G \cdot \mathbf{w}_G + \\
&+ \hat{\rho}^G\,(\varepsilon^L - \varepsilon^G + \tfrac{1}{2}\,\mathbf{w}_L \cdot \mathbf{w}_L - \tfrac{1}{2}\,\mathbf{w}_G \cdot \mathbf{w}_G)\,.
\end{aligned}
\tag{4.46}
$$

The free *Helmholtz* energies ψ^S, ψ^W are defined the same as in (4.17), whereas ψ^L, ψ^G have a different form. In particular, ψ^L depends not only on temperature θ and density ρ^{LR} of the supercritical CO_2 as for model I, but also on the saturation function s^L. An inclusion of s^L into the dependence of ψ^L can be explained by a necessity to cover the existence of the capillary pressure between CO_2 phases. ψ^G is the free *Helmholtz* energy of the CO_2 constituent in the gaseous state and is a function of the temperature and corresponding density.

$$
\begin{array}{rclcrcl}
\psi^S & = & \psi^S(\theta,\, \mathbf{F}_S) & \longrightarrow & (\psi^S)'_S & = & \dfrac{\partial \psi^S}{\partial \theta}\, \theta'_S \;+\; \dfrac{\partial \psi^S}{\partial \mathbf{F}_S}\, \mathbf{F}_S^T \cdot \mathbf{L}_S\,, \\
\psi^W & = & \psi^W(\theta,\, s^W) & \longrightarrow & (\psi^W)'_W & = & \dfrac{\partial \psi^W}{\partial \theta}\, \theta'_W \;+\; \dfrac{\partial \psi^W}{\partial s^W}\, (s^W)'_W\,, \\
\psi^L & = & \psi^L(\theta,\, \rho^{LR},\, s^L) & \longrightarrow & (\psi^L)'_L & = & \dfrac{\partial \psi^L}{\partial \theta}\, \theta'_L \;+\; \dfrac{\partial \psi^L}{\partial \rho^{LR}}\, (\rho^{LR})'_L \;+ \\
 & & & & & & \;+\; \dfrac{\partial \psi^L}{\partial s^L}\, (s^L)'_L\,, \\
\psi^G & = & \psi^G(\theta,\, \rho^{GR}) & \longrightarrow & (\psi^G)'_G & = & \dfrac{\partial \psi^G}{\partial \theta}\, \theta'_G \;+\; \dfrac{\partial \psi^G}{\partial \rho^{GR}}\, (\rho^{GR})'_G\,,
\end{array}
\tag{4.47}
$$

where the derivatives of the saturations have a following form:

$$
\begin{aligned}
(s^W)'_W &= -\frac{1}{n^F}\Big[\frac{n^W}{\rho^{WR}} \frac{\mathrm{d}\rho^{WR}}{\mathrm{d}\theta}\, \theta'_W + n^W\, \mathbf{L}_W \cdot \mathbf{I} + s^W \frac{n^S}{\rho^{SR}} \frac{\mathrm{d}\rho^{SR}}{\mathrm{d}\theta}\, \theta'_S + \\
&\qquad + s^W n^S\, \mathbf{L}_S \cdot \mathbf{I} + s^W \operatorname{grad} n^F \cdot \mathbf{w}_W \Big]\,, \\
(s^L)'_L &= -\frac{1}{n^F}\Big[\frac{n^L}{\rho^{LR}} (\rho^{LR})'_L + n^L\, \mathbf{L}_L \cdot \mathbf{I} + s^L \frac{n^S}{\rho^{SR}} \frac{\mathrm{d}\rho^{SR}}{\mathrm{d}\theta}\, \theta'_S - \frac{\hat{\rho}^L}{\rho^{LR}} \\
&\qquad + s^L n^S\, \mathbf{L}_S \cdot \mathbf{I} + s^L \operatorname{grad} n^F \cdot \mathbf{w}_L \Big]\,.
\end{aligned}
\tag{4.48}
$$

Going further, the free energies are inserted into the entropy inequality (4.44) yielding

$$
\begin{aligned}
&(\underbrace{\mathbf{T}^S + \Lambda\, n^S\, \mathbf{I}}_{\mathbf{T}^S_E} + n^S\,(s^W)^2\,\rho^{WR}\,\frac{\partial\psi^W}{\partial s^W}\,\mathbf{I} + \\
&\qquad\qquad + n^S\,(s^L)^2\,\rho^{LR}\,\frac{\partial\psi^L}{\partial s^L}\,\mathbf{I} - \rho^S\,\frac{\partial\psi^S}{\partial\mathbf{F}_S}\,\mathbf{F}_S^T\,)\cdot\mathbf{L}_S + \\
&+(\underbrace{\mathbf{T}^W + \Lambda\, n^W\,\mathbf{I}}_{\mathbf{T}^W_E} + n^W\,s^W\,\rho^{WR}\,\frac{\partial\psi^W}{\partial s^W}\,\mathbf{I}\,)\cdot\mathbf{L}_W + \\
&+(\underbrace{\mathbf{T}^L + \Lambda\, n^L\,\mathbf{I}}_{\mathbf{T}^L_E} + n^L\,s^L\,\rho^{LR}\,\frac{\partial\psi^L}{\partial s^L}\,\mathbf{I})\cdot\mathbf{L}_L + (\underbrace{\mathbf{T}^G + \Lambda\, n^G\,\mathbf{I}}_{\mathbf{T}^G_E})\cdot\mathbf{L}_G - \\
&-\rho^S\,\theta'_S\,(\underbrace{\eta^S - \Lambda\,\frac{1}{(\rho^{SR})^2}\,\frac{\mathrm{d}\rho^{SR}}{\mathrm{d}\theta}}_{\eta^S_E} - \frac{(s^W)^2\,\rho^{WR}}{(\rho^{SR})^2}\,\frac{\mathrm{d}\rho^{SR}}{\mathrm{d}\theta}\,\frac{\partial\psi^W}{\partial s^W} - \\
&\qquad\qquad\qquad - \frac{(s^L)^2\,\rho^{LR}}{(\rho^{SR})^2}\,\frac{\mathrm{d}\rho^{SR}}{\mathrm{d}\theta}\,\frac{\partial\psi^L}{\partial s^L} + \frac{\partial\psi^S}{\partial\theta}) - \\
&-\rho^W\,\theta'_W\,(\underbrace{\eta^W - \Lambda\,\frac{1}{(\rho^{WR})^2}\,\frac{\mathrm{d}\rho^{WR}}{\mathrm{d}\theta}}_{\eta^W_E} - \frac{s^W}{\rho^{WR}}\,\frac{\mathrm{d}\rho^{WR}}{\mathrm{d}\theta}\,\frac{\partial\psi^W}{\partial s^W} + \frac{\partial\psi^W}{\partial\theta}) - \\
&-\rho^L\,\theta'_L\,(\eta^L + \frac{\partial\psi^L}{\partial\theta}) + (\rho^{LR})'_L\,(\Lambda\,\frac{n^L}{\rho^{LR}} + s^L\,n^L\frac{\partial\psi^L}{\partial s^L} - \rho^L\frac{\partial\psi^L}{\partial\rho^{LR}}) - \\
&-\rho^G\,\theta'_G\,(\eta^G + \frac{\partial\psi^G}{\partial\theta}) + (\rho^{GR})'_G\,(\Lambda\,\frac{n^G}{\rho^{GR}} - \rho^G\frac{\partial\psi^G}{\partial\rho^{GR}}) - \\
&-(\underbrace{\hat{p}^W - \Lambda\,\mathrm{grad}\,n^W}_{\hat{p}^W_E} - (s^W)^2\,\rho^{WR}\,\frac{\partial\psi^W}{\partial s^W}\,\mathrm{grad}\,n^F)\cdot\mathbf{w}_W - \\
&-(\underbrace{\hat{p}^L - \Lambda\,\mathrm{grad}\,n^L}_{\hat{p}^L_E} - (s^L)^2\,\rho^{LR}\,\frac{\partial\psi^L}{\partial s^L}\,\mathrm{grad}\,n^F)\cdot\mathbf{w}_L - (\underbrace{\hat{p}^G - \Lambda\,\mathrm{grad}\,n^G}_{\hat{p}^G_E})\cdot\mathbf{w}_G \\
&+\hat{\rho}^G\,(\psi^L + \frac{1}{2}\,\mathbf{w}_L\cdot\mathbf{w}_L + \frac{\Lambda}{\rho^{LR}} - \psi^G - \frac{1}{2}\,\mathbf{w}_G\cdot\mathbf{w}_G - \frac{\Lambda}{\rho^{GR}} + s^L\frac{\partial\psi^L}{\partial\rho^{LR}}) - \\
&-\frac{1}{\theta}\,\mathbf{q}\cdot\mathrm{grad}\theta \geq 0\,.
\end{aligned}
\tag{4.49}
$$

Herein, $\mathbf{T}_E^\alpha$ with $\alpha \in \{S,\, W,\, L,\, G\}$ are the extra stresses, η_E^S, η_E^W are the extra entropies and $\hat{p}_E^\beta$ with $\beta \in \{W,\, L,\, G\}$ are the extra momentum production terms assigned to

$$\begin{aligned}
\mathbf{T}_E^\alpha &= \mathbf{T}^\alpha + \Lambda\, n^\alpha\, \mathbf{I}\,,\\
\eta_E^S &= \eta^S - \Lambda\, \frac{1}{(\rho^{SR})^2}\, \frac{\mathrm{d}\rho^{SR}}{\mathrm{d}\theta}\,,\\
\eta_E^W &= \eta^W - \Lambda\, \frac{1}{(\rho^{WR})^2}\, \frac{\mathrm{d}\rho^{WR}}{\mathrm{d}\theta}\,,\\
\hat{p}_E^\beta &= \hat{p}^\beta - \Lambda\, \mathrm{grad}\, n^\beta\,.
\end{aligned} \tag{4.50}$$

Following the same procedure of evaluation of the entropy inequality as performed for model I, the expressions in front of the free parameters $\mathbf{L}_S$, θ'_α, $(\rho^{LR})'_L$ and $(\rho^{GR})'_G$ with arbitrary values have to disappear in order to fulfil the inequality. This leads to the constraints for the mechanical extra stress terms $\mathbf{T}^S_{E\,\mathrm{mech}}$, $\mathbf{T}^W_{E\,\mathrm{mech}}$ and $\mathbf{T}^L_{E\,\mathrm{mech}}$:

$$\begin{aligned}
\mathbf{T}^S_{E\,\mathrm{mech}} &= \mathbf{T}_E^S + n^S\,(s^W)^2\,\rho^{WR}\,\frac{\partial\psi^W}{\partial s^W} + n^S\,(s^L)^2\,\rho^{LR}\,\frac{\partial\psi^L}{\partial s^L} = \rho^S\,\frac{\partial\psi^S}{\partial\mathbf{F}_S}\,\mathbf{F}_S^T\,,\\
\mathbf{T}^W_{E\,\mathrm{mech}} &= \mathbf{T}_E^W + s^W\,\rho^W\,\frac{\partial\psi^W}{\partial s^W}\,,\\
\mathbf{T}^L_{E\,\mathrm{mech}} &= \mathbf{T}_E^L + s^L\,\rho^L\,\frac{\partial\psi^L}{\partial s^L}\,,
\end{aligned} \tag{4.51}$$

for the mechanical extra entropies $\eta^S_{E\,\mathrm{mech}}$, $\eta^W_{E\,\mathrm{mech}}$ and for the entropies η^L, η^G:

$$\begin{aligned}
\eta^S_{E\,\mathrm{mech}} &= \eta_E^S - \frac{(s^W)^2\,\rho^{WR}}{(\rho^{SR})^2}\,\frac{\mathrm{d}\rho^{SR}}{\mathrm{d}\theta}\,\frac{\partial\psi^W}{\partial s^W} - \frac{(s^L)^2\,\rho^{LR}}{(\rho^{SR})^2}\,\frac{\mathrm{d}\rho^{SR}}{\mathrm{d}\theta}\,\frac{\partial\psi^L}{\partial s^L} = -\frac{\partial\psi^S}{\partial\theta}\,,\\
\eta^W_{E\,\mathrm{mech}} &= \eta_E^W - \frac{s^W}{\rho^{WR}}\,\frac{\mathrm{d}\rho^{WR}}{\mathrm{d}\theta}\,\frac{\partial\psi^W}{\partial s^W} = -\frac{\partial\psi^W}{\partial\theta}\,,\\
\eta^L &= -\frac{\partial\psi^L}{\partial\theta}\,,\\
\eta^G &= -\frac{\partial\psi^G}{\partial\theta}\,,
\end{aligned} \tag{4.52}$$

and for the extra momentum production terms $\hat{p}^W_{E\,\mathrm{mech}}$ and $\hat{p}^L_{E\,\mathrm{mech}}$:

$$\begin{aligned}
\hat{p}^W_{E\,\mathrm{mech}} &= \hat{p}_E^W - (s^W)^2\,\rho^{WR}\,\frac{\partial\psi^W}{\partial s^W}\,\mathrm{grad}\, n^F\,,\\
\hat{p}^L_{E\,\mathrm{mech}} &= \hat{p}_E^L - (s^L)^2\,\rho^{LR}\,\frac{\partial\psi^L}{\partial s^L}\,\mathrm{grad}\, n^F\,.
\end{aligned} \tag{4.53}$$

Examining the expression in front of $(\rho^{GR})'_G$, the *Lagrange*an multiplier Λ is defined as:

$$\Lambda \;=\; (\rho^{GR})^2\,\frac{\partial\psi^G}{\partial\rho^{GR}} \;=\; p^{GR}\,. \tag{4.54}$$

Considering the coefficient ahead of $(\rho^{LR})'_L$, the following relation is obtained

$$\Lambda \,+\, s^L\,\rho^{LR}\,\frac{\partial\psi^L}{\partial s^L} \;=\; (\rho^{LR})^2\,\frac{\partial\psi^L}{\partial\rho^{LR}}\,, \tag{4.55}$$

where by definition the right hand side of the relation represents the pressure p^{LR}. Therefore, the left hand side of the relation also equals to p^{LR}, which is in agreement with the later determination of the $\overset{\equiv}{\Lambda}$ in (4.60).

The dissipation part of the entropy inequality reads

$$\begin{aligned} \mathcal{D} \;=\; & -\hat{p}^W_{E\,\mathrm{mech}}\cdot\mathbf{w}_W \,-\, \hat{p}^L_E\cdot\mathbf{w}_L \,-\, \hat{p}^G_E\cdot\mathbf{w}_G \,-\, \frac{1}{\theta}\,\mathbf{q}\cdot\mathrm{grad}\theta \,+ \\ & +\hat{\rho}^G\,(\psi^L \,+\, \frac{1}{2}\,\mathbf{w}_L\cdot\mathbf{w}_L \,+\, \frac{\Lambda}{\rho^{LR}} \,+\, s^L\,\frac{\partial\psi^L}{\partial\rho^{LR}} \,- \\ & -\psi^G \,-\, \frac{1}{2}\,\mathbf{w}_G\cdot\mathbf{w}_G \,-\, \frac{\Lambda}{\rho^{GR}})\;\geq\;0\,, \end{aligned} \tag{4.56}$$

where the extra momentum production terms are

$$\begin{aligned} \hat{p}^W_{E\,\mathrm{mech}} &= \hat{p}^W_E \,-\, (s^W)^2\,\rho^{WR}\,\frac{\partial\psi^W}{\partial s^W}\mathrm{grad}\,n^F\,, \\ \hat{p}^L_E &= \hat{p}^L \,-\, \Lambda\,\mathrm{grad}\,n^L\,, \\ \hat{p}^G_E &= \hat{p}^G \,-\, \Lambda\,\mathrm{grad}\,n^G\,. \end{aligned} \tag{4.57}$$

In order to fulfil the $\mathcal{D}$ inequality, appropriate constitutive assumptions for $\hat{p}^W_{E\,\mathrm{mech}}$, $\hat{p}^L_E$, $\mathbf{q}$ and $\hat{\rho}^G$ have to be developed such that $\mathcal{D}\geq 0$. Using the same argumentation as for model I, the momentum production terms yield

$$\begin{aligned} \hat{p}^W_{E\,\mathrm{mech}} &= -(n^W)^2\,\gamma^{WR}(\mathbf{K}^W_r)^{-1}\,\mathbf{w}_W\,, \\ \hat{p}^L_E &= -(n^L)^2\,\gamma^{LR}(\mathbf{K}^L_r)^{-1}\,\mathbf{w}_L\,, \\ \hat{p}^G_E &= -(n^G)^2\,\gamma^{GR}(\mathbf{K}^G_r)^{-1}\,\mathbf{w}_G\,, \end{aligned} \tag{4.58}$$

with parameters given in (4.28) and valid for $\beta\in\{W,\,L,\,G\}$.

The remaining variables, namely, the heat flux $\mathbf{q}$ is defined above in (4.45) and the mass production term $\hat{\rho}^G$ in Section 5.

Based on the notations in (4.49) and relations (4.51), the *Cauchy* stress tensors yield

$$
\begin{aligned}
\mathbf{T}^S_{E\,\mathrm{mech}} &= \mathbf{T}^S + n^S\,(\underbrace{\Lambda + (s^W)^2\,\rho^{WR}\,\frac{\partial\psi^W}{\partial s^W} + (s^L)^2\,\rho^{LR}\,\frac{\partial\psi^L}{\partial s^L}}_{\bar{\Lambda}})\,\mathbf{I}\,,\\
\mathbf{T}^W_{E\,\mathrm{mech}} &= \mathbf{T}^W + n^W\,(\underbrace{\Lambda + s^W\,\rho^{WR}\,\frac{\partial\psi^W}{\partial s^W}}_{\bar{\bar{\Lambda}}})\,\mathbf{I}\,,\\
\mathbf{T}^L_{E\,\mathrm{mech}} &= \mathbf{T}^L + n^L\,(\underbrace{\Lambda + s^L\,\rho^{LR}\,\frac{\partial\psi^L}{\partial s^L}}_{\bar{\bar{\bar{\Lambda}}}})\,\mathbf{I}\,,\\
\mathbf{T}^G_E &= \mathbf{T}^G + n^G\,\Lambda\,\mathbf{I}\,.
\end{aligned}
\tag{4.59}
$$

The variables $\bar{\Lambda}$, $\bar{\bar{\Lambda}}$ and $\bar{\bar{\bar{\Lambda}}}$ are introduced similar to the variables in (4.31), in particular, by the effective pressures p^{WR}, p^{LR} and pore pressure p^{FR}:

$$
\begin{aligned}
\bar{\bar{\bar{\Lambda}}} &= \Lambda + s^L\,\rho^{LR}\,\frac{\partial\psi^L}{\partial s^L} = p^{LR},\\
\bar{\bar{\Lambda}} &= \Lambda + s^W\,\rho^{WR}\,\frac{\partial\psi^W}{\partial s^W} = p^{WR},\\
\bar{\Lambda} &= \Lambda + (s^W)^2\,\rho^{WR}\,\frac{\partial\psi^W}{\partial s^W} + (s^L)^2\,\rho^{LR}\,\frac{\partial\psi^L}{\partial s^L} = p^{FR}\,.
\end{aligned}
\tag{4.60}
$$

Here, it is essential to remember that in this model two capillary pressures p^C_{LW} and p^C_{GL} are defined. The term p^C_{LW} represents the capillary pressure between water and supercritical CO_2, whereas p^C_{GL} describes the difference between the pressures of supercritical and gaseous CO_2:

$$
p^C_{LW} = p^{LR} - p^{WR}\,, \quad p^C_{GL} = p^{GR} - p^{LR}\,.
\tag{4.61}
$$

According to the relations (4.60), these capillary pressures could be defined as

$$
\begin{aligned}
p^C_{LW} &= s^L\,\rho^{LR}\,\frac{\partial\psi^L}{\partial s^L} - s^W\,\rho^{WR}\,\frac{\partial\psi^W}{\partial s^W}\,,\\
p^C_{GL} &= -s^L\,\rho^{LR}\,\frac{\partial\psi^L}{\partial s^L}\,.
\end{aligned}
\tag{4.62}
$$

Respectively, the pore pressure p^{FR} is defined as

$$
p^{FR} = s^W\,p^{WR} + s^L\,p^{LR} + s^G\,p^{GR}\,.
\tag{4.63}
$$

Following the argumentation given for model I, the extra stresses of the fluid constituents $\mathbf{T}^W_{E\,\mathrm{mech}}$, $\mathbf{T}^L_E$ and $\mathbf{T}^G_E$ are negligible in comparison to the mechanical extra momentum production terms, which represent the fluid viscosity in the model. The *Cauchy* stress tensors have a form

$$\begin{aligned} \mathbf{T}^S &= -n^S\, p^{FR}\, \mathbf{I} + \mathbf{T}^S_{E\,\text{mech}}\,, \\ \mathbf{T}^W &= -n^W\, p^{WR}\, \mathbf{I}\,, \\ \mathbf{T}^L &= -n^L\, p^{LR}\, \mathbf{I}\,, \\ \mathbf{T}^G &= -n^G\, p^{GR}\, \mathbf{I}\,, \end{aligned} \tag{4.64}$$

and the entropies yield

$$\begin{aligned} \eta^S &= \frac{1}{(\rho^{SR})^2}\frac{\mathrm{d}\rho^{SR}}{\mathrm{d}\theta}\, p^{FR} && - \frac{\partial\psi^S}{\partial\theta}\,, \\ \eta^W &= \frac{1}{(\rho^{WR})^2}\frac{\mathrm{d}\rho^{WR}}{\mathrm{d}\theta}\, p^{WR} && - \frac{\partial\psi^W}{\partial\theta}\,, \\ \eta^L &= && -\frac{\partial\psi^L}{\partial\theta}\,, \\ \eta^G &= && -\frac{\partial\psi^G}{\partial\theta}\,. \end{aligned} \tag{4.65}$$

The remaining constitutive settings are defined in the next sections, specifically, for the solid and fluid constituents. Based on the derived relations for the stress tensors and production terms as well as setting $\rho = \sum_\alpha \rho^\alpha$, the system (4.3) of the governing equations for model II is reformulated and read

momentum balance:

$$\operatorname{div}(\mathbf{T}^S_E - p^{FR}\,\mathbf{I}) + \rho\,\mathbf{g} - \hat{\rho}^L\,\mathbf{w}_L - \hat{\rho}^G\,\mathbf{w}_G = \mathbf{0}\,, \tag{4.66}$$

mass balances:

$$\begin{aligned} (\rho^W)'_S &+ \operatorname{div}(\rho^W\,\mathbf{w}_W) + \rho^W \operatorname{div}(\mathbf{u}_S)'_S &&= 0\,, \\ (\rho^L)'_S &+ \operatorname{div}(\rho^L\,\mathbf{w}_L) + \rho^L \operatorname{div}(\mathbf{u}_S)'_S - \hat{\rho}^L &&= 0\,, \\ (\rho^G)'_S &+ \operatorname{div}(\rho^G\,\mathbf{w}_G) + \rho^G \operatorname{div}(\mathbf{u}_S)'_S - \hat{\rho}^G &&= 0\,, \end{aligned} \tag{4.67}$$

energy balance:

$$\begin{aligned} &\rho^S(\varepsilon^S)'_S + \rho^W(\varepsilon^W)'_W + \rho^L(\varepsilon^L)'_L - \mathbf{T}^S_E\cdot\mathbf{L}_S + n^S\,p^{FR}\operatorname{div}(\mathbf{u}_S)'_S + \\ &+ n^W\,p^{WR}\operatorname{div}\overset{\prime}{\mathbf{x}}_W + n^L\,p^{LR}\operatorname{div}\overset{\prime}{\mathbf{x}}_L + n^G\,p^{GR}\operatorname{div}\overset{\prime}{\mathbf{x}}_G + \\ &+ \operatorname{div}\mathbf{q} + \hat{\mathbf{p}}^W\cdot\mathbf{w}_W + \hat{\mathbf{p}}^L\cdot\mathbf{w}_L + \hat{\mathbf{p}}^G\cdot\mathbf{w}_G + \\ &+ \hat{\rho}^G\,(\varepsilon^G + \tfrac{1}{2}\,\mathbf{w}_G\cdot\mathbf{w}_G) + \hat{\rho}^L\,(\varepsilon^L + \tfrac{1}{2}\,\mathbf{w}_L\cdot\mathbf{w}_L) = 0\,. \end{aligned} \tag{4.68}$$

4.4 The Solid Constituent

For the purpose of simplification of the modelling procedure, the deformation of the solid skeleton is limited to elastic behaviour within the current investigation. However, it is possible to include plastic or visco-plastic properties for the solid skeleton into the model, cf. Graf [53], Ehlers *et al.* [43]. Due to the assumption that only small deformations occur within the considered continuum mechanical model, the geometrically linear theory is used to describe the deformations of the solid constituent. Also, it should be noted that in the framework of the two considered approaches (model I and model II), the constitutive relations for the solid skeleton have the same form.

Effective Density:

The constitutive relation for the partial density ρ^S of the solid skeleton is derived by time integration of the corresponding mass balance without the mass production term and results in

$$\rho^S \;=\; \rho^S_{0S}\,(\det\mathbf{F}_S)^{-1}\,, \tag{4.69}$$

where ρ^S_{0S} is the partial solid density at the reference configuration. Following Ghadiani [51], the material gradient $\mathbf{F}_S$ can be split into a mechanical $\mathbf{F}_{S_m}$ and a thermal $\mathbf{F}_{S_\theta}$ part:

$$\mathbf{F}_S \;=\; \mathbf{F}_{S_m}\,\mathbf{F}_{S_\theta}\,. \tag{4.70}$$

Thus, the density of the solid skeleton leads to

$$\rho^S \;=\; \rho^S_{0S}\,(\det\mathbf{F}_{S_\theta})^{-1}\,(\det\mathbf{F}_{S_m})^{-1}\,. \tag{4.71}$$

The partial density of the solid skeleton, which deformation is caused only by purely thermal loads, is denoted ρ^S_θ and equals

$$\rho^S_\theta = \rho^S_{0S}\,(\det\mathbf{F}_{S_\theta})^{-1}\,. \tag{4.72}$$

Further, looking at the definition of ρ^S via the volume fraction n^S and substituting ρ^S_θ into (4.71), the density ρ^S yields

$$\rho^S \;=\; n^S\,\rho^{SR} \;=\; \rho^S_\theta\,(\det\mathbf{F}_{S_m})^{-1} \;=\; n^S_\theta\,\rho^{SR}_\theta\,(\det\mathbf{F}_{S_m})^{-1}\,. \tag{4.73}$$

It is assumed that the effective density ρ^{SR} of the solid skeleton is governed only by the temperature θ, which means that $\rho^{SR} = \rho^{SR}_\theta$. The thermal loading only yields a homogeneous expansion, or in other words, the changes of the volume fractions are only caused by the mechanical loads: $n^S_\theta = n^S_{0S}$. Based on these assumptions, (4.72) is transformed into

$$\rho^{SR} = \rho^{SR}_{0R}\,(\det\mathbf{F}_{S_\theta})^{-1}\,, \tag{4.74}$$

and (4.73) turns out to

$$n^S \;=\; n^S_\theta\,(\det\mathbf{F}_{S_m})^{-1} \;=\; n^S_{0S}\,(\det\mathbf{F}_{S_m})^{-1}\,. \tag{4.75}$$

According to Ghadiani [51], an *a priori* constitutive relation for the determinant of the thermal part of the deformation gradient is introduced in the form

$$\det \mathbf{F}_{S_\theta} \;=\; e^{3\alpha_S\,(\theta\,-\,\theta_0)}\,, \tag{4.76}$$

where α_S is the thermal expansion coefficient of the solid skeleton, θ_0 is the temperature at the reference configuration (initial temperature). Finally, the expression for the effective density of the solid skeleton reads

$$\rho^{SR} \;=\; \rho^{SR}_{0S}\, e^{-3\alpha_S\,(\theta\,-\,\theta_0)}\,. \tag{4.77}$$

In order to use the geometrically linear theory for a description of the deformations of the solid skeleton, the linearisation procedure has to be performed for the effective density ρ^{SR} and volume fraction n^S. Proceeding from Graf [53], it results in

$$\begin{aligned} \rho^{SR}_{\mathrm{lin}} \;&=\; \rho^{SR}_{0S}\,[1\,-\,3\alpha_S\,(\theta\,-\,\theta_0)]\,,\\ n^S_{\mathrm{lin}} \;&=\; n^S_{0S}\,[1\,-\,\mathrm{Div}_S\,\mathbf{u}_S\,+\,3\,\alpha_S\,(\theta\,-\,\theta_0)]\,. \end{aligned} \tag{4.78}$$

Moreover, there is no need to distinguish between reference and actual configurations in case of small deformations. It means that there is no difference between div $(\cdot)$ and Div $(\cdot)$ resulting into

$$n^S_{\mathrm{lin}} \;=\; n^S_{0S}\,[1\,-\,\mathrm{div}\,\mathbf{u}_S\,+\,3\,\alpha_S\,(\theta\,-\,\theta_0)]\,. \tag{4.79}$$

Free Helmholtz Energy:

The free *Helmholtz* energy of the solid constituent φ^S is defined as a function of the temperature and the deformation gradient, cf. $(4.17)_1$. In addition, the *principle of material frame indifference*, also known as principle of the material objectivity, requires the dependence of ψ^S on the *Cauchy-Green* tensor $\mathbf{C}_S \,=\, \mathbf{F}^T_S\,\mathbf{F}_S$. Then, $\mathbf{C}_S$ can be substituted via the *Green-Lagrange*an tensor $\mathbf{E}_S$ from (3.26), which after linearisation is denoted as $\boldsymbol{\varepsilon}_S$ and equals to

$$\boldsymbol{\varepsilon}_S \;=\; \tfrac{1}{2}\,[\,\mathrm{grad}\,\mathbf{u}_S\,+\,\mathrm{grad}^T\,\mathbf{u}_S]\,. \tag{4.80}$$

Herein, there is no difference between the grad$(\cdot)$ and Grad$_S(\cdot)$ operators because of the assumption that small deformations occur in the problem.

Thus, the free *Helmholtz* energy ψ^S_{lin} for the solid skeleton in the frame of the geometrically linear theory and non-isothermal problem depends on the temperature θ and the strain tensor $\boldsymbol{\varepsilon}_S$ and is defined as

$$\begin{aligned} \rho^S_{0S}\,\psi^S_{\mathrm{lin}}\,(\theta,\,\boldsymbol{\varepsilon}_S) \;=\;& \mu^S\,\boldsymbol{\varepsilon}_S\cdot\boldsymbol{\varepsilon}_S\,+\,\tfrac{1}{2}\,\lambda^S\,(\boldsymbol{\varepsilon}_S\cdot\mathbf{I})^2\,+\,m^S\,(\theta\,-\,\theta_0)\,\boldsymbol{\varepsilon}_S\cdot\mathbf{I}\,-\\ &-\,\rho^S_{0S}\,C^S_V\left[\theta\ln\frac{\theta}{\theta_0}\,-\,(\theta\,-\,\theta_0)\right], \end{aligned} \tag{4.81}$$

where μ^S, λ^S are the *Lamé* constants, $m^S = -(2\mu^S + 3\lambda^S)\alpha^S$ is the stress-temperature modulus and C_V^S is the specific heat for the solid skeleton.

Effective Stress, Entropy and Internal Energy:

As a consequence of $(4.51)_1$, the linearised mechanical extra stress for the solid constituent denoted as $\boldsymbol{\sigma}^S_{E\text{mech}}$ is obtained based on (4.81) in the following form:

$$\boldsymbol{\sigma}^S_{E\text{mech}} = \rho^S_{0S}\,\frac{\partial \psi^S_{\text{lin}}}{\partial \boldsymbol{\varepsilon}^S} = 2\,\mu^S\,\boldsymbol{\varepsilon}_S + \lambda^S\,(\boldsymbol{\varepsilon}_S \cdot \mathbf{I})\,\mathbf{I} + m^S\,(\theta - \theta_0)\,\mathbf{I}\,. \tag{4.82}$$

Having ψ^S_{lin} from (4.81) and ρ^{SR}_{lin} from $(4.78)_1$, the linearised entropy function η^S_{lin} can be deduced from $(4.36)_1$ in the from

$$\eta^S_{\text{lin}} = C_V^S \ln\frac{\theta}{\theta_0} - \frac{1}{\rho^S_{0S}}\,m^S\,\boldsymbol{\varepsilon}_S\cdot\mathbf{I} - p^{FR}\,\frac{3\,\alpha^S}{\rho^{SR}_{0S}}\,, \tag{4.83}$$

with an additional assumption that for small α^S: $(\rho^{SR}_{\text{lin}})^2 \approx (\rho^{SR}_{0S})^2$.

In addition, taking the second derivative of (4.81), the specific heat for the solid skeleton can be determined:

$$C_V^S = -\theta\,\frac{\partial^2\psi^S}{(\partial\theta)^2}\bigg|_{\rho^{SR}=\text{const}}\,. \tag{4.84}$$

The internal energy of the solid constituent ε^S can be defined from an expression for the *Helmholtz* energy ψ^S introduced via the *Legendre* transformation between the conjugated variables entropy η^S and temperature θ, cf. Appendix B:

$$\psi^S := \varepsilon^S - \theta\,\eta^S\,. \tag{4.85}$$

4.5 The Pore-Fluid Constituents

At the beginning of this subsection, the capillary pressure as well as the capillary pressure-saturation relationships are introduced. Afterwards, the definition of the seepage velocities of the fluid constituents and the constitutive settings specific to the different modelling approaches are discussed.

4.5.1 Capillary Pressure

In general, the *capillary pressure* p^C is defined for a multiphasic material composed of two or more fluid phases. These fluid phases could be divided into two classes according to their wettability, which depends on the contact angle ϑ between the solid skeleton and fluid interface. A fluid is a *wetting* fluid W, if $0^0 \leq \vartheta < 90^0$, and a *non-wetting* fluid NW, if $90^0 < \vartheta \leq 180^0$. If $\vartheta = 90^0$, there are no capillary forces in the system, cf. Figure 4.2.

At the microscopic level, capillarity is caused by the cohesion (adhesion) effects within (between) the phases or, simply, by the surface tension σ at the interface between the fluids. The difference between the pressures of the corresponding phases is called the capillary pressure p^C:

$$p^C = p^{NW} - p^W , \tag{4.86}$$

where p^{NW} is a pressure of a non-wetting phase and p^W of a wetting phase. In this case, the capillary pressure can be also represented via

$$p^C = \frac{2\,\sigma \cos\vartheta}{r} , \tag{4.87}$$

where r is the meniscus radius, cf. Helmig [57].

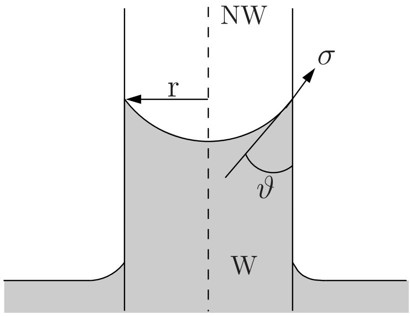

Figure 4.2: Capillary tube.

At the macroscopic level, it is noted that as the saturations of the phases change the capillary pressure also changes. Therefore, it is realised that p^C depends on the saturation

$$p^C = p^C\,(s^W) . \tag{4.88}$$

However, it is found that there are also other factors, which should be included into the capillary-pressure-saturation relation (4.88). For example, according to the modelling approach suggested in the publications by Pop *et al.* [84], Niessner & Hassanizadeh [76] and others, $p^C\,(s^W)$ does not only involve the saturation s^W, but also specific interfacial areas. Nevertheless, since in the present contribution the models are considered at the macroscopic scale, it is assumed that the capillary pressure depends only on the saturation of the wetting phases as in (4.88).

Many scientists have tried to derive the relationship between capillary pressure and saturation. Among others, the most widely used formulations for a system with two fluid phases were developed by *Brooks & Corey* (1964) and *van Genuchten* (1980). The basic principles of these laws can be found in Brooks & Corey [23, 24] and van Genuchten [50].

The *Brooks & Corey* law with the material parameters p_d, λ and the *van Genuchten* law with the parameters n, m, γ are defined in $(4.89)_1$, $(4.89)_2$ as the dependence between an effective saturation s_{eff} and the capillary pressure p^C:

$$\begin{aligned} \text{Brooks\,\&\,Corey}: \quad s_{eff} &= \left(\frac{p_d}{p^C}\right)^{\lambda} , \\ \text{van Genuchten}: \quad s_{eff} &= (1 + (\gamma\, p^C)^n)^{-m} . \end{aligned} \tag{4.89}$$

The effective saturation s_{eff} can be derived through the residual saturation s^W_{res} such as

$$s_{eff} = \frac{s^W - s^W_{res}}{1 - s^W_{res}} \quad \text{for} \quad s^W_{res} \leq s^W \leq 0\,, \tag{4.90}$$

or in a different way

$$s_{eff} = \frac{s^W - s^W_{res}}{1 - s^W_{res} - s^{NW}_{res}} \quad \text{for} \quad s^W_{res} \leq s^W \leq 1 - s^{NW}_{res}\,. \tag{4.91}$$

The choice of the definition of s_{eff} can be done based on the hydrodynamic situation of the considered problem.

Inverting the relations (4.89), the capillary pressures lead to

$$\begin{aligned} \text{Brooks\,\&\,Corey}: \quad p^C\,(s^W) &= p_d\, s_{eff}^{-\frac{1}{\lambda}} && \text{for} \quad p_c \geq p_d\,, \\ \text{van Genuchten}: \quad p^C\,(s^W) &= \frac{1}{\gamma}\,(s_{eff}^{-\frac{1}{m}} - 1)^{\frac{1}{n}} && \text{for} \quad p_c > 0\,, \end{aligned} \tag{4.92}$$

where s_{eff} is defined via (4.90) or (4.91). The main difference between the *Brooks & Corey* and the *van Genuchten* laws is in the behaviour of the corresponding capillary-pressure-saturation relation $p^C\,(s^W)$ in the fully-saturated region. In particular, the *Brooks & Corey* law results in a non-zero value of the capillary pressure at the fully-saturated conditions whereas the *van Genuchten* law does not. As an example, $p^C\,(s^W)$ curves related to both laws for a gas-water system under identical physical conditions are schematically illustrated in Figure 4.3. More detailed information about this topic can be found, for instance, in the book by Helmig [57] and references therein.

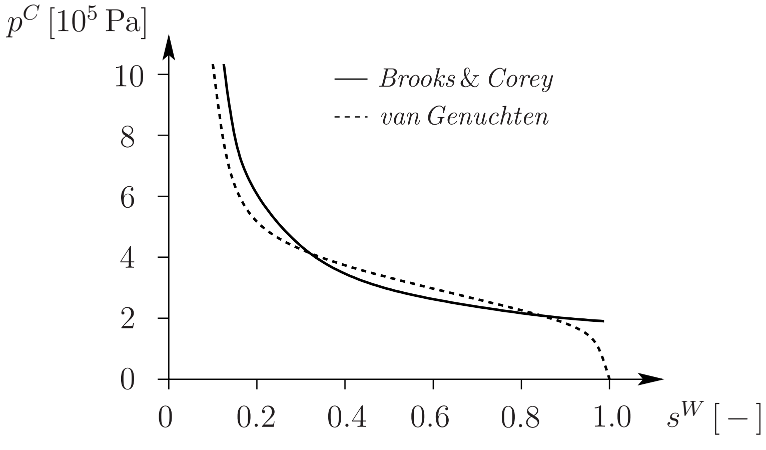

Figure 4.3: *Brooks & Corey* and *van Genuchten* $p^C(s^W)$ relations.

There are several limitations of these laws. One of them is the omission of the temperature influence on the capillary pressure, resulting from the temperature-dependence of the surface tension, cf. Class [26]. Also, the required material parameters can be determined only by fitting to experimental data and are, therefore, often not available.

Going further into a discussion about the capillary-pressure-saturation relations, for the model II a proper capillary-pressure-saturation relation between three fluid phases is required. Different scenarios could be suggested to describe a capillary-pressure-saturation relation for a model with more than two fluid phases. One approach among others suggested by Holm *et al.* [58] is based on the idea to create a capillary-pressure-saturation surface by using a pore network model. Another possibility is to split the problem with three fluid phases into two problems with two phases, cf. Class [26], Helmig [57]. Within the current work, the second concept is used, which requires the definition of a capillary pressure p^C_{LW} between the supercritical CO_2 (L) and water (W), and p^C_{GL} between gaseous CO_2 (G) and the supercritical CO_2 (L). Proceeding from (4.61) and (4.62), these capillary pressures read

$$\begin{aligned} p^C_{LW} &= p^{LR} - p^{WR} &&= s^L\,\rho^{LR}\,\frac{\partial\psi^L}{\partial s^L} - s^W\,\rho^{WR}\,\frac{\partial\psi^W}{\partial s^W}\,, \\ p^C_{GL} &= p^{GR} - p^{LR} &&= -s^L\,\rho^{LR}\,\frac{\partial\psi^L}{\partial s^L}\,, \end{aligned} \tag{4.93}$$

where according to (4.47), the *Helmholtz* energies are defined as $\psi^L = \psi^L(\theta, \rho^{LR}, s^L)$ and $\psi^W = \psi^W(\theta, s^W)$. This leads to the following dependence of the capillary pressures p^C_{LW}, p^C_{GL} on the variables $\theta, \rho^{LR}, s^L, s^W$:

$$p^C_{LW} = p^C_{LW}(\theta, \rho^{LR}, s^L, s^W) \quad \text{and} \quad p^C_{GL} = p^C_{GL}(\theta, \rho^{LR}, s^L). \tag{4.94}$$

For the description of the capillary-pressure-saturation relation for p^C_{LW} given in (4.94), the standard *van Genuchten* or *Brooks* & *Corey* laws are used. In this regard, a broad of the multiphasic pore models considering the interaction between CO_2 and water were also discussed in Spycher *et al.* [96], Span & Wagner [94] and some experimental results can be found in Plug & Bruining [82] among others. The capillary-pressure-saturation relation for p^C_{GL} given (4.94) is also described by the *van Genuchten* or *Brooks* & *Corey* laws in this thesis, because of the lack of data and information about an interaction and a behaviour of the CO_2 phases.

4.5.2 Filter Velocity

By definition, the filter velocity $n^\beta \mathbf{w}_\beta$ is the product of the volume fraction n^β and the seepage velocity $\mathbf{w}_\beta$, presented in Section 3.3. Incorporating the momentum production terms (4.57) with (4.58) into the corresponding momentum balances, the individual relation for the filter velocity is obtained:

$$n^\beta\,\mathbf{w}_\beta = -\frac{k_r^\beta\,\mathbf{K}^\beta}{\gamma^{\beta R}}\,(\operatorname{grad} p^{\beta R} - \rho^{\beta R}\,\mathbf{g})\,. \tag{4.95}$$

This is a well-known relation to obtain the seepage velocity $\mathbf{w}_\beta$ of the multiphasic material, which is valid for all fluid constituents $\beta \in \{W, L, G\}$ within the present work. Moreover, this relation represents the standard *Darcy* law derived from the experiments for the multiphase flow problems, cf. Helmig [57].

4.5.3 Specific Constitutive Relations for Model I

The constitutive relations for the fluid phases, water and supercritical CO_2, are introduced for a discussion here. The derivation procedure for these constitutive settings is similar to the procedure used for the solid constituent in Section 4.4. Mainly, the relations for the effective properties, such as density, CO_2 pressure, stress as well as entropy, free energy and heat fluxes are defined in this section.

Effective Density:

The effective density for the fluid constituent represented by the water phase φ^W reads

$$\rho^{WR} = \rho^{WR}_{0W} \, e^{-\gamma^W (\theta - \theta_0)} \, , \tag{4.96}$$

where γ^W is the volumetric thermal expansion coefficient and ρ^{WR}_{0W} is the density in the reference configuration with the corresponding temperature θ_0.

Concerning the supercritical CO_2, its density ρ^{LR} is obtained by solving the *Peng-Robinson* EOS (Peng & Robinson [81]) with respect to the density, cf. Appendix B. Herein, the effective pressure of the supercritical CO_2 is defined by the *Peng-Robinson* EOS, which was discussed in Section 3.5.2:

$$p^{LR} = \frac{R^L \, \theta}{v - b} - \frac{a \, \alpha_\omega}{v^2 + 2 \, b \, v - b^2} \, . \tag{4.97}$$

Therein, $v = 1/\rho^{LR}$ is the specific volume, $R^L = R/M_{CO_2}$ is the specific gas constant given by a ratio between the universal gas constant R and the molar mass M_{CO_2}. The constants a, b and α_ω are defined in (3.59) and (3.60) via the critical pressure $p_{\rm cr}$, the critical temperature $\theta_{\rm cr}$ and an acentric factor ω. The required parameters for CO_2 for the *Peng-Robinson* EOS yield, cf. Metz *et al.* [73],

$$\begin{aligned} R &= 8.31 \quad [\,\mathrm{J/(K\,mol)}\,] \, , \\ M_{CO_2} &= 0.044 \quad [\,\mathrm{kg/mol}\,] \, , \\ p_{\rm cr} &= 7.38 \quad [\mathrm{MPa}] \, , \\ \theta_{\rm cr} &= 304.1 \quad [\,\mathrm{K}\,] \, , \\ \omega &= 0.239 \quad [\,-\,] \, . \end{aligned} \tag{4.98}$$

Free Helmholtz Energies:

The free *Helmholtz* energies for the fluid constituents φ^W and φ^L are derived using the procedure proposed by Ghadiani [51] and extended by Graf [53]. The main idea is to combine properly the derivatives $\frac{\partial \psi^W}{\partial \theta}$, $\frac{\partial \psi^L}{\partial \theta}$ via the specific heat C_V^α with the derivatives $\frac{\partial \psi^W}{\partial s^W}$, $\frac{\partial \psi^L}{\partial \rho^{LR}}$ via the capillary and liquid pressures in order to obtain the relation for ψ^W and ψ^L.

Thus, on the one hand, the second derivative of the free *Helmholtz* energy with respect to temperature is by definition the specific heat coefficient C_V^α, $\alpha \in \{S,\, W,\, L\}$ reads

$$C_V^\alpha \;=\; -\theta\; \frac{\partial^2 \psi^\alpha}{(\partial\theta)^2}\bigg|_{\rho^{\alpha R}=\text{const}} \,. \tag{4.99}$$

And integration of (4.99) by use of (4.17) results in

$$\begin{aligned} \frac{\partial \psi^W}{\partial \theta} \;&=\; -\int \frac{C_V^W}{\theta}\,\mathrm{d}\,\theta \,+\, g^W(s^W) \;&=\; -\,C_V^W \ln\theta \,+\, g^W(s^W)\,, \\ \frac{\partial \psi^L}{\partial \theta} \;&=\; -\int \frac{C_V^L}{\theta}\,\mathrm{d}\,\theta \,+\, g^L(\rho^{LR}) \;&=\; -\,C_V^L \ln\theta \,+\, g^L(\rho^{LR})\,. \end{aligned} \tag{4.100}$$

On the other hand, the derivative of the free energy with respect to the saturation can be expressed via the capillary pressure similar to (4.34):

$$p^C \;=\; -s^W\,\rho^{WR}\,\frac{\partial \psi^W}{\partial s^W}\,, \tag{4.101}$$

and its integration turns out as

$$\psi^W \;=\; -\int \frac{p^C}{s^W\,\rho^{WR}}\,\mathrm{d}\,s^W \,+\, f^W(\theta)\,. \tag{4.102}$$

In the framework of the present investigation, p^C could be inserted either based on the *Brooks & Corey* or *van Genuchten* laws given in (4.92). For example, the *Brooks & Corey* law, which has a simpler form for the purpose of integration with an assumption of $s_{eff} \approx s^W$, is inserted into (4.102) and free energy leads to

$$\psi^W \;=\; \frac{\lambda\,p^C}{\rho^{WR}} \,+\, f^W(\theta)\,. \tag{4.103}$$

Taking the derivative of ψ^W from (4.103) with respect to temperature and inserting ρ^{WR} from (4.96), the expression for $\frac{\partial \psi^W}{\partial \theta}$ is obtained

$$\frac{\partial \psi^W}{\partial \theta} \;=\; \frac{\lambda\,\gamma^W\,p^C}{\rho^{WR}} \,+\, \frac{\partial f^W(\theta)}{\partial \theta}\,. \tag{4.104}$$

Comparing (4.104) with $(4.100)_1$, the functions $f^W(\theta)$ and $g^W(s^W)$ are assigned

$$f^W(\theta) \;=\; -C_V^W\,(\theta\ln\theta \,-\, \theta) \quad \text{and} \quad g^W(s^W) \;=\; \frac{\lambda\,\gamma^W\,p^C}{\rho^{WR}}\,, \tag{4.105}$$

and the free *Helmholtz* energy for the water reads

$$\psi^W \;=\; \frac{\lambda\,p^C}{\rho^{WR}} \,-\, C_V^W\,(\theta\ln\theta \,-\, \theta)\,. \tag{4.106}$$

In the same way, the free *Helmholtz* energy of the supercritical CO_2 is defined. In this case instead of (4.34), the relation for $\frac{\partial \psi^L}{\partial \rho^{LR}}$ via p^{LR} obtained as a result of evaluation of the entropy principle is used:

$$p^{LR} = (\rho^{LR})^2 \frac{\partial \psi^L}{\partial \rho^{LR}} . \tag{4.107}$$

Integrating (4.107) with the pressure p^{LR} given by the *Peng-Robinson* EOS (4.97), ψ^L reads

$$\psi^L = R^L \theta \ln \frac{\rho^{LR}}{1 - b\,\rho^{LR}} - \frac{a\,\alpha_\omega}{2\sqrt{2}\,b} \ln \frac{1 - \sqrt{2} - b\,\rho^{LR}}{1 + \sqrt{2} - b\,\rho^{LR}} + f^L(\theta) . \tag{4.108}$$

The derivative of ψ^L with respect to θ based on (4.108) is

$$\frac{\partial \psi^L}{\partial \theta} = R^L \ln \frac{\rho^{LR}}{1 - b\,\rho^{LR}} + \frac{\partial f^L(\theta)}{\partial \theta} . \tag{4.109}$$

Comparing (4.109) and $(4.100)_2$, the functions $f^L(\theta)$ and $g^L(\rho^{LR})$ are defined as

$$f^L(\theta) = -C_V^L (\theta \ln \theta - \theta) \quad \text{and} \quad g^L(\rho^{LR}) = R^L \ln \frac{\rho^{LR}}{1 - b\,\rho^{LR}} . \tag{4.110}$$

Finally, proceeding from (4.108), ψ^L yields

$$\psi^L = R^L \theta \ln \frac{\rho^{LR}}{1 - b\,\rho^{LR}} - \frac{a\,\alpha_\omega}{2\sqrt{2}\,b} \ln \frac{1 - \sqrt{2} - b\,\rho^{LR}}{1 + \sqrt{2} - b\,\rho^{LR}} - C_V^L (\theta \ln \theta - \theta) . \tag{4.111}$$

Effective Stress, Entropy and Internal Energy:

It was mentioned in the previous sections that the effective fluid stresses $\mathbf{T}_E^W$ and $\mathbf{T}_E^L$ could be neglected in comparison to the mechanical part of the momentum production terms,

$$\mathbf{T}_E^W \approx 0 \quad \text{and} \quad \mathbf{T}_E^L \approx 0 . \tag{4.112}$$

The entropy function η^W is derived using $(4.36)_2$ and (4.106) as

$$\eta^W = C_V^W \ln \theta - \frac{\gamma^W p^{WR}}{\rho^{WR}} . \tag{4.113}$$

Similarly, the entropy function η^L is derived proceeding from $(4.36)_3$ and (4.111) in the form

$$\eta^L = C_V^L \ln \theta - R^L \ln \frac{\rho^{LR}}{1 - b\,\rho^{LR}} . \tag{4.114}$$

The internal energy of the fluid constituents can be obtained from the introduction of the *Helmholtz* energy via the *Legendre* transformation for entropy η^β and θ, cf. Appendix B, $\beta \in \{W, L\}$:

$$\psi^\beta := \varepsilon^\beta - \theta\,\eta^\beta . \tag{4.115}$$

4.5.4 Specific Constitutive Relations for Model II

This section introduces the constitutive relations for the water phase and both CO_2 phases in the frame of model II. Although the constitutive settings for the water and supercritical CO_2 have been already defined in Section 4.5.3, some of them will be briefly repeated and reformulated here. The main difference of model II compared to model I is in possessing the additional CO_2 phase and the mass production term in the balance relations, which is separately defined in Section 5.

Effective Density:

The effective density of the water phase φ^W is defined in (4.96). The effective densities ρ^{LR}, ρ^{GR} of the supercritical and gaseous CO_2 are defined via an expression presented in Appendix B. The effective pressures of the CO_2 phases are given by the *Peng-Robinson* EOS as follows

$$\begin{aligned} p^{LR} &= \frac{R^L\,\theta}{v^L - b} - \frac{a\,\alpha_\omega}{v^{L^2} + 2\,b\,v^L - b^2}\,, \\ p^{GR} &= \frac{R^G\,\theta}{v^G - b} - \frac{a\,\alpha_\omega}{v^{G^2} + 2\,b\,v^G - b^2}\,, \end{aligned} \tag{4.116}$$

where $v^L = 1/\rho^{LR}$ and $v^G = 1/\rho^{GR}$ are the specific volumes. The constants R^L and R^G, a, b and α_ω have the same value for both phases, since they are defined specifically for the CO_2 component and do not depend on the phase of CO_2. All required parameters are listed in (4.98).

Free Helmholtz Energies:

The free *Helmholtz* energies for the fluid constituents φ^W, φ^L and φ^G are derived here using the same algorithm as for model I. Thus, the free *Helmholtz* energy for the water phase $\psi^W(\theta,\, s^W)$ is derived based on the relations (4.99) and (4.62), namely,

$$\begin{aligned} C_V^W &= -\theta\,\frac{\partial^2\psi^W}{(\partial\theta)^2}\bigg|_{\rho^{WR}=\text{const}}\,, \\ p_{LW}^C &= s^L\,\rho^{LR}\,\frac{\partial\psi^L}{\partial s^L} - s^W\,\rho^{WR}\,\frac{\partial\psi^W}{\partial s^W}\,, \\ p_{GL}^C &= -s^L\,\rho^{LR}\,\frac{\partial\psi^L}{\partial s^L}\,. \end{aligned} \tag{4.117}$$

Integration of $(4.117)_1$ leads to

$$\frac{\partial\psi^W}{\partial\theta} = -\,C_V^W\ln\theta + g^W(s^W)\,. \tag{4.118}$$

Inserting $(4.117)_3$ into $(4.117)_2$, and then, integrating $(4.117)_2$ with respect to s^W, the ψ^W results in

$$\psi^W \;=\; \frac{\lambda\, p^C_{LW}}{\rho^{WR}} - \frac{p^C_{GL}}{\rho^{WR}} \ln s^W \;+\; f(\theta)\,. \tag{4.119}$$

Taking the derivative of ψ^W from (4.119) with respect to temperature and comparing to the (4.118), the ψ^W reads

$$\psi^W = \frac{\lambda\, p^C_{LW}}{\rho^{WR}} - \frac{p^C_{GL}}{\rho^{WR}} \ln s^W \;-\; C^W_V\,(\theta \ln \theta \;-\; \theta)\,. \tag{4.120}$$

The free *Helmholtz* energy ψ^L for the supercritical CO_2 is defined in $(4.47)_3$ as a function of the temperature θ, density ρ^{LR} and saturation s^L. Therefore, it would be reasonably to presume that $\psi^L\,(\theta, \rho^{LR}, s^L)$ should have a mixed form between the free energies depending on $(\theta, \rho^{\beta R})$ and on (θ, s^β). In order to derive $\psi^L\,(\theta, \rho^{LR}, s^L)$, the following relations are used:

$$\begin{aligned} C^L_V \;&=\; -\theta\, \frac{\partial^2 \psi^L}{(\partial\theta)^2}\bigg|_{\rho^{LR}=\text{const}}\,, \\ p^{LR} \;&=\; (\rho^{LR})^2\, \frac{\partial \psi^L}{\partial \rho^{LR}}\,, \\ p^C_{GL} \;&=\; -s^L\,\rho^{LR}\, \frac{\partial \psi^L}{\partial s^L}\,, \end{aligned} \tag{4.121}$$

where the first relation is a definition of the specific heat coefficient via the free energy function, and the next two relations appear during the evaluation of the entropy principle, cf. (4.55) and $(4.62)_2$. Assuming that the function $\psi^L\,(\theta, \rho^{LR}, s^L)$ can be presented by the sum of the functions explicitly depending on the internal variables θ, ρ^{LR}, s^L, the first relation in (4.121) after integration yields

$$\frac{\partial \psi^L}{\partial \theta} = -\,C^L_V \ln \theta \;+\; g^L\,(s^L) \;+\; h^L(\rho^{LR})\,. \tag{4.122}$$

The other relations in (4.121) after integration lead to

$$\psi^L \;=\; R^L\,\theta \ln \frac{\rho^{LR}}{1 \,-\, b\,\rho^{LR}} \;-\; \frac{a\,\alpha_\omega}{2\,\sqrt{2}\,b} \ln \frac{1 \,-\, \sqrt{2} \,-\, b\,\rho^{LR}}{1 \,+\, \sqrt{2} \,-\, b\,\rho^{LR}} \;+\; f^L(\theta) \;+\; g^L(s^L)\,, \tag{4.123}$$

and

$$\psi^L \;=\; \frac{\lambda\, p^C_{GL}}{\rho^{LR}} \;+\; h^L(\rho^{LR}) \;+\; f^L(\theta)\,. \tag{4.124}$$

Therein, $f^L(\theta)$, $g^L\,(s^L)$ and $h^L(\rho^{LR})$ are functions which have to be defined. This is done by solving the system of equations (4.122) - (4.124). Then, the ψ^L results in

$$\begin{aligned} \psi^L \;=\;& R^L\,\theta \ln \frac{\rho^{LR}}{1 \,-\, b\,\rho^{LR}} \;-\; \frac{a\,\alpha_\omega}{2\,\sqrt{2}\,b} \ln \frac{1 \,-\, \sqrt{2} \,-\, b\,\rho^{LR}}{1 \,+\, \sqrt{2} \,-\, b\,\rho^{LR}} \;-\; C^L_V\,(\theta \ln \theta \;-\; \theta) \;+ \\ &+ \frac{\lambda\, p^C_{GL}}{\rho^{LR}}\,. \end{aligned} \tag{4.125}$$

The free *Helmholtz* energy $\psi^G(\theta, \rho^{GR})$ for the gaseous CO_2 is defined based on the *Peng-Robinson* EOS and has the same form as the ψ^L for model I in (4.111), namely,

$$\psi^G = R^G \theta \ln \frac{\rho^{GR}}{1 - b\,\rho^{GR}} - \frac{a\,\alpha_\omega}{2\sqrt{2}\,b} \ln \frac{1 - \sqrt{2} - b\,\rho^{GR}}{1 + \sqrt{2} - b\,\rho^{GR}} - C_V^G(\theta \ln\theta - \theta)\,. \tag{4.126}$$

Effective Stress, Entropy and Internal Energy:

As for the other fluid constituents φ^W and φ^L, the effective stress $\mathbf{T}_E^G$ for φ^G is neglected in comparison to the mechanical part of the momentum production terms

$$\mathbf{T}_E^W \approx 0 \quad \text{and} \quad \mathbf{T}_E^L \approx 0 \quad \text{and} \quad \mathbf{T}_E^G \approx 0\,. \tag{4.127}$$

Proceeding from the relations for the free *Helmholtz* energies and the entropies in (4.65), the entropy functions η^W, η^L and η^G yield

$$\begin{aligned} \eta^W &= C_V^W \ln\theta - \frac{\gamma^W p^{WR}}{\rho^{WR}}\,, \\ \eta^L &= C_V^L \ln\theta - R^L \ln\frac{\rho^{LR}}{1 - b\,\rho^{LR}}\,, \\ \eta^G &= C_V^G \ln\theta - R^G \ln\frac{\rho^{GR}}{1 - b\,\rho^{GR}}\,. \end{aligned} \tag{4.128}$$

The internal energies are defined via the *Legendre* transformation in the same way as for model I, cf. (4.85).

Chapter 5:
Mass Interaction

One of the goals of the present investigation is to model the mass interaction process between two different phases of the CO_2 component. Within the framework of the present contribution, "mass interaction" means the same as "phase interaction", "phase exchange" or "phase transfer", although these definitions could be contradictory according to the classical theories.

This chapter focuses on the particular aspects needed to understand the phase transition process in detail. The discussion begins with the description of the existing constitutive relations for the mass production term $\hat{\rho}^\alpha$. After that, a new constitutive law for $\hat{\rho}^\alpha$ is introduced. At the end, the "switching mechanism" that distinguishes between the processes with phase transition ($\hat{\rho}^\alpha \neq 0$) and without phase transition ($\hat{\rho}^\alpha = 0$) can be found.

5.1 State of the Art

The derivation of the constitutive equation for the mass production term in the context of the TPM was discussed before in the literature by de Boer, Kowalski, Bluhm, Ricken and by others. For example, in the paper by de Boer & Kowalski [17], the considered model consists of three constituents φ^α, $\alpha \in \{S, L, G\}$ (solid, liquid, gas) and the mass exchange process takes place only between fluid constituents: $\hat{\rho}^L = -\,\hat{\rho}^G$, $\hat{\rho}^S = 0$. The constitutive equation for the mass production term $\hat{\rho}^L$ is proposed in the form:

$$\hat{\rho}^L \;=\; -\,\alpha^R\,(\mu^L \,-\, \mu^G)\,, \tag{5.1}$$

where α^R is a positive response parameter and μ^L, μ^G are defined as the chemical potentials for the liquid and the gaseous phases. The form of the constitutive equation (5.1) was chosen in order to satisfy the dissipation part of the entropy inequality:

$$\begin{aligned} \mathcal{D} \;=\;& \frac{1}{\theta}\,\mathrm{grad}\,\theta\cdot\mathbf{q} \,-\, (\overset{\prime}{\mathbf{x}}_L \,-\, \overset{\prime}{\mathbf{x}}_S)\cdot(\hat{\mathbf{p}}^L \,-\, \Lambda\,\mathrm{grad}\,n^L)\,- \\ &-(\overset{\prime}{\mathbf{x}}_G \,-\, \overset{\prime}{\mathbf{x}}_S)\cdot(\hat{\mathbf{p}}^G \,-\, \Lambda\,\mathrm{grad}\,n^G) \,-\, \hat{\rho}^L\,(\mu^L \,-\, \mu^G) \;\geq\; 0\,. \end{aligned} \tag{5.2}$$

where Λ is the *Lagrange*an multiplier, which can be interpreted as an "interface pressure", and the chemical potentials μ^β with $\beta \in \{L,\, G\}$ are defined as

$$\mu^\beta \;=\; \psi^\beta \,+\, \frac{1}{\rho^\beta}\,(n^\beta\,\Lambda \,+\, {\rho^\beta}^2\,\frac{\partial\psi^\beta}{\partial\rho^\beta})\,. \tag{5.3}$$

According to de Boer & Kowalski [17], the *Helmholtz* energies ψ^β in (5.3) do not depend on the saturation function s^β in comparison with the energies defined in the current contribution in (4.47). It leads to the minor difference between the dissipation part $\mathcal{D}$ given in (5.2) and $\mathcal{D}$ obtained in this work, cf. (4.56). Moreover, the aforementioned authors confirm that relation (5.1) is in good agreement with the main principles of the classical thermodynamics theory, where it is postulated that the mass-exchange process does not take place when the chemical potentials are equal to each other. However, this fact is valid only if additional assumptions about the equilibrium between the phases are done, cf. Section 3.5.3. Moreover, there are no numerical examples in this publication which can prove the suggested constitutive equation and no hints from the authors on how the coefficient α can be defined.

A similar form of the constitutive relation for the mass production term is suggested by de Boer & Bluhm [15], $\beta \in \{L, G\}$:

$$\hat{\rho}^\beta = -\,\xi^\beta \Big(\frac{\mu^\beta}{\theta^\beta} - \frac{\mu^S}{\theta^S} \Big) , \tag{5.4}$$

with a positive response parameter ξ^β. In comparison to (5.1), the mass production term (5.4) additionally depends on the temperature. Nevertheless, there is no indication as to how the response parameter has to be defined.

There are several other constitutive relations which have been derived specifically for the problem at hand. For example, in the paper by Ricken & Ustohalova [90], an organic mass-exchange term $\hat{\rho}^O$ is discussed and is defined as

$$\hat{\rho}^O = -\,\delta^O_{\psi^{OG}} \, \frac{1}{\theta} \, (\psi^O - \psi^G) , \tag{5.5}$$

wherein $\delta^O_{\psi^{OG}}$ defines a constant for the chemical potential functions Ψ^O and Ψ^G.

In the work published by Ricken *et al.* [89], the mass exchange between the solid and the nutrient phase ($\hat{\rho}^N = -\hat{\rho}^S$) in the case of biological tissues is considered such as

$$\begin{aligned} \hat{\rho}^S &= \hat{\rho}^S_{max} \, \hat{\rho}^S_{n^N} \, \hat{\rho}^S_{\tau_{vMi}} , \\ \hat{\rho}^S_{n^N} &= -\, e^{k_{n^N} \, (n^N)^2} + 1 , \\ \hat{\rho}^S_{\tau_v Mi} &= -\,2 \, e^{-\,log(2) \, \tau_{vMi}/\tau_{vMi0}} + 1 , \end{aligned} \tag{5.6}$$

where τ_{vMi} is the effective stress related to the distortion strain energy according to *von Mises* and n^N is the nutrient content. For the numerical examples presented in the aforementioned paper, the required material parameters from (5.6) were chosen by the authors in a way that the obtained solution is reasonable. It means that these parameters are defined for a specific case, and consequently, could not be used to describe the phase exchange process between CO_2 phases.

In Steeb *et al.* [98], where the erosion problem is considered, the mass production term for the solid constituent $\hat{\rho}^S$ is chosen proportionally to the intensity of the total fluid discharge $\mathbf{q}$:

$$\hat{\rho}^S = \xi(c, \phi) \, \rho^{SR} \, \mathbf{q} \cdot \mathbf{q} , \tag{5.7}$$

where the erosion modulus ξ has to be calibrated experimentally. There are also other variations of the constitutive relation, for example in the publications by Kruschwitz & Bluhm [64] and Kowalski [62].

It can be seen that up to now, the developed constitutive relations for $\hat{\rho}^\alpha$ were defined for specific cases without explanations on how to choose the parameters and corroborative numerical examples. It means that these relations could not be used for the CO_2 storage problem, and therefore, another constitutive relation is required. First endeavours to develop a constitutive relation for the mass production term, which in general can be used for any type of problem, are presented in the following.

5.2 Developed Constitutive Relation

In order to derive a constitutive relation for the mass production term, the entropy balance for the individual constituent φ^α is taken into consideration

$$\rho^\alpha\,(\eta^\alpha)'_\alpha = \operatorname{div}\,(-\frac{1}{\theta}\,\mathbf{q}^\alpha) + \frac{1}{\theta}\,\rho^\alpha\,r^\alpha + \hat{\zeta}^\alpha\,, \tag{5.8}$$

where η^α is the entropy and $\hat{\zeta}^\alpha$ is the entropy production term, which equals to

$$\hat{\zeta}^\alpha = \hat{\eta}^\alpha - \hat{\rho}^\alpha\eta^\alpha\,. \tag{5.9}$$

It is known that for a closed system the sum of the total entropy production terms has to be non-negative, cf. (3.49):

$$\sum_\alpha \hat{\eta}^\alpha \geq 0\,. \tag{5.10}$$

However, if the considered process is reversible as it is assumed to be in the present work, restriction (5.10) can be enforced in the sense that the sum of the entropy productions terms yields zero:

$$\sum_\alpha \hat{\eta}^\alpha = 0\,. \tag{5.11}$$

Substituting (5.9) into (5.8) with the assumption (5.11), the relation for the mass production term $\hat{\rho}^G = -\hat{\rho}^L$ can be easily derived as

$$\hat{\rho}^G = \frac{1}{\eta^G - \eta^L}\sum_\alpha \Big(-\operatorname{div}\,(\frac{1}{\theta}\,\mathbf{q}^\alpha) - \rho^\alpha(\eta^\alpha)'_\alpha + \frac{1}{\theta}\,\rho^\alpha\,r^\alpha\Big)\,. \tag{5.12}$$

Herein, the entropy change $\eta_G - \eta_L$ can be represented by definition through the enthalpy difference $\zeta_G - \zeta_L$ as

$$\eta_G - \eta_L = \frac{\zeta_G - \zeta_L}{\theta}\,. \tag{5.13}$$

Moreover, applying the divergence theorem to the term with the heat flux

$$\operatorname{div}\,(\frac{1}{\theta}\,\mathbf{q}^\alpha) = -\frac{1}{\theta^2}\,\mathbf{q}^\alpha\cdot\operatorname{grad}\theta + \frac{1}{\theta}\operatorname{div}\mathbf{q}^\alpha\,, \tag{5.14}$$

equation (5.12) is modified and leads to

$$\hat{\rho}^G = \frac{1}{\theta\,(\zeta^L - \zeta^G)} \sum_\alpha \Big(\theta^2 \rho^\alpha\,(\eta^\alpha)'_\alpha + \theta \operatorname{div} \mathbf{q}^\alpha - \mathbf{q}^\alpha \cdot \operatorname{grad}\theta - \theta\,\rho^\alpha\, r^\alpha\Big)\,. \tag{5.15}$$

The enthalpy difference is also called *latent heat* and represents the amount of energy which is necessary for the realisation of the phase transition process. It can be seen that if $\zeta_G = \zeta_L$, then the equation (5.15) can not be used for the calculation of the mass production term (zero in the denominator). It means that in this case the mass transition is not taking place, which is in agreement with the definition of the latent heat.

For a full description of the mass-exchange process between the phases, some type of switching mechanism indicating whether the phase transition takes place or not, should be defined.

5.2.1 Switching criterion

One of the ways to define a switching criterion is based on the principle from the *theory of plasticity*, where a certain yielding surface splits the stress domain into the elastic and plastic regions. In case of the mass transition process, the "yielding surface" can be represented by a phase transition surface in the three-dimensional space shown in Figure 3.5. Based on the position of a point (p, ν, θ) on the phase diagram, the phase region, where the points are located, can be determined. In order to implement this criterion, an equation for a transition surface has to be derived. This is not straightforward to accomplish because of the complicated shape of this surface. The alternative method would be to use so-called *lookup tables*, where the $p - \nu - \theta$ data are collected. The *lookup-table* concept is widely used and can be taken as a reference methodology to define the state of a substance. However, the idea within the current work is to find a more general switching criterion, which can be also used in the future for other substances, even if there is no *lookup-table* data available.

The criterion suggested here is based on a combined condition between the saturation functions and chemical potentials, which are taken in the form defined in (3.71). This criterion proceeds from the fact that, in the phase diagram, there are regions occupied only by one phase, where the saturation can be determine as $s^\beta = 1$ or $s^\beta = 0$ and no mass transition takes place. In contrast, in phase diagram there are also transition curves (surfaces), where the saturation has a value between $0 < s^\beta < 1$ and a mass-exchange process may occur. However, the last aspect should be checked supplementary, and thus, some type of additional constraint is required. This refers to the idea of using the relation between the chemical potentials during the phase transition process discussed in Section 3.5.3. Having a look at the dissipative part of the entropy inequality (4.56) and remembering that in the current investigation, a system with non-dissipative, fully reversible processes is under consideration, the next condition is deduced: if the chemical potentials of two phases are equal, a phase transition process can occur, otherwise, there is no mass transfer.

Finally, the switching criterion for the phase transition process between two phases L and G is stated as a correlation of a relation between the chemical potentials μ^L, μ^G and saturation functions s^L, s^G and reads

$$\begin{array}{llllll}
\text{if} & s^G = 1,\, s^L = 0 & \text{or} & s^G = 0\,,\, s^L = 1\,, & \text{then} & \hat{\rho}^G = 0\,; \\
\text{if} & 0 < s^G,\, s^L < 1 & \text{and} & \mu^L = \mu^G\,, & \text{then} & \hat{\rho}^G \neq 0\,; \\
\text{if} & 0 < s^G,\, s^L < 1 & \text{and} & \mu^L \lessgtr \mu^G\,, & \text{then} & \hat{\rho}^G = 0\,.
\end{array} \tag{5.16}$$

In the current work, a relation between calculated chemical potentials for the phases is used in the simulations as an indicator of the phase transition process.

Chapter 6: Numerical Treatment

This chapter concerns the solution procedure for the system of partial differential equations associated with the problem studied herein. The best way to solve such a system of equations is to obtain its analytical solution, which can be difficult to achieve for the challenging problems discussed in the present work. Alternatively, an approximate solution can be derived using an appropriate numerical method.

In this context, the numerical solution of the governing equations from Section 4 presented by the partial differential equations (PDE) is introduced. The PDE with the corresponding boundary and initial conditions constitute an initial-boundary-value problem (IBVP). Herein, the IBVP is formulated for the weak (integral) form of the PDE based on the fact that the strong form of the PDE is too strict for numerical solution of the considered problem. However, for several relatively simple numerical examples presented in Section 7, the strong formulation of the problem is used. A derivation of the weak form of the equations, the required ansatz and test functions are presented in this chapter and valid for the Finite-Element Solver PANDAS. Furthermore, the obtained equations should be discretised in order to solve the postulated IBVP. This is accomplished using the finite-element method (FEM) in the spatial domain and by the implicit *Euler* method in the temporal domain.

6.1 Weak Formulations of the Governing Equations

The transformation of the strong form of the governing equations into the corresponding weak form requires several steps. Firstly, the trial (ansatz) and test functions have to be defined. Then, each governing equation is multiplied by the corresponding test function and integrated over the domain Ω using the *Gauss* theorem, cf. Appendix B. At the end, it results in the weak formulation of the problem.

Herein, the trial functions are defined as follows

$$\begin{array}{lclclclclcll}
\mathcal{S}_{\mathbf{u}_S}(t) & = & \{\, \mathbf{u}_S & \in & H^1(\Omega)^d & : & \mathbf{u}_S\,(\mathbf{x}) & = & \bar{\mathbf{u}}_S\,(\mathbf{x},t) & \text{on} & \Gamma_{\mathbf{u}_S} & \}\,, \\
\mathcal{S}_{p^{WR}}(t) & = & \{\, p^{WR} & \in & H^1(\Omega) & : & p^{WR}\,(\mathbf{x}) & = & \bar{p}^{WR}\,(\mathbf{x},t) & \text{on} & \Gamma_{p^{WR}} & \}\,, \\
\mathcal{S}_{p^{LR}}(t) & = & \{\, p^{LR} & \in & H^1(\Omega) & : & p^{LR}\,(\mathbf{x}) & = & \bar{p}^{LR}\,(\mathbf{x},t) & \text{on} & \Gamma_{p^{LR}} & \}\,, \\
\mathcal{S}_{p^{GR}}(t) & = & \{\, p^{GR} & \in & H^1(\Omega) & : & p^{GR}\,(\mathbf{x}) & = & \bar{p}^{GR}\,(\mathbf{x},t) & \text{on} & \Gamma_{p^{GR}} & \}\,, \\
\mathcal{S}_{\theta}(t) & = & \{\, \theta & \in & H^1(\Omega) & : & \theta\,(\mathbf{x}) & = & \bar{\theta}\,(\mathbf{x},t) & \text{on} & \Gamma_{\theta} & \}\,,
\end{array} \tag{6.1}$$

where $H^1(\Omega)$ represents the *Sobolev* space with $d \in \{1, 2, 3\}$ as a dimension of the problem and $\Gamma_{(\cdot)}$ the boundaries of the domain Ω for a corresponding primary variable.

Any boundary $\Gamma_{(\cdot)}$ can be usually split into two regions: the *Dirichlet* boundary, where the value of the primary variable itself is specified, and the *Neumann* boundary, where the flux over the boundary is given. Respectively to the primary variables chosen for the current investigation, the *Dirichlet* boundary conditions are presented on $\Gamma_{\mathbf{u}_S}$, $\Gamma_{p^{WR}}$, $\Gamma_{p^{LR}}$, $\Gamma_{p^{GR}}$ and Γ_θ, the *Neumann* boundary conditions on $\Gamma_{\mathbf{t}}$, Γ_{v^W}, Γ_{v^L}, Γ_{v^G} and Γ_q and $\emptyset$ denotes an empty set:

$$\begin{array}{lllllllll} \Gamma & = & \Gamma_{\mathbf{u}_S} & \cup & \Gamma_{\mathbf{t}}\,, & \Gamma_{\mathbf{u}_S} & \cap & \Gamma_{\mathbf{t}} & = \emptyset\,, \\ \Gamma & = & \Gamma_{p^{WR}} & \cup & \Gamma_{v^W}\,, & \Gamma_{p^{WR}} & \cap & \Gamma_{v^W} & = \emptyset\,, \\ \Gamma & = & \Gamma_{p^{LR}} & \cup & \Gamma_{v^L}\,, & \Gamma_{p^{LR}} & \cap & \Gamma_{v^L} & = \emptyset\,, \\ \Gamma & = & \Gamma_{p^{GR}} & \cup & \Gamma_{v^G}\,, & \Gamma_{p^{GR}} & \cap & \Gamma_{v^G} & = \emptyset\,, \\ \Gamma & = & \Gamma_{\theta} & \cup & \Gamma_{q}\,, & \Gamma_{\theta} & \cap & \Gamma_{q} & = \emptyset\,. \end{array} \tag{6.2}$$

The test functions of the corresponding primary variables disappear on the *Dirichlet* boundaries and are defined as

$$\begin{array}{lllllllll} \mathcal{T}_{\mathbf{u}_S} & = & \{\, \delta\mathbf{u}_S & \in & H^1(\Omega)^d & : & \delta\mathbf{u}_S\,(\mathbf{x}) & = \mathbf{0} & \text{on } \Gamma_{\mathbf{u}_S} \,\}\,, \\ \mathcal{T}_{p^{WR}} & = & \{\, \delta p^{WR} & \in & H^1(\Omega) & : & \delta p^{WR}\,(\mathbf{x}) & = 0 & \text{on } \Gamma_{p^{WR}} \,\}\,, \\ \mathcal{T}_{p^{LR}} & = & \{\, \delta p^{LR} & \in & H^1(\Omega) & : & \delta p^{LR}\,(\mathbf{x}) & = 0 & \text{on } \Gamma_{p^{LR}} \,\}\,, \\ \mathcal{T}_{p^{GR}} & = & \{\, \delta p^{GR} & \in & H^1(\Omega) & : & \delta p^{GR}\,(\mathbf{x}) & = 0 & \text{on } \Gamma_{p^{GR}} \,\}\,, \\ \mathcal{T}_{\theta} & = & \{\, \delta\theta & \in & H^1(\Omega) & : & \delta\theta\,(\mathbf{x}) & = 0 & \text{on } \Gamma_{\theta} \,\}\,. \end{array} \tag{6.3}$$

Further, the weak form of the governing equations for both models, I and II, can be represented. In this regard, based on the set of equations (4.37) - (4.39) for model I, the weak form of the momentum balance for the overall aggregate leads to

$$\begin{aligned} \mathcal{G}_{\mathbf{u}_S} \;=\; & \int\limits_\Omega (\mathbf{T}^S_E - p^{FR}\,\mathbf{I}) \cdot \operatorname{grad}\delta\mathbf{u}_S\,\mathrm{d}v - \int\limits_\Omega \rho\,\mathbf{b}\cdot\delta\mathbf{u}_S\,\mathrm{d}v - \\ & - \int\limits_{\Gamma_{\mathbf{t}}} \bar{\mathbf{t}}\cdot\delta\mathbf{u}_S\,\mathrm{d}a \;=\; 0\,, \end{aligned} \tag{6.4}$$

where $\bar{\mathbf{t}} = (\mathbf{T}^S_E - p^{FR}\,\mathbf{I})\,\mathbf{n}$ is an external load vector acting on the boundary $\Gamma_{\mathbf{t}}$ with outward-oriented normal $\mathbf{n}$.

The weak from of the mass balances for the water and supercritical CO_2 phases yield

$$\begin{aligned} \mathcal{G}_{p^{WR}} \;=\; & \int\limits_\Omega \{(\rho^W)'_S + \rho^W \operatorname{div}(\mathbf{u}_S)'_S\}\,\delta p^{WR}\,\mathrm{d}v - \int\limits_\Omega \rho^W\,\mathbf{w}_W \cdot \operatorname{grad}\delta p^{WR}\,\mathrm{d}v + \\ & + \int\limits_{\Gamma_{v^W}} \bar{v}^W\,\delta p^{WR}\,\mathrm{d}a \;=\; 0\,, \end{aligned} \tag{6.5}$$

and

$$\begin{aligned}\mathcal{G}_{p^{LR}} \;=\; & \int\limits_{\Omega} \{(\rho^L)'_S \,+\, \rho^L \operatorname{div}(\mathbf{u}_S)'_S\}\,\delta p^{LR}\,\mathrm{d}v \,-\, \int\limits_{\Omega} \rho^L\,\mathbf{w}_L \,\cdot\, \operatorname{grad}\delta p^{LR}\,\mathrm{d}v\,+ \\ & +\int\limits_{\Gamma_{v^L}} \bar{v}^L\,\delta p^{LR}\,\mathrm{d}a \,=\, 0\,,\end{aligned} \tag{6.6}$$

where $\bar{v}^W = \rho^W \mathbf{w}_W \cdot \mathbf{n}$ and $\bar{v}^L = \rho^L \mathbf{w}_L \cdot \mathbf{n}$ are the mass effluxes over the boundaries Γ_{v^W} and Γ_{v^L}, respectively.

Based on (4.39) the weak form of the energy balance for the overall aggregate reads

$$\begin{aligned}\mathcal{G}_\theta \;=\; & \int\limits_{\Omega} \{\rho^S\,(\varepsilon^S)'_S \,-\, \mathbf{T}^S_E \cdot \mathbf{L}_S \,+\, \rho^W\,(\varepsilon^W)'_W \,+\hat{\mathbf{p}}^W \cdot \mathbf{w}_W\,+ \\ & +\rho^L\,(\varepsilon^L)'_L \,+\hat{\mathbf{p}}^L \cdot \mathbf{w}_L \,+\, p^{FR}\operatorname{div}(\mathbf{u}_S)'_S\,\}\,\delta\theta\,\mathrm{d}v\,- \\ & -\int\limits_{\Omega} \{\mathbf{q} \,+\, n^W p^{WR}\,\mathbf{w}_W \,+\, n^L p^{LR}\,\mathbf{w}_L\} \,\cdot\, \operatorname{grad}\delta\theta\,\mathrm{d}v\,+ \\ & +\int\limits_{\Gamma_q} \bar{q}\,\delta\theta\,\mathrm{d}a \,=\, 0\,,\end{aligned} \tag{6.7}$$

where the *Neumann* boundary conditions on Γ_q are governed by $\bar{q} = (\mathbf{q} + n^W p^{WR}\,\mathbf{w}_W + n^L p^{LR}\,\mathbf{w}_L) \cdot \mathbf{n} = (\mathbf{q}^S + \mathbf{q}^W + \mathbf{q}^L + n^W p^{WR}\,\mathbf{w}_W + n^L p^{LR}\,\mathbf{w}_L) \cdot \mathbf{n}$.

Similarly to model I, the weak formulation for model II is presented in the following based on the set of the governing equations (4.66) - (4.68). The weak form of the momentum balance reads

$$\begin{aligned}\mathcal{G}_{\mathbf{u}_S} \;=\; & \int\limits_{\Omega} (\mathbf{T}^S_E \,-\, p^{FR}\,\mathbf{I}) \,\cdot\, \operatorname{grad}\delta\mathbf{u}_S\,\mathrm{d}v \,-\, \int\limits_{\Omega} \rho\,\mathbf{b} \cdot \delta\mathbf{u}_S\,\mathrm{d}v\,- \\ & -\int\limits_{\Omega} \hat{\rho}^G\,(\mathbf{w}_L \,-\, \mathbf{w}_G)\,\delta\mathbf{u}_S\,\mathrm{d}v \,-\, \int\limits_{\Gamma_{\mathbf{t}}} \bar{\mathbf{t}} \cdot \delta\mathbf{u}_S\,\mathrm{d}a \,=\, 0\,,\end{aligned} \tag{6.8}$$

with the external load vector: $\bar{\mathbf{t}} = (\mathbf{T}^S_E \,-\, p^{FR}\,\mathbf{I})\,\mathbf{n}$.

The weak mass balances are presented correspondingly for the water and both CO_2 phases:

$$\begin{aligned}\mathcal{G}_{p^{WR}} \;=\; & \int\limits_{\Omega} \{(\rho^W)'_S \,+\, \rho^W \operatorname{div}(\mathbf{u}_S)'_S\}\,\delta p^{WR}\,\mathrm{d}v \,-\, \int\limits_{\Omega} \rho^W\,\mathbf{w}_W \,\cdot\, \operatorname{grad}\delta p^{WR}\,\mathrm{d}v\,+ \\ & +\int\limits_{\Gamma_{v^W}} \bar{v}^W\,\delta p^{WR}\,\mathrm{d}a \,=\, 0\,,\end{aligned} \tag{6.9}$$

where $\bar{v}^W = \rho^W \mathbf{w}_W \cdot \mathbf{n}$;

$$
\begin{aligned}
\mathcal{G}_{p^{LR}} \;=\; & \int\limits_{\Omega} \{(\rho^L)'_S \,+\, \rho^L \operatorname{div}(\mathbf{u}_S)'_S\}\,\delta p^{LR}\,\mathrm{d}v \;-\; \int\limits_{\Omega} \rho^L\,\mathbf{w}_L \,\cdot\, \operatorname{grad}\delta p^{LR}\,\mathrm{d}v \,- \\
& - \int\limits_{\Omega} \hat{\rho}^L\,\delta p^{LR}\,\mathrm{d}v \,+\, \int\limits_{\Gamma_{v^L}} \bar{v}^L\,\delta p^{LR}\,\mathrm{d}a \;=\; 0\,,
\end{aligned}
\tag{6.10}
$$

with $\bar{v}^L = \rho^L \mathbf{w}_L \cdot \mathbf{n}$;

$$
\begin{aligned}
\mathcal{G}_{p^{GR}} \;=\; & \int\limits_{\Omega} \{(\rho^G)'_S \,+\, \rho^L \operatorname{div}(\mathbf{u}_S)'_S\}\,\delta p^{GR}\,\mathrm{d}v \;-\; \int\limits_{\Omega} \rho^G\,\mathbf{w}_G \,\cdot\, \operatorname{grad}\delta p^{GR}\,\mathrm{d}v \,- \\
& - \int\limits_{\Omega} \hat{\rho}^G\,\delta p^{GR}\,\mathrm{d}v \,+\, \int\limits_{\Gamma_{v^G}} \bar{v}^G\,\delta p^{GR}\,\mathrm{d}a \;=\; 0\,,
\end{aligned}
\tag{6.11}
$$

where $\bar{v}^G = \rho^G \mathbf{w}_G \cdot \mathbf{n}$.

Based on (4.68) the energy balance in the weak form leads to

$$
\begin{aligned}
\mathcal{G}_{\theta} \;=\; & \int\limits_{\Omega} \{\rho^S\,(\varepsilon^S)'_S \,-\, \mathbf{T}^S_E \cdot \mathbf{L}_S \,+\, p^{FR} \operatorname{div}(\mathbf{u}_S)'_S \,+\, \rho^W\,(\varepsilon^W)'_W \,+\, \hat{\mathbf{p}}^W \cdot \mathbf{w}_W \,+ \\
& + \rho^L\,(\varepsilon^L)'_L \,+ \hat{\mathbf{p}}^L \cdot \mathbf{w}_L \,+\, \rho^G\,(\varepsilon^G)'_G \,+ \hat{\mathbf{p}}^G \cdot \mathbf{w}_G - \\
& - \hat{\rho}^G\,(\varepsilon^L \,-\, \varepsilon^G \,+\, \tfrac{1}{2}\,\mathbf{w}_L \cdot \mathbf{w}_L \,-\, \tfrac{1}{2}\,\mathbf{w}_G \cdot \mathbf{w}_G)\}\,\delta\theta\,\mathrm{d}v \,+ \\
& - \int\limits_{\Omega} \{\mathbf{q} \,+\, n^W p^{WR}\,\mathbf{w}_W \,+\, n^L p^{LR}\,\mathbf{w}_L \,+\, n^G p^{GR}\,\mathbf{w}_G\} \,\cdot\, \operatorname{grad}\delta\theta\,\mathrm{d}v \,+ \\
& + \int\limits_{\Gamma_q} \bar{q}\,\delta\theta\,\mathrm{d}a \;=\; 0\,,
\end{aligned}
\tag{6.12}
$$

where $\bar{q} = (\mathbf{q} + n^W p^{WR}\,\mathbf{w}_W + n^L p^{LR}\,\mathbf{w}_L + n^G p^{GR}\,\mathbf{w}_G) \cdot \mathbf{n}$.

6.2 Spatial and Time Discretisation

The numerical solution of an IBVP requires the discretisation of the weak form of the governing equations in space and time. Within the current work, a spatial discretisation is carried out by the FEM, whereas a time integration is implemented by the implicit *Euler* method. For more comprehensive information about FEM, the readership is referred to Zienkiewicz & Taylor [106], Segerlind [93], Hughes [59] among others. The particular information about the FE procedure in the frame of the TPM is given in Ammann [3], Ellsiepen [48].

6.2.1 Finite-Element Method in Space

The FEM is a numerical algorithm used to define an approximate solution of differential equations describing the different physical processes. To be more precise, the domain Ω is approximated by a spatially discretised domain Ω^h, which is represented by the union of the non-overlapping subdomains Ω_e:

$$\Omega \approx \Omega^h = \bigcup_{e=1}^{N_e} \Omega_e \,, \tag{6.13}$$

where N_e is a number of the subdomains (FE). The corresponding number of nodes is denoted as N_n.

Correspondingly, the infinite dimensional trial space $\mathcal{S}_{(\cdot)}(t)$ defined in (6.1) and test space $\mathcal{T}_{(\cdot)}$ from (6.3) could be transformed into the corresponding discrete spaces $\mathcal{S}^h_{(\cdot)}(t)$ and $\mathcal{T}^h_{(\cdot)}$, where the discrete trial functions for both models, I and II, are defined as

$$\begin{array}{lllllll}
\mathbf{u}_S(\mathbf{x},t) & \approx \mathbf{u}^h_S(\mathbf{x},t) & = & \bar{\mathbf{u}}^h_S(\mathbf{x},t) & + & \displaystyle\sum_{j=1}^{N_n} \boldsymbol{\phi}^j_{\mathbf{u}_S}(\mathbf{x})\, \mathbf{u}^j_S(t) & \in \mathcal{S}^h_{\mathbf{u}_S}(t)\,, \\
p^{WR}(\mathbf{x},t) & \approx p^{WR^h}(\mathbf{x},t) & = & \bar{p}^{WR^h}(\mathbf{x},t) & + & \displaystyle\sum_{j=1}^{N_n} \phi^j_{p^{WR}}(\mathbf{x})\, p^{WR^j}(t) & \in \mathcal{S}^h_{p^{WR}}(t)\,, \\
p^{LR}(\mathbf{x},t) & \approx p^{LR^h}(\mathbf{x},t) & = & \bar{p}^{LR^h}(\mathbf{x},t) & + & \displaystyle\sum_{j=1}^{N_n} \phi^j_{p^{LR}}(\mathbf{x})\, p^{LR^j}(t) & \in \mathcal{S}^h_{p^{LR}}(t)\,, \\
p^{GR}(\mathbf{x},t) & \approx p^{GR^h}(\mathbf{x},t) & = & \bar{p}^{GR^h}(\mathbf{x},t) & + & \displaystyle\sum_{j=1}^{N_n} \phi^j_{p^{GR}}(\mathbf{x})\, p^{GR^j}(t) & \in \mathcal{S}^h_{p^{GR}}(t)\,, \\
\theta(\mathbf{x},t) & \approx \theta^h(\mathbf{x},t) & = & \bar{\theta}^h(\mathbf{x},t) & + & \displaystyle\sum_{j=1}^{N_n} \phi^j_{\theta}(\mathbf{x})\, \theta^j(t) & \in \mathcal{S}^h_{\theta}(t)\,.
\end{array} \tag{6.14}$$

Therein, $\bar{\mathbf{u}}^h_S$, $\bar{p}^{WR^h}$, $\bar{p}^{LR^h}$, $\bar{p}^{GR^h}$ and $\bar{\theta}^h$ represent the *Dirichlet* boundary conditions. The functions $\boldsymbol{\phi}^j_{\mathbf{u}_S} = \{\phi^j_{u1}, ...\phi^j_{ud}\}$, $\phi^j_{p^{WR}}$, $\phi^j_{p^{LR}}$, $\phi^j_{p^{GR}}$ and ϕ^j_θ are the global basis functions of the respective trial functions, which correspond to the set of the nodal points N_n and normalised such that

$$\begin{array}{lll}
\phi^j(\mathbf{x}) & = 0, & \text{if } \ \mathbf{x} \notin \displaystyle\bigcup_{e \in N_{ej}} \Omega_e \,,\ j = 1, ..., N_n \,, \\
\phi^j_d(\mathbf{x}_i) & = \delta^j_i, & \qquad i, j = 1, ..., N_n \,,
\end{array} \tag{6.15}$$

where δ^j_i is the *Kronecker* symbol. The nodal values of the primary variables or the so-called degrees of freedom (DOF) $\mathbf{u}^j_S$, p^{WR^j}, p^{LR^j}, p^{GR^j}, θ^j depend only on time t, while the basis functions depend only on the spatial position $\mathbf{x}$.

In order to derive the discrete test functions, the *Bubnov-Galerkin* approximate method is applied. In the framework of this method, the equal global basis functions are used for trial and test functions. Moreover, in contrast to the discrete trial functions, the discrete test functions disappear at the *Dirichlet* boundaries $\Gamma_{\mathbf{u}_S}$, $\Gamma_{p^{WR}}$, $\Gamma_{p^{LR}}$, $\Gamma_{p^{GR}}$ and Γ_θ and are given in the following form

$$\begin{aligned}
\delta\mathbf{u}_S(\mathbf{x}) &\approx \delta\mathbf{u}_S^h(\mathbf{x}) = \sum_{j=1}^{N_n} \boldsymbol{\phi}^j_{\mathbf{u}_S}(\mathbf{x})\,\delta\mathbf{u}_S^j && \in \mathcal{T}^h_{\mathbf{u}_S}\,,\\
\delta p^{WR}(\mathbf{x}) &\approx \delta p^{WR^h}(\mathbf{x}) = \sum_{j=1}^{N_n} \phi^j_{p^{WR}}(\mathbf{x})\,\delta p^{WRj} && \in \mathcal{T}^h_{p^{WR}}\,,\\
\delta p^{LR}(\mathbf{x}) &\approx \delta p^{LR^h}(\mathbf{x}) = \sum_{j=1}^{N_n} \phi^j_{p^{LR}}(\mathbf{x})\,\delta p^{LRj} && \in \mathcal{T}^h_{p^{LR}}\,,\\
\delta p^{GR}(\mathbf{x}) &\approx \delta p^{GR^h}(\mathbf{x}) = \sum_{j=1}^{N_n} \phi^j_{p^{GR}}(\mathbf{x})\,\delta p^{GRj} && \in \mathcal{T}^h_{p^{GR}}\,,\\
\delta\theta(\mathbf{x}) &\approx \delta\theta^h(\mathbf{x}) = \sum_{j=1}^{N_n} \phi^j_{\theta}(\mathbf{x})\,\delta\theta^j && \in \mathcal{T}^h_{\theta}\,.
\end{aligned} \tag{6.16}$$

The whole procedure of the spatial discretisation leads to a system of linear independent equations for each unknown nodal quantity (each DOF). However, for the multiphasic problem modelled in the present work, several primary variables appear in all equations of the coupled system of equations. Thus they have to be approximated simultaneously. It requires the modification of the FE within the FEM to the so-called mixed FE.

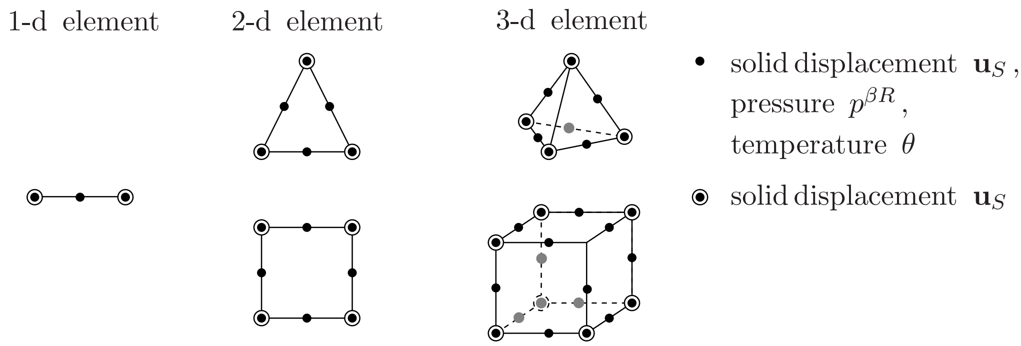

Figure 6.1: 1-d, 2-d and 3-d *Taylor-Hood* elements.

In the framework of the mixed finite element formulation, a proper choice of the trial functions is based on the *Ladyzhenskaya-Babuška-Brezzi* conditions (or inf-sup conditions), which have to be fulfilled to prevent possible oscillations in the numerical solution, cf. Brezzi & Fortin [22], Zienkiewicz *et al.* [105]. Based on the weak form of the equations from Section 6.1, assumptions about the order of approximation of the primary variables can be made. To obtain an equal order of the variables belonging to one equation, quadratic basis functions are chosen for the displacement $\mathbf{u}_S^h$ and linear basis functions for the fluid pressure p^{WR^h}, p^{LR^h}, p^{GR^h} and temperature θ^h. In this context, the mixed FE is designed to consider the aforementioned conditions and is used for the spatial discretisation of the studied problem, was suggested by *Taylor* and *Hood* and is shown in Figure 6.1.

Numerical Integration:

For the numerical treatment of the integral representation of the governing equations within the FE implementation, the equations should be reformulated with respect to the local coordinates $\boldsymbol{\xi}$ of the element. This can be carried out, for example, by the *Gauss* quadrature method, cf. Ellsiepen [48], Zienkiewicz & Taylor [106]. Using this numerical integration technique and the geometrical relation of the local coordinates $\boldsymbol{\xi}$ to the global coordinates $\mathbf{x}$ via $\boldsymbol{\xi} \mapsto \mathbf{x} = \mathbf{h}^e(\boldsymbol{\xi})$, an integral can be approximated as follows

$$\int\limits_{\Omega_e} f(\mathbf{x})\,\mathrm{d}\mathbf{x} = \sum_{k=1}^{N_k} f(\mathbf{h}^e(\boldsymbol{\xi}_k))J_e(\boldsymbol{\xi}_k)\,\omega_k\,. \tag{6.17}$$

Therein, N_k is the number of integration (*Gauss*) points $\boldsymbol{\xi}_k$, ω_k is a certain weight factor and J_e denotes the *Jacobi*an determinant.

Semi-Discrete Initial-Value Problem:

Up to this point, the considered problem is discretised only in the spatial domain, but still depends on time. This fact leads to the formulation of the semi-discrete initial-value problem. Afterwards, the suitable discretisation method for the temporal domain can be defined.

In this context, the system of the governing equations leads to

$$\boldsymbol{F}(t,\,\boldsymbol{u},\,\boldsymbol{u}') = \boldsymbol{M}\,\boldsymbol{u}' + \boldsymbol{k}(\boldsymbol{u}) - \boldsymbol{f} = \mathbf{0} \quad \text{with} \quad \boldsymbol{u}(t_0) = \boldsymbol{u}_0\,, \tag{6.18}$$

where $\boldsymbol{M}$ is the generalised mass matrix, $\boldsymbol{k}$ the generalised stiffness vector and $\boldsymbol{f}$ the generalised force vector, cf. Ammann [3], Acartürk [2]. The space-discrete vector $\boldsymbol{u}$ is defined at N_n nodal points and consists of all DOF:

$$\boldsymbol{u} = [(\mathbf{u}_S^1,\,p^{WR^1},\,p^{LR^1},\,p^{GR^1},\,\theta^1),\cdots,(\mathbf{u}_S^{N_n},\,p^{WR^{N_n}},\,p^{LR^{N_n}},\,p^{GR^{N_n}},\,\theta^{N_n})]^T\,. \tag{6.19}$$

For the simplification of this formulation, it is assumed that all DOF are approximated by the same order, or in other words, at each nodal point all primary variables are present, although this is not the case for the used *Taylor - Hood* element.

It should be noted that, if plastic deformations are taken into consideration, the plastic evaluation equations and additional space-discrete variables should be included into (6.18), cf. Graf [53], Karajan [60].

6.2.2 Time Integration

In order to complete the whole discretisation procedure, a suitable discretisation scheme for the time domain should be defined. Within a wide range of available numerical schemes generally given by the series of *Runge-Kutta* methods, the implicit (backward) *Euler* scheme is chosen here to carry out the time discretisation. Numerical methods considering explicit schemes are not unconditionally stable compared to implicit ones and might lead to the unstable results or require high numerical efforts, because of a choice of a relatively small time step. Therefore, the explicit schemes are not applied here.

The implicitness of the scheme can be explained by the form of an approximate solution for the standard first order PDE $y' = f(x, y)$ such as

$$y_{n+1} = y_n + h\, f(x_{n+1},\, y_{n+1}), \quad n = 0, 1, \dots, \tag{6.20}$$

where y_{n+1} is obtained implicitly via y_n and h is the step size, cf. Kreyszig [63].

Regarding the numerical problem discussed in this work, the time derivative of vector $\boldsymbol{u}$ depending on time t_{n+1} is discretised as

$$\boldsymbol{u}'(t_{n+1}) = \boldsymbol{u}'_{n+1} = \frac{\Delta \boldsymbol{u}_{n+1}}{\Delta t_{n+1}} = \frac{\boldsymbol{u}_{n+1} - \boldsymbol{u}_n}{t_{n+1} - t_n} \tag{6.21}$$

where n denotes the old time step. More details about time integration schemes can be found, for instance, in Ellsiepen [48], Ammann [3].

6.2.3 Solution Procedure

Substituting (6.21) into (6.18) yields the following system of nonlinear equations:

$$\boldsymbol{F}_{n+1}\,(t_{n+1},\, \boldsymbol{u}_{n+1},\, \boldsymbol{u}'_{n+1}) = \boldsymbol{M}\,\boldsymbol{u}'_{n+1} + \boldsymbol{k}\,(\boldsymbol{u}_{n+1}) - \boldsymbol{f}_{n+1} = \boldsymbol{0}\,. \tag{6.22}$$

In the current work, this system of equations is solved by the *Newton-Raphson* iteration method. This method consists of several iterative steps within each time step. In order to apply the *Newton-Raphson* method to the actual problem, firstly, the global tangent should be defined. In this work, the global tangent is calculated numerically at each step, and according to Eipper [47] it reads

$$\mathrm{D}\boldsymbol{F}^k_{n+1} = \frac{\mathrm{d}\boldsymbol{F}^k_{n+1}}{\mathrm{d}\boldsymbol{u}^k_{n+1}}\,. \tag{6.23}$$

After obtaining the global tangent of the system $\mathrm{D}\boldsymbol{F}^k_{n+1}$, a system of equations

$$\mathrm{D}\boldsymbol{F}^k_{n+1}\,\Delta\boldsymbol{u}^k_{n+1} = -\,\boldsymbol{F}^k_{n+1} \tag{6.24}$$

has to be solved at an iteration step k and time t_{n+1}, where the solution vector

$$\boldsymbol{u}^{k+1}_{n+1} = \boldsymbol{u}^k_{n+1} + \Delta\boldsymbol{u}^k_{n+1} \tag{6.25}$$

is updated until the remainder or the so-called residual part $\boldsymbol{R}^{k+1}_{n+1}$ becomes less than a certain tolerance value $\varepsilon_{\mathrm{tol}}$:

$$\|\boldsymbol{F}^{k+1}_{n+1}\| = \|\boldsymbol{R}^{k+1}_{n+1}\| < \varepsilon_{\mathrm{tol}}\,, \tag{6.26}$$

The details on the steps discussed above could be found in Ellsiepen [48], Ehlers & Ellsiepen [44] and Eipper [47].

Chapter 7: Numerical Application

This chapter introduces the application of the developed theoretical models to the description of the phase transition and CO_2 injection processes. In this regard, several numerical examples are presented here. The first group of numerical examples examines the phase transition process for the different models. The goal of these numerical examples is to verify the constitutive relation for the mass production term derived in Section 5. In particular, there is an example, which describes the water vaporisation process, and another example, which illustrates the mass exchange process between the CO_2 phases. The second group of examples is dedicated to the simulation of the CO_2 injection problem. Herein, an ideal scenario of CO_2 injection is presented based on the model I from Section 4.

The numerical treatment of the problems is carried out by the implementation of the weak forms of the governing equations into the Finite-Element Solver PANDAS (**P**orous media **A**daptive **N**onlinear finite element solver based on **D**ifferential **A**lgebraic **S**ystems), cf. PANDAS [79] and of the strong forms of the governing equations into the software FlexPDE. The FlexPDE tool is a multi-physics finite-element solution environment for partial-differential equations.

7.1 Phase Transition

Water Vaporisation:

The water vaporisation process is considered here in order to describe the phase exchange process between two fluid phases and to check the constitutive relation for the mass production term (5.12).

The geometry of the model is given in Figure 7.1, where a rectangular container with a height of $h = 0.2\,\text{m}$ and a width of $h/2$ is illustrated. After applying a heat flux on the bottom of the container filled with a water saturated porous material, the vaporisation process should start.

The examined model consists of a solid skeleton S percolated by two fluid phases: materially incompressible water L and materially compressible vapour G. The solid skeleton is deformable, but the characteristic *Lamé* parameters are chosen in the way that a behaviour of a solid constituent is very close to the behaviour of a rigid solid skeleton, and therefore, its deformation can be neglected in this numerical example. The capillary pressure between the fluid phases is described by the *van Genuchten* law. The phase transition process takes place between the water and vapour, which means that $\hat{\rho}^L = -\hat{\rho}^G$.

The applied initial conditions are chosen as follows:

$$
\begin{aligned}
\theta_0 &= 370 && [\,\mathrm{K}\,]\,, \\
p_0^G &= p_{\mathrm{atm}} = 101325 && [\,\mathrm{Pa}\,]\,, \\
s_0^L &= 0.95 && [-]\,,
\end{aligned}
\tag{7.1}
$$

where θ_0 is the initial temperature, p_0^G denotes the initial vapour pressure and equals to the atmospheric pressure p_{atm} and s_0^L is the initial water saturation corresponding to the condition of a nearly fully-saturated domain.

The boundary conditions are illustrated in Figure 7.1(a). On the bottom of the domain, the heat flux $\bar{\mathbf{q}} = 100\,[\mathrm{J/m^2s}]$ and the pressures p^{GR}, p^{LR} with the values corresponded to the water saturation $s^L = 0.95$ are applied. On the other sides of the domain, the *Neumann* boundary conditions are set.

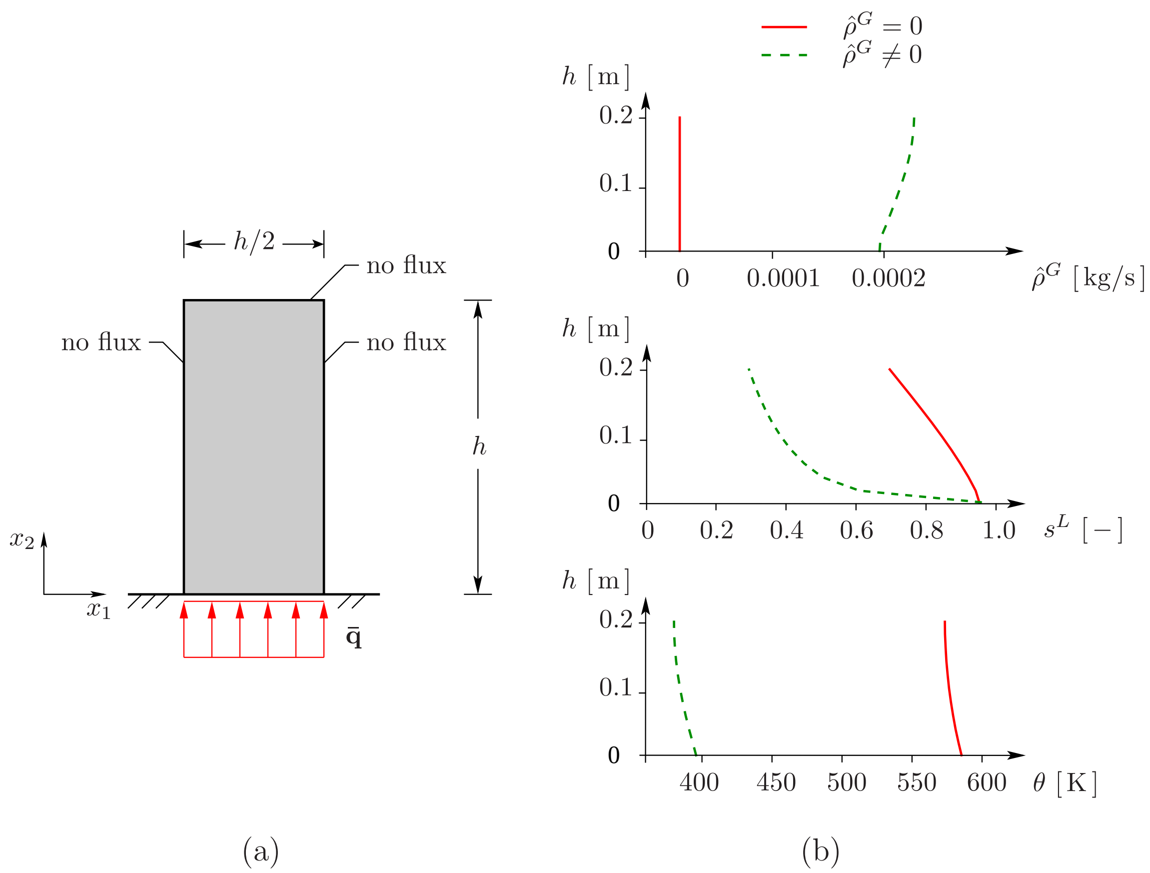

Figure 7.1: (a) Geometry and boundary conditions; (b) mass production term $\hat{\rho}^G$, saturation s^L and temperature θ versus height of the domain h.

The material parameters needed for the simulation are summarised in the following:

Lamé coefficients	μ^S	$=$	$5.58 \cdot 10^7$	$[\,\mathrm{N/m^2}\,]$
	λ^S	$=$	$8.36 \cdot 10^7$	$[\,\mathrm{N/m^2}\,]$
intrinsic permeability	$K^S_{0\mathrm{S}}$	$=$	10^{-12}	$[\,\mathrm{m^2}\,]$
porosity	n^F_{0F}	$=$	$1 - n^S_{0S} = 0.4$	$[-]$
specific heat	C^L_V	$=$	4187	$[\,\mathrm{J/(kg\,K)}\,]$
	C^V_G	$=$	1618	$[\,\mathrm{J/(kg\,K)}\,]$
	C^S_V	$=$	700	$[\,\mathrm{J/(kg\,K)}\,]$
gas constant	R^V	$=$	287.17	$[\,\mathrm{J/(kg\,K)}\,]$
viscosities	μ^{GR}	$=$	$2.01 \cdot 10^{-5}$	$[\,\mathrm{N\,s/m^2}\,]$
	μ^{LR}	$=$	$2.94 \cdot 10^{-4}$	$[\,\mathrm{N\,s/m^2}\,]$
heat conductivity	h^L	$=$	0.62	$[\,\mathrm{W/(m\,K)}\,]$
	h^G	$=$	0.2	$[\,\mathrm{W/(m\,K)}\,]$
	h^S	$=$	1.0	$[\,\mathrm{W/(m\,K)}\,]$
van Genuchten parameters	γ	$=$	0.0002	$[\,\mathrm{1/Pa}\,]$
	n	$=$	1.5	$[\,-\,]$
	m	$=$	2.3	$[\,-\,]$
residual saturations	s^L_{res}	$=$	$s^G_{res} = 0.05$	$[\,-\,]$
effective densities	ρ^{SR}	$=$	2600	$[\,\mathrm{kg/m^3}\,]$
	ρ^{LR}	$=$	1000	$[\,\mathrm{kg/m^3}\,]$
gravitation	g	$=$	9.81	$[\,\mathrm{m/s^2}\,]$

Two different cases with respect to the mass production term are examined here: with and without mass exchange term. In both cases, the boundary conditions and the computational time are identical. The numerical simulations are done within PANDAS. As a switching criterion for the mass-exchange process, the relation between the saturation function and the chemical potential is chosen, cf. Section 5.2.1. In particular, $\hat{\rho}^G = 0$ if $s^L < 0.05$ or $s^L > 0.95$, otherwise if $0.05 < s^L < 0.95$, the values for the chemical potentials have to be calculated. In this case, if $\mu^L \approx \mu^G$, the mass transition process takes place.

The graphical interpretation of the results is given in Figure 7.1(b). These results show that including the mass production term $\hat{\rho}^G$ into the equations affects the saturation and temperature profile. In particular, the temperature increases dramatically in the case where the $\hat{\rho}^G$ term is not considered compared to the case with $\hat{\rho}^G$. This can be explained by the fact that, if the phase transition process takes place, part of the heat is used by the substance to transform from one phase into another phase and only the rest of the heat influences the increase of temperature over the whole domain. Furthermore, having a look at the saturation profile, it can be noted that a different amount of vapour is created within the same simulation time. These differences in the saturation and temperature magnitudes can govern the variety in the pressure values and, as a result, the deformation of the solid skeleton (if the deformation of the solid is relevant for the problem in hand). Therefore, the mass transition process should not be neglected, but included into the model.

Phase Transition between CO_2 Phases:

This numerical example focuses on the modelling of the phase transition process between supercritical CO_2 (L) and gaseous CO_2 (G). At the beginning of the simulations, the considered domain is under constant temperature and almost fully occupied by supercritical CO_2, see Figure 7.2. With time the pressure of the supercritical CO_2 (p^{LR}) is reduced on the top of the domain leading to a phase change of the CO_2. According to the phase diagram shown in Figure 2.4, a pressure change between 6.8 and 7.8 MPa is enough to observe a phase transition between supercritical and gaseous CO_2. Moreover, this pressure range corresponds to the depth of CO_2 injection in real applications.

The examined model consists of two materially compressible fluid phases: supercritical and gaseous CO_2. The solid skeleton is not included into the model. Both fluid phases are described by the *Peng-Robinson* EOS introduced in Section 3.5.2. The densities of the fluid phases are estimated by an expression, which is obtained by inversion of the *Peng-Robinson* EOS with respect to the density, cf. Appendix B. The capillary pressure between the phases is given by the *Brooks* & *Corey* law, cf. Section 4.5.1. Two specific cases are chosen here for consideration in order to analyse the influence of the mass production term on the results. The first case corresponds to the model, where the mass production term is included into the system of the governing equations ($\hat{\rho}^G \neq 0$), while in the second case, the mass production term is assumed to be zero ($\hat{\rho}^G = 0$). However, it should noted that the phase transition with different intensity takes place in both cases: in the first case, this process is modelled directly by an inclusion of the mass production term into system of equations ($\hat{\rho}^G \neq 0$), and in the second case, where $\hat{\rho}^G = 0$, the phase transition process is governed by the EOS.

The initial conditions for the current problem are given via

$$\begin{aligned} \theta_0 &= 313 \quad [\,\mathrm{K}\,]\,, \quad p_0^{LR} = 7.8 \quad [\,\mathrm{MPa}\,]\,, \\ s_0^L &= 0.95 \quad [-]\,, \quad p_0^{GR} = 6.8 \quad [\,\mathrm{MPa}\,]\,, \end{aligned} \tag{7.2}$$

where θ_0 is the initial temperature, p_0^{LR} and p_0^{GR} are the initial pressures of the supercritical and gaseous CO_2 correspondently and s_0^L is the initial saturation of the supercritical CO_2. It is assumed that there is a small residual amount of gaseous CO_2 within the domain at the beginning of the simulations, $s_0^G = 0.05$ (to prevent numerical problems).

The applied boundary conditions are illustrated in Figure 7.2. The left and the right sides of the domain are impermeable for both CO_2 phases. On the bottom of the domain the pressures of supercritical and gaseous CO_2 are set to a constant value:

$$x_2 = 0: \quad p^{GR} = p_0^{GR}, \, p^{LR} = p_0^{LR}. \tag{7.3}$$

On the top of the domain, p^{LR} is reduced with time t by the scale factor k. Herein, the scale factor k is chosen in a way that the pressure of supercritical CO_2 (p^{LR}) is decreased in order to keep the simulation within the pressure range between 6.8 and 7.8 MPa,

$$x_2 = h: \quad p^{LR} = p_0^{LR} - \mathrm{k\,t}. \tag{7.4}$$

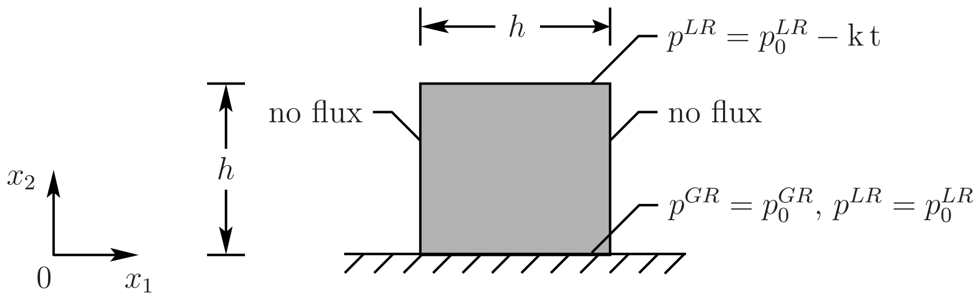

Figure 7.2: IBVP for the CO_2 phase transition problem.

The mass production term $\hat{\rho}^G$ is estimated by the constitutive relation (5.12), and the corresponding switching criterion is taken from Section 5.2.1. The chemical potentials for the switching criterion are given as follows, cf. (3.71):

$$\mu^\beta = \psi^\beta + \frac{p^{\beta R}}{\rho^{\beta R}}, \quad \beta \in \{G, L\}. \tag{7.5}$$

Furthermore, the *Helmholtz* energies ψ^β and entropy functions η^β should be evaluated in order to obtain the mass production term $\hat{\rho}^G$ and the chemical potentials μ^β. In this regard, repeating the procedure for deriving ψ^β and η^β proposed in Section 4.5.3 and assuming that the system has a non-zero reference state (in this case also the initial state), the *Helmholtz* energies yield

$$\begin{aligned}\psi^\beta = {} & R^\beta \theta \ln \frac{\rho^{\beta R}(1 - b\,\rho_0^{\beta R})}{\rho_0^{\beta R}(1 - b\,\rho^{\beta R})} - \frac{a\,\alpha_\omega}{2\sqrt{2}\,b} \ln \frac{(1 - \sqrt{2} - b\,\rho^{\beta R})(1 + \sqrt{2} - b\,\rho_0^{\beta R})}{(1 + \sqrt{2} - b\,\rho^{\beta R})(1 - \sqrt{2} - b\,\rho_0^{\beta R})} \\ & - C_V^\beta \Big(\theta \ln \frac{\theta}{\theta_0} - (\theta - \theta_0)\Big) + \psi_0^\beta + \eta_0^\beta\,(\theta - \theta_0),\end{aligned} \tag{7.6}$$

and the entropy functions lead to

$$\eta^\beta = C_V^\beta \ln \frac{\theta}{\theta_0} - R^\beta \frac{\rho^{\beta R}(1 - b\,\rho_0^{\beta R})}{\rho_0^{\beta R}(1 - b\,\rho^{\beta R})} + \eta_0^\beta. \tag{7.7}$$

The required material parameters are summarised in the following:

porosity	n^F	=	0.6	[−]
intrinsic permeability	K_{0S}^S	=	10^{-7}	[m^2]
specific heat	C_V^β	=	868	[J/(kg K)]
gas constant	R^β	=	189	[J/(kg K)]
heat conductivity	h^β	=	0.014	[W/(m K)]
viscosities	μ^{GR}	=	$1.85 \cdot 10^{-5}$	[$\mathrm{N\,s/m^2}$]
	μ^{LR}	=	$2.1 \cdot 10^{-5}$	[$\mathrm{N\,s/m^2}$]
reference densities	ρ_0^{GR}	=	186.87	[$\mathrm{kg/m^3}$]
	ρ_0^{LR}	=	257.57	[$\mathrm{kg/m^3}$]
reference temperature	θ_0	=	313	[K]
reference Helmholtz energy	ψ_0^β	=	0	[J/kg]
reference entropy	η_0^β	=	0	[J/(kg K)]
Brooks & Corey parameters	p^D	=	$2.31 \cdot 10^5$	[Pa]
	λ	=	2.0	[−]
residual saturations	s_{res}^L	=	$s_{res}^G = 0.05$	[−]
CO_2 critical pressure	p_{cr}	=	7.38	[MPa]
CO_2 critical temperature	θ_{cr}	=	304.1	[K]
gravitation	g	=	9.81	[$\mathrm{m/s^2}$]

The numerical treatment of this example is carried out by using FlexPDE. The resulting distributions of the pressures, densities and saturation over the domain are shown in Figure 7.3. It can be seen that during the same simulation time t, which is set to 50 s, the profiles of the densities, pressures and saturation for both considered cases are different. These differences can be explained by the inclusion of $\hat{\rho}^G$ into the system of equations in the one case and by the exclusion of $\hat{\rho}^G$ in the other case. In order to clarify these differences in the results, the graphical interpretation of the results is presented at the last time step in Figure 7.3 and is analysed in the following.

According to the EOS, the pressure of CO_2 is a function of density and temperature. In the current simulation the temperature is constant, which leads to the fact that the pressures of the CO_2 phases depends only on the corresponding densities. Therefore, it is obvious that the shape of the curve describing the pressure behaviour repeats the shape of the curve presenting the density behaviour and vice versa, cf. in Figure 7.3(a)-(d).

Based on the phase diagram for CO_2 introduced in Figure 2.4, it can be seen that under constant temperature the reduction of the pressure of supercritical CO_2 causes the passing of the critical pressure level p_{cr} and leads to a phase transition process of the supercritical CO_2 into gaseous CO_2. Also, it can be observed in Figure 7.3(a) and (d), where the pressure and the density of the supercritical CO_2 decreased during the simulations. For the current numerical example, the density obtained from the *Peng-Robinson* EOS for the temperature $\theta = 313\,\mathrm{K}$ and the critical pressure $p_{\mathrm{cr}} = 7.38\,\mathrm{MPa}$ has the value of $\rho_{\mathrm{cr}} = 229\,\mathrm{kg/m^3}$.

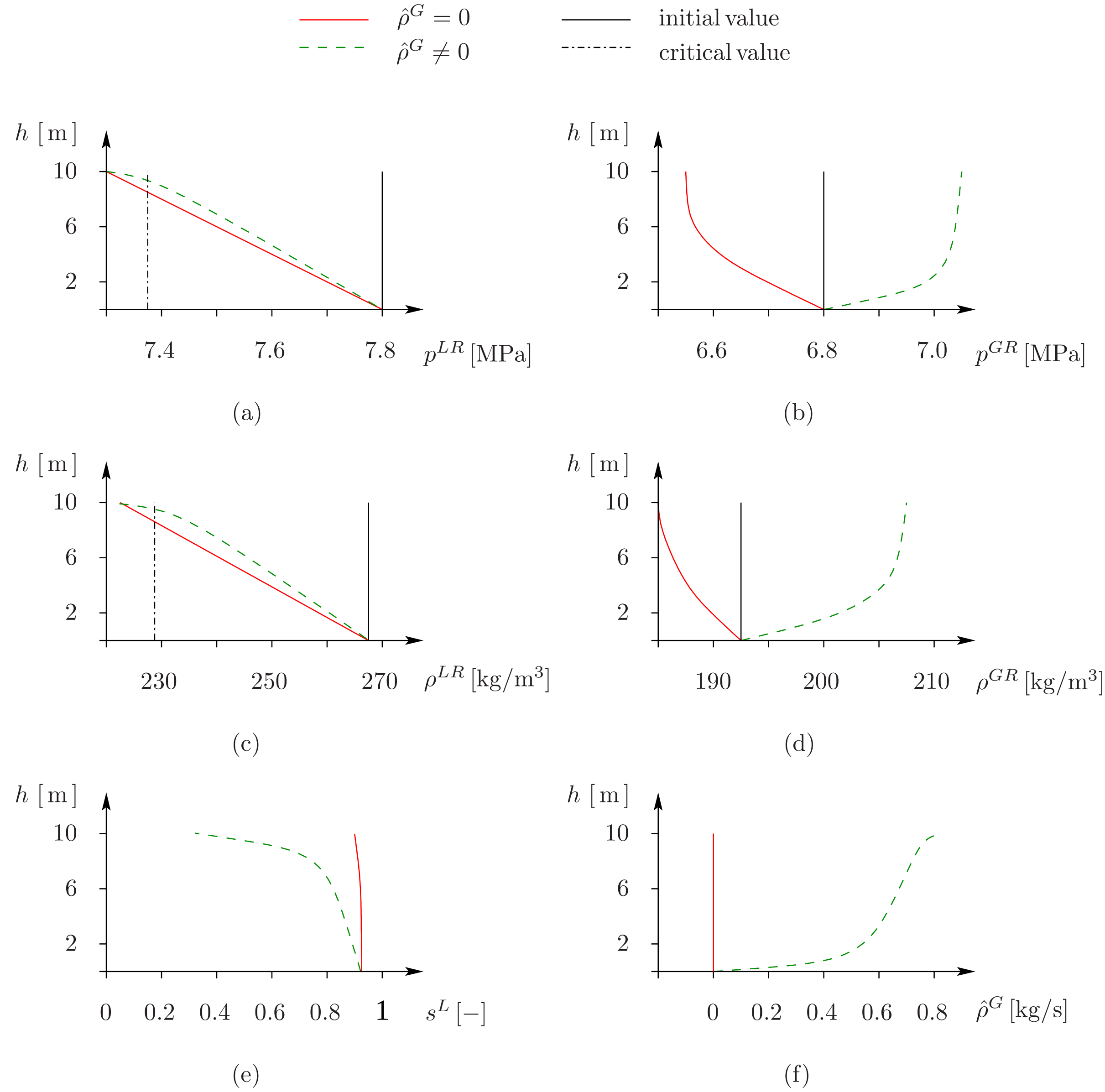

Figure 7.3: Results of the simulation: (a) pressure p^{LR} versus h; (b) pressure p^{GR} versus h; (c) density ρ^{LR} versus h; (d) density ρ^{LR} versus h; (e) saturation s^L versus h; (f) mass production term $\hat{\rho}^G$ versus h.

The difference in the saturation profile for the cases with and without $\hat{\rho}^G$ can be seen in Figure 7.3(e). Moreover, from the results of the calculation it can be noted that for the model with $\hat{\rho}^G$ the supercritical CO_2 occupies the layer $0 < h < 1$ at the end of the simulation and in case without $\hat{\rho}^G$ this layer is $0 < h < 2.1$. It means that an inclusion of $\hat{\rho}^G$ accelerates a phase transition process. In addition, the mass production term itself $\hat{\rho}^G$ is plotted in Figure 7.3(f). To summarise, taking the phase transition process into consideration is necessary to describe the processes within the system properly and to control the speed of the phase transition.

7.2 Carbon-Dioxide Injection

This numerical example represents the behaviour of supercritical CO_2 during its injection into an aquifer as well as the propagation of CO_2 plume through a reservoir. In particular, the present simulations are focused on the estimation of the deformation of a solid skeleton within an reservoir after CO_2 injection.

The model I from Section 4 corresponding to the ideal scenario of injection process is used here for modelling. This multiphasic model consists of three phases and three components: materially incompressible solid (S) with elastic properties, materially incompressible water (W) and materially compressible supercritical CO_2 (L). Following the ideal scenario of an injection process, the pumped supercritical CO_2 should stay in the supercritical state during the whole propagation process. Moreover, the temperature within a domain slightly changes compared to the injection point whereas CO_2 propagates through an aquifer. This non-isothermal character of the process is described by model I.

However, for simplification and reduction of calculation time, the following assumptions are made in this example. The behaviour of CO_2 is described by the ideal gas law. Temperature θ is assumed to be constant during the whole propagation process, which means that the energy balance can be excluded form the system of equations. Assuming that the temperature and pressure are above the critical values θ_{cr} and p_{cr}, a phase transition process between CO_2 phases is omitted from a consideration.

The observed domain consists of four layers: layers with a high intrinsic permeability K^S_{0S1} and Lamé constants μ^S_1, λ^S_1 with corresponding index 1, such as an aquifer and an aquitard, and layers with lower permeability K^S_{0S2} and μ^S_2, λ^S_2 with index 2, namely, a cap-rock and impermeable layer. The geometry and the respective boundary conditions are illustrated in Figure 7.4. The length of the domain is $l = 500\,\text{m}$ and the height is $h = 250\,\text{m}$. The size of the domain is large enough for neglecting the influence of the CO_2 distribution around the injection well on the solid deformation and CO_2 propagation on the right side of the domain. The bottom of the domain corresponds to a depth of 850 m under the subsurface. Injection and distribution of CO_2 take place in the aquifer layer, which has a thickness of 100 m. The cap-rock is 20 m in vertical direction and acts as a barrier for the injected CO_2. The upper aquitard layer with thickness of 80 m and a lower impermeable layer (50 m) are modelled here in order to show possible deformations of these layers under the CO_2 pressure.

At the beginning of the simulations, on the right and left sides of the domain, the hydrostatic pressure is applied, whereas the other sides are impermeable for water and CO_2. The CO_2 under pressure 8 MPa is injected into an aquifer from the left side of a domain,

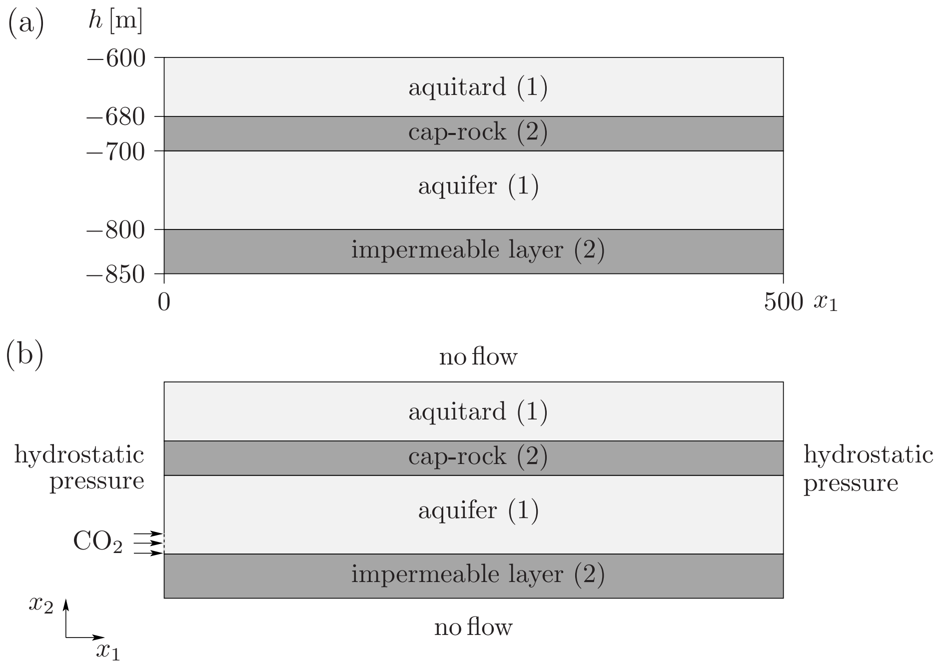

Figure 7.4: CO_2 injection problem: (a) geometry; (b) boundary conditions.

see Figure 7.4(b). After a certain time, the injection pressure is equalised to the pressure in the aquifer and the injection stops. Therefore, in order to proceed with the CO_2 injection into the aquifer, the injection pressure should be increased a little bit with time (herein, 0.001MPa with each time step).

The capillary-pressure-saturation relationship and relative permeabilities between water and supercritical CO_2 are described by the *van Genuchten* law with the material parameters presented below.

The required material parameters are presented in the following:

porosity	n^F	=	0.4	[−]
Lamé constants	μ_1^S	=	$2500 \cdot 10^6$	[Pa]
	λ_1^S	=	$1667 \cdot 10^6$	[Pa]
	μ_2^S	=	$8695 \cdot 10^6$	[Pa]
	λ_2^S	=	$3726 \cdot 10^6$	[Pa]
intrinsic permeability	K_{0S1}^S	=	10^{-10}	[m^2]
	K_{0S2}^S	=	10^{-14}	[m^2]
gas constant	R^L	=	188.86	[J/(kg K)]
viscosities	μ^{WR}	=	$1.0 \cdot 10^{-3}$	[N s/m^2]
	μ^{LR}	=	$2.1 \cdot 10^{-5}$	[N s/m^2]

densities	ρ^{SR}	=	2 720	[kg/m^3]
	ρ^{WR}	=	1 000	[kg/m^3]
	ρ^{LR}	=	136	[kg/m^3]
material parameter	π	=	1.0	[−]
van Genuchten parameters	γ	=	0.0002	[1/Pa]
	n	=	1.5	[−]
	m	=	2.3	[−]
residual saturations	s^L_{res}	=	0.1	[−]
	s^G_{res}	=	0.01	[−]
temperature	θ	=	310	[K]
initial injection pressure	p^{LR}	=	$8 \cdot 10^6$	[Pa]
gravitation	g	=	9.81	[m/s^2]

The injection of CO_2 is stopped when the plume reaches approximately the middle of the aquifer in the horizontal direction. The results of the simulation are presented at different time steps: t_1 is the time step at the beginning of the injection, t_2, t_3 are in the middle of the injection and t_4 is at the end of the injection process. The resulting saturation profile for the water s^W is shown in Figure 7.5.

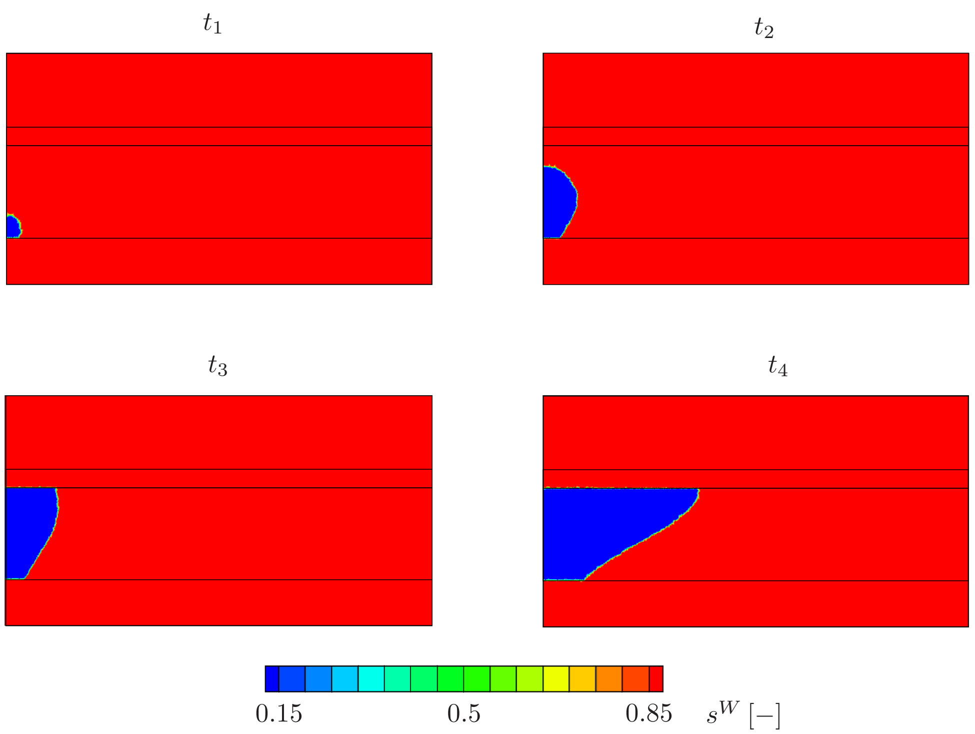

Figure 7.5: Resulting saturation profile s^W.

It can be seen that the more CO_2 is pumped into aquifer the more CO_2 migrates upwards due to buoyancy forces (density difference) until it reaches the cap-rock layer. Then, CO_2 accumulates under the cap-rock and propagates further along the aquifer due to the pressure gradient (advection).

The pressure distribution of the injected CO_2 is given in Figure 7.6. The character of the distribution is correspondent to the form of the saturation profile represented in Figure 7.5. The small oscillation of the pressure, which appear around the CO_2 plume in Figure 7.6, could be explained by some limitations of the chosen numerical scheme.

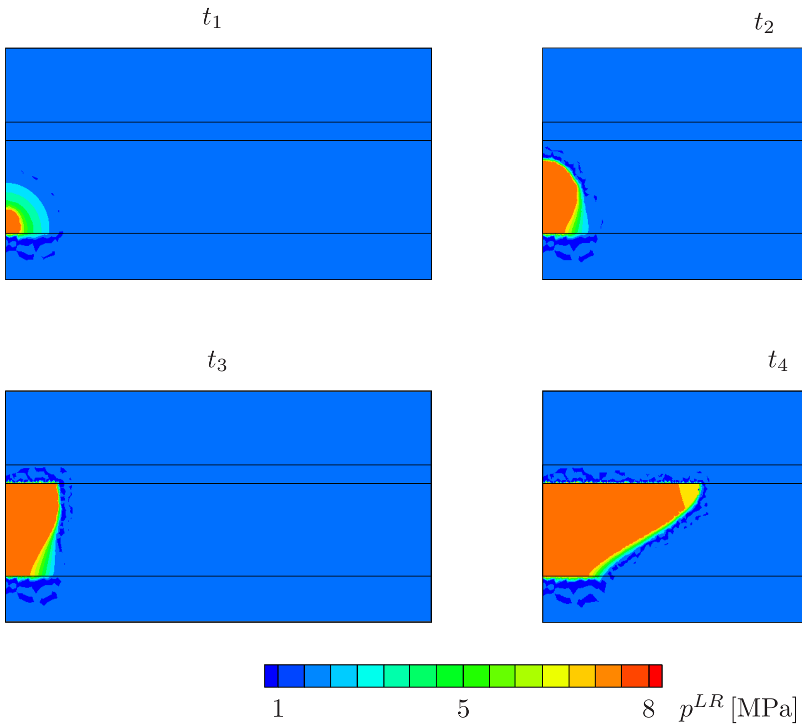

Figure 7.6: CO_2 pressure distribution p^{LR}.

It should be noted that the deformation of the solid skeleton within an aquifer and in a cap-rock layer can cause serious problems for the storage process. For example, appearing cracks and faults in a cap-rock layer could provide possibilities for the escaping of CO_2 from a storage reservoir. The estimated displacement u_2 in the vertical direction at the particular points A, B, C and D versus time could be found in Figure 7.7. The time period for an estimation of u_y starts approximately at the beginning of the CO_2 injection and ends, when the simulations are stopped.

It can be seen that the maximum amplitude of the displacement in the vertical direction is less than 0.01 % of the thickness of the aquifer. It means that in this particular example, a deformation of a solid skeleton has uncritical values and plastic properties of the solid skeleton are not needed to be described.

The current numerical example is solved using PANDAS and describes a proper behaviour of the CO_2 within the aquifer. Nevertheless, the results could be improved in order to have

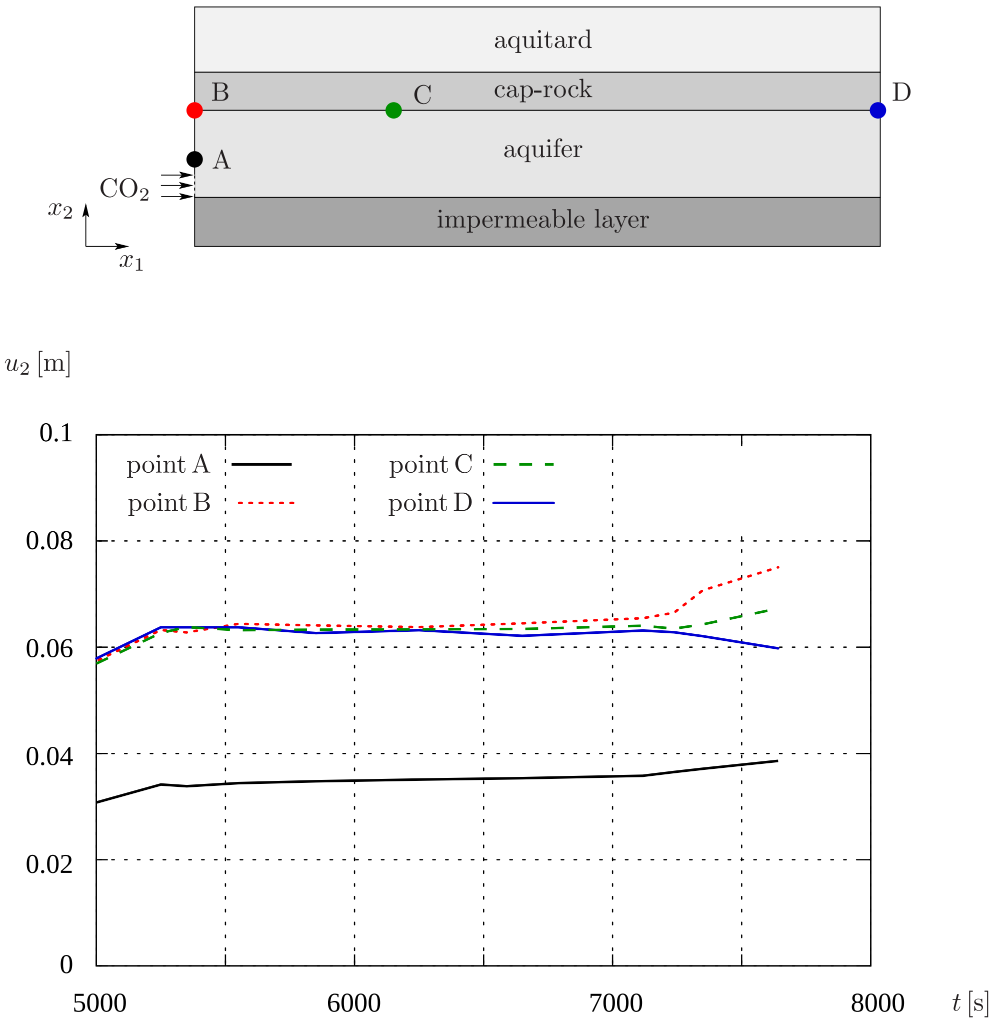

Figure 7.7: Vertical displacement at the particular points of the aquifer.

more realistic representation of the CO_2 injection process. For example, in this numerical example the behaviour of CO_2 is described by the ideal gas law. This simplification is done in order to omit a reformulation of the problem with respect to other primary variables, what should be done if the *Peng-Robinson* EOS is used (indirect representation of density, cf. Section 3.5.2 and Appendix B). However, the *Peng-Robinson* EOS for CO_2 can be implemented for the simulations to perform more realistic propagation of the CO_2 trough the aquifer. Moreover, the distribution of the CO_2 over the domain shows that considering a deformation of the solid skeleton within the aquifer is important for the injection process. It is also important to note that during propagation, CO_2 can change its phase what requires a description of the phase-transition process. The relevant theoretical model corresponding to the critical scenario of the CO_2 injection is developed within the current work in Section 4.1. Using the model II, it is possible to model the phase transition process of CO_2 during its propagation trough an aquifer. However, in the current work, there are no numerical simulations performed for the model II. Therefore, further investigations have to be carried out in the field of the phase transition process for the CO_2 injection problem.

Chapter 8: Summary and Outlook

8.1 Summary

The CO_2 capture and storage problem is a widely discussed issue at the present time. In order to predict the problems that may occur during and after CO_2 injection in the subsurface, scientists from different research areas developed a variety of models and scenarios of the CO_2 sequestration process. The distinct feature of the current investigation is to model two particular processes taking place in the storage reservoir (aquifer): phase transition phenomena and solid deformation. A multiphasic model describing these processes was derived based on the continuum-mechanical framework of the well-founded TPM.

Two different approaches regarding the number of fluid phases were considered in the current research. The main difference between these two formulations was in the description of the CO_2 state. In the frame of the first formulation, CO_2 was present only in one (supercritical) phase without any phase transition, whereas the second formulation included phase transition between the CO_2 phases (gaseous and supercritical).

Within the modelling procedure, the deformation of the solid skeleton was limited to elastic material behaviour and described by the linear elastic *Hooke*an law. The phase transition process between the CO_2 phases was modelled by the inclusion of the mass production term into the corresponding mass balance relations. For this term, a new constitutive relation was derived from the entropy balance relations based on the assumption of full reversibility of the considered processes. To complete the description of the phase transition process, a so-called switching criterion was defined in the form of a combined condition for the saturation functions and chemical potentials.

In order to describe the realistic behaviour of the CO_2 in any state, the *Peng-Robinson* EOS was implemented into the model. This is a cubic equation and its inversion with respect to the density has a relatively complicated form. Moreover, the new form of the *Helmholtz* energies for the CO_2 phases was derived based on the *Peng-Robinson* EOS.

The numerical treatment of the problem was carried out by the FEM in the spatial space and by the implicit *Euler* scheme in the temporal domain. Numerical examples were performed in order to confirm the proposed modelling approach for the distribution of the CO_2 plume in the reservoir after injection and verify the developed constitutive equation for the mass production term.

Throughout this thesis, it has been demonstrated that the solid deformation affects the propagation of the CO_2 plume within the aquifer after the injection. Moreover, it has been shown that the phase transition process has a significant influence on the property change for the discussed models and, therefore, should be included into the modelling to describe the processes in a system properly.

However, in the CCS research field, a number of questions remain open, which are important for future discussion and vital for further investigation.

8.2 Outlook

The developed multiphasic models are capable of describing the coupled behaviour of the injected supercritical CO_2 and the deformable solid skeleton within the aquifer and the cap-rock layer. Also, the phase exchange process between the CO_2 phases is modelled by the additional thermodynamical constitutive relation for the mass production term. However, the numerical example corresponding to the critical scenario of CO_2 injection should be still implemented into the numerical tool in order to show the joint influence of both discussed aspects of solid deformation and phase transition on the CO_2 propagation within the aquifer.

Additionally, there are several aspects, which can be further investigated in order to improve the existing model. In this regard, further work on this topic should focus on the following items:

- *Phase transition process*: The suggested switching criterion was not compared to other possible criteria and may have some potential disadvantages. Therefore, an alternative transition rule for the phase transition process can be defined. Afterwards, the criteria should be compared in order to define a more realistic criterion.

  The derived constitutive relation for the mass production term was found with the strong assumption of full reversibility of the processes taking place within the problem. In this context, the constitutive equation can be reconsidered and improved such that it is valid for any type of processes.

- *Deformation of the solid skeleton*: Within the model presented in this thesis, the behaviour of the solid skeleton was described by the geometrically linear elasticity theory, which is sufficient for numerous applications. Nevertheless, there are some cases, where large elasto-plastic deformations may take place as the result of inhomogeneities in the sequestration process. In other locations, such as the cap-rock layer, cracks may occur leading to leakage phenomena of the sequestrated CO_2. Consequently, an extension of the solid behaviour towards elasto-plasticity as well as to crack initiation and propagation is required.

- *Chemical reactions*: A part of the CO_2 sequestration process over time is the dissolution process of CO_2 into the aquifer. As a result of the CO_2 reacting with the water, salt species appear and may block the path for the further propagation of the CO_2 plume, especially around the injection well. This can be very critical for the whole sequestration process. In this regard, the modelling of the dissolution process would be an appropriate and useful extension of the problem.

- *Computational schemes*: The coupled CO_2 sequestration problem was computed by a fully coupled implicit monolithic scheme. However, if the developed model will be extended by an inclusion of, for example, the modelling of the crack propagation process or another complexity, the suggested numerical scheme may not work properly requiring an improvement of numerical performance.
- *Capillary-pressure-saturation relation*: In contrast to the model introduced in this thesis, the different capillary-pressure-saturation relations with various material parameters for the water-supercritical CO_2 interface and for the interface between the CO_2 phases can be implemented.

Although in the current work, the developed models give a realistic description of the CO_2 injection problem, the implementation of the aforementioned suggestions may result into a more detailed and appropriate description of problem. Therefore, it is recommended to consider and include the discussed aspects in future research efforts.

Appendix A: Tensor Calculus

This appendix presents some selected principles of the tensor calculus. For the presented relations, arbitrary scalars $\alpha, \beta \in R$ are defined in the real space R; vectors $\mathbf{a}, \mathbf{b}, \mathbf{c}, \mathbf{d} \in \mathcal{V}^3$ in the *Euclid*ean vector space $\mathcal{V}^3$ and second-order tensors $\mathbf{A}, \mathbf{B}, \mathbf{C} \in \mathcal{V}^3 \otimes \mathcal{V}^3$ in the dyadic product space $\mathcal{V}^3 \otimes \mathcal{V}^3$. More detailed information about the notations and tensor calculus operations can be found in de Boer [13] and Ehlers [39].

A.1 Selected Rules for Second-Order Tensors

Multiplication of tensors by scalars:

$$\begin{aligned} \text{associative law:} \quad \alpha\,(\beta\,\mathbf{A}) &= (\alpha\,\beta)\,\mathbf{A} \\ \text{distributive laws:} \quad (\alpha + \beta)\,\mathbf{A} &= \alpha\,\mathbf{A} + \beta\,\mathbf{A} \\ \alpha\,(\mathbf{A} + \mathbf{B}) &= \alpha\,\mathbf{A} + \alpha\,\mathbf{B} \\ \text{commutative law:} \quad \alpha\,\mathbf{A} &= \mathbf{A}\,\alpha \end{aligned} \tag{A.1}$$

Linear mapping between tensors and vectors:

$$\begin{aligned} \text{associative law:} \quad \mathbf{A}\,(\alpha\,\mathbf{a}) &= \alpha(\mathbf{A}\,\mathbf{a}) = (\alpha\,\mathbf{A})\,\mathbf{a} \\ \text{distributive laws:} \quad \mathbf{A}\,(\mathbf{a} + \mathbf{b}) &= \mathbf{A}\,\mathbf{a} + \mathbf{A}\,\mathbf{b} \\ (\mathbf{A} + \mathbf{B})\,\mathbf{a} &= \mathbf{A}\,\mathbf{a} + \mathbf{B}\,\mathbf{a} \end{aligned} \tag{A.2}$$

The scalar product of tensors:

$$\begin{aligned} \text{associative law:} \quad (\alpha\,\mathbf{A}) \cdot \mathbf{B} &= \mathbf{A} \cdot (\alpha\,\mathbf{B}) = \alpha\,(\mathbf{A} \cdot \mathbf{B}) \\ \text{distributive law:} \quad \mathbf{A} \cdot (\mathbf{B} + \mathbf{C}) &= \mathbf{A} \cdot \mathbf{B} + \mathbf{A} \cdot \mathbf{C} \\ \text{commutative laws:} \quad \mathbf{A} \cdot \mathbf{B} &= \mathbf{B} \cdot \mathbf{A} \\ \mathbf{A} \cdot \mathbf{B} &= 0 \quad \forall\,\mathbf{A}\,,\ \text{if } \mathbf{B} \equiv \mathbf{0} \\ \mathbf{A} \cdot \mathbf{A} &> 0 \quad \forall\,\mathbf{A} \neq \mathbf{0} \end{aligned} \tag{A.3}$$

The tensor product of tensors:

$$
\begin{aligned}
\text{associate law :} \qquad \alpha\,(\mathbf{A}\,\mathbf{B}) &= (\alpha\,\mathbf{A})\,\mathbf{B} = \mathbf{A}\,(\alpha\,\mathbf{B}) \\
(\mathbf{A}\,\mathbf{B})\,\mathbf{a} &= \mathbf{A}\,(\mathbf{B}\,\mathbf{a}) \\
(\mathbf{A}\,\mathbf{B})\,\mathbf{C} &= \mathbf{A}\,(\mathbf{B}\,\mathbf{C}) \\
\text{distributive laws :} \qquad \mathbf{A}\,(\mathbf{B}+\mathbf{C}) &= \mathbf{A}\,\mathbf{B}+\mathbf{A}\,\mathbf{C} \\
(\mathbf{A}+\mathbf{B})\,\mathbf{C} &= \mathbf{A}\,\mathbf{C}+\mathbf{B}\,\mathbf{C} \\
\text{no commutative law :} \qquad \mathbf{A}\,\mathbf{B} &\neq \mathbf{B}\,\mathbf{A} \\
(\mathbf{a}\otimes\mathbf{b})\,(\mathbf{c}\otimes\mathbf{d}) &= (\mathbf{b}\cdot\mathbf{c})\,\mathbf{a}\otimes\mathbf{d}
\end{aligned}
\tag{A.4}
$$

The transposition and inversion of a tensor:

$$
\begin{aligned}
(\mathbf{a}\otimes\mathbf{b})^T &= (\mathbf{b}\otimes\mathbf{a}) \\
(\alpha\,\mathbf{A})^T &= \alpha\,\mathbf{A}^T \\
(\mathbf{A}\,\mathbf{B})^T &= \mathbf{B}^T\,\mathbf{A}^T \\
(\mathbf{A}\,+\,\mathbf{B})^T &= \mathbf{A}^T\,+\,\mathbf{B}^T
\end{aligned}
\tag{A.5}
$$

The inversion of a tensor:

$$
\begin{aligned}
\mathbf{A}^{-1} &\quad \text{exists if } \det\mathbf{A}\neq 0 \\
\mathbf{A}\,\mathbf{A}^{-1} &= \mathbf{A}^{-1}\,\mathbf{A} = \mathbf{I} \\
(\mathbf{A}^{-1})^T &= (\mathbf{A}^T)^{-1} =: \mathbf{A}^{T-1} \\
(\mathbf{A}\,\mathbf{B})^{-1} &= \mathbf{B}^{-1}\,\mathbf{A}^{-1}
\end{aligned}
\tag{A.6}
$$

The trace operator:

$$
\begin{aligned}
\operatorname{tr}\mathbf{A} &= \mathbf{A}\cdot\mathbf{I} \\
\operatorname{tr}(\alpha\,\mathbf{A}) &= \alpha\operatorname{tr}\mathbf{A} \\
\operatorname{tr}(\mathbf{a}\otimes\mathbf{b}) &= \mathbf{a}\cdot\mathbf{b} \\
\operatorname{tr}\mathbf{A}^T &= \operatorname{tr}\mathbf{A} \\
\operatorname{tr}(\mathbf{A}\,\mathbf{B}) &= \operatorname{tr}(\mathbf{B}\,\mathbf{A}) = \mathbf{A}\cdot\mathbf{B}^T = \mathbf{A}^T\cdot\mathbf{B}
\end{aligned}
\tag{A.7}
$$

A.2 Principal Invariants of Second-Order Tensors

The principle invariants of a tensor $\mathbf{A}$ can be obtained by solving the eigenvalue problem: $(\mathbf{A}-\gamma_A\mathbf{I})\,\mathbf{a}=0$, where γ_A is the eigenvalue and $\mathbf{a}$ is the eigenvector. Thus, the first I_A, second II_A and third III_A invariants of any tensor $\mathbf{A}$ have a form:

$$\begin{aligned} I_A &= \mathbf{A} \cdot \mathbf{I} = \operatorname{tr} \mathbf{A} \, , \\ II_A &= \tfrac{1}{2}(I_A^2 - \mathbf{A}^T \cdot \mathbf{A}) \, , \\ III_A &= \tfrac{1}{6} I_A^3 - \tfrac{1}{2} I_A^2 \, (\mathbf{A}^T \cdot \mathbf{A}) + \tfrac{1}{3} \mathbf{A}^T \mathbf{A}^T \cdot \mathbf{A} \, . \end{aligned} \tag{A.8}$$

Appendix B: Specific Evaluations

Legendre Transformation for the ε and ψ:

The internal energy ε can be related to the free *Helmholtz* energy ψ by the *Legendre* transformation. In order to perform this, conjugate variables are used, in particular the mechanical pair $\{\frac{1}{\rho_0}\mathbf{S}, \mathbf{E}\}$ and the thermodynamical pair $\{\eta, \theta\}$. Thus, the derivative of the internal energy as a function of strain and entropy $\varepsilon(\mathbf{E}, \eta)$ leads to

$$\dot{\varepsilon}(\mathbf{E}, \eta) = \frac{\partial \varepsilon}{\partial \mathbf{E}} \cdot \dot{\mathbf{E}} + \frac{\partial \varepsilon}{\partial \eta} \dot{\eta} = \frac{1}{\rho_0} \mathbf{S} \cdot \dot{\mathbf{E}} + \theta \, \dot{\eta} \, . \tag{B.1}$$

Substituting $\theta \, \dot{\eta} = (\theta \, \eta)^{\dot{}} - \dot{\theta} \, \eta$ into (B.1), the following relation is obtained

$$(\varepsilon - \theta \, \eta)^{\dot{}} = \frac{1}{\rho_0} \mathbf{S} \cdot \dot{\mathbf{E}} - \dot{\theta} \, \eta \, , \tag{B.2}$$

where the *Helmholtz* energy reads

$$\psi(\mathbf{E}, \theta) = \varepsilon(\mathbf{E}, \eta) - \theta \, \eta \, . \tag{B.3}$$

Other examples of the *Legendre* transformations can be found, for instance, in Ehlers [39].

Inversion of the Peng-Robinson EOS with respect to the Density:

The *Peng-Robinson* EOS is a cubic EOS and has the following form:

$$p = \frac{R \, \theta}{v - b} - \frac{a \, \alpha_\omega}{v^2 + 2 \, b \, v - b^2} \, , \tag{B.4}$$

where v is a specific volume, p is a pressure, θ is a temperature, a, b, α_ω are the constants depending on the critical pressure and temperature of a substance (here CO_2) and R is the universal gas constant, cf. Section 3.5.2.
Inserting a specific volume v as $v = 1/\rho$ into equation (B.4), it yields

$$p = \frac{R \, \theta \, \rho}{1 - b \, \rho} - \frac{a \, \alpha_\omega \, \rho^2}{1 + 2 \, b \, \rho - b^2 \, \rho^2} \, . \tag{B.5}$$

Equation (B.5) is reformulated with respect to the density as follows

$$A \, \rho^3 + B \, \rho^2 + C \, \rho + D = 0 \, , \tag{B.6}$$

where

$$\begin{aligned} A &= -p\,b^3 + a\alpha_\omega\, b - R\,\theta\, b^2\,, \\ B &= 2\,b\,R\theta + 3\,p\,b^2 - a\,\alpha_\omega\,, \\ C &= R\theta - b\,p\,, \\ D &= -p\,. \end{aligned} \tag{B.7}$$

Before solving equation (B.6), the following discriminant has to be evaluated

$$\Delta = 18\,A\,B\,C\,D - 4\,B^3\,D + B^2\,C^2 - 4A\,C^3 - 27\,A^2\,D^2\,. \tag{B.8}$$

There are several cases depending on the value of Δ, which can be distinguished: if $\Delta > 0$, then the equation has three distinct real roots; if $\Delta = 0$, then the equation has a multiple roots and all these roots are real; if $\Delta < 0$, then the equation has one real root and two non-real complex conjugate roots.

For the specific substance considered in the current work, namely CO_2, $\Delta < 0$. It leads to the fact that equation (B.6) has one real root, which is required in the expression for CO_2 density:

$$\rho = -\frac{B}{3\,A} - \frac{1}{3\,A}\Big(\frac{E+F}{2}\Big)^{\frac{1}{3}} - \frac{1}{3\,A}\Big(\frac{E-F}{2}\Big)^{\frac{1}{3}}\,, \tag{B.9}$$

where

$$\begin{aligned} E &= 2\,B^3 - 9\,A\,B\,C + 27\,A^2\,D\,, \\ F &= \sqrt{(2\,B^3 - 9\,A\,B\,C + 27\,A^2\,D)^2 - 4\,(B^2 - 3\,A\,C)^3}\,. \end{aligned} \tag{B.10}$$

Bibliography

[1] Abbott, M. M. & van Ness, H. C.: *Schaum's Outline of Thermodynamics with Chemical Applications*. McGraw-Hill, New-York 1989, 2nd edn.

[2] Acartürk, A. Y.: *Simulation of Charged Hydrated Porous Materials*. Dissertation, Bericht Nr. II-18 aus dem Institut für Mechanik (Bauwessen), Universität Stuttgart 2009.

[3] Ammann, M.: *Parallel Finite Element Simulations of Localization Phenomena in Porous Media*. Dissertation, Bericht Nr. II-11 aus dem Institut für Mechanik (Bauwessen), Universität Stuttgart 2005.

[4] Bachu, S.: CO_2 storage in geological media: Role, means, status and barriers to deployment. *Progress in Energy and Combustion Science* **34** (2008), 254–273.

[5] Bachu, S.; Bonijoly, D.; Bradshaw, J.; Burruss, R.; Holloway, S.; Christensen, N. P. & Mathiassen, O. M.: CO_2 storage capacity estimation: Methodology and gaps. *International Journal of Greenhouse Gas Control* **I** (2007), 430–443.

[6] Baines, S. J. & Worden, R. H. (eds.): *Geological Storage of Carbon Dioxide*. The Geological Society, London 2004.

[7] Barragán-Aroche, J. F. & Bazúa-Rueda, E. R.: A local composition extension of the van der Waals mixing rule for PR cubic equation of state. *Fluid Phase Equilibria* **227** (2005), 97–112.

[8] Bear, J.: *Dynamics of Fluids im Porous Media*. Elsevier, New York 1972.

[9] Bear, J.: *Hydraulics of Groundwater*. McGraw-Hill, New York 1979.

[10] Benedict, M.; Webb, G. W. & Rubin, L. C.: An empirical equation for thermodynamic properties of light hydrocarbons and their mixtures. *Journal Chemical Physics* **10** (1942), 747–758.

[11] Bielinski, A.: *Numerical Simulation of CO_2 Sequestration in Geological Formations*. Dissertation, Mitteilungsheft Nr. 155 aus dem Institut für Wasserbau, Universität Stuttgart 2007.

[12] Blome, K. P.: *Ein Mehrphasen-Stoffmodell für Böden mit Übergang auf Interface-Gesetze*. Dissertation, Bericht Nr. II-10 aus dem Institut für Mechanik (Bauwessen), Universität Stuttgart 2003.

[13] de Boer, R.: *Vektor- und Tensorrechnung für Ingenieure*. Springer-Verlag, Berlin 1982.

[14] de Boer, R.: *Theory of Porous Media*. Springer-Verlag, Berlin 2000.

[15] de Boer, R. & Bluhm, J.: Phase transition in gas- and liquid-saturated porous solids. *Transport in Porous Media* **34** (1999), 249–267.

[16] de Boer, R. & Ehlers, W.: *Theorie der Mehrkomponentenkontinua mit Anwendungen auf bodenmechanische Probleme*. Forschungsberichte aus dem Fachbereich Bauwesen Heft 40, Universität-GH-Essen (1986).

[17] de Boer, R. & Kowalski, S. J.: Thermodynamics of fluid-saturated porous media with a phase change. *Acta Mechanica* **109** (1995), 167–189.

[18] Bowen, R. M.: Theory of mixtures. In *Continuum Physics*, Eringen, A. C., ed., Academic Press, New York 1976, vol. III, pp. 1–127.

[19] Bowen, R. M.: Incompressible porous media models by use of the theory of mixtures. *International Journal of Engineering Science* **18** (1980), 1129–1148.

[20] Bowen, R. M.: Compressible porous media models by use of the theory of mixtures. *International Journal of Engineering Sciences* **20** (1982), 697–735.

[21] Bradshaw, J.; Bachu, S.; Bonijoly, D.; Burrus, R.; Holloway, S.; Christensen, N. P. & Mathiassen, O. M.: CO_2 storage capacity estimation: Issues and development of standards. *Greenhouse Gas Control* **I** (2007), 62–68.

[22] Brezzi, F. & Fortin, M.: *Mixed and Hybrid Finite Element Methods*. Spinger-Verlag, New-York 1991.

[23] Brooks, R. H. & Corey, A. T.: *Hydraulic Properties of Porous Media*. No. 3, Hydrology Papers 1964.

[24] Brooks, R. H. & Corey, A. T.: Properties of porous media affecting fluid flow. *ASCE: Journal of the Irrigation and Drainage Division* **92** (1966), 61–88.

[25] Class, H.: *Theorie und numerische Modellierung nichtisothermer Mehrphasenprozesse in NAPL-kontaminieren porösen Medien*. Dissertation, Mitteilungsheft Nr.105 aus dem Institut für Wasserbau, Universität Stuttgart 2001.

[26] Class, H.: *Models for Non-Isothermal Compositional Gas-Liquid Flow and Transport in Porous Media*. Habilitationsschrift, Der Fakultät für Bau- und Umweltingenieurwissenschaften der Universität Stuttgart 2009.

[27] Coleman, B. D. & Noll, W.: The thermodynamics of elastic materials with heat conduction and viscosity. *Archive for Rational Mechanics and Analysis* **13** (1963), 167–178.

[28] Damen, K.; Faaij, A. & Turkenburg, W.: Health, safety and environmental risks of underground CO_2 storage - overview of mechanisms and current knowledge. *Climatic Change* **74** (2006), 289–318.

[29] Doughty, C. & Pruess, K.: Modeling supercritical carbon dioxide injection in heterogeneous porous media. *Vadose Zone Journal* **3** (2004), 837–847.

[30] Durucan, S. & Shi, J.-Q.: Improving the CO_2 well injectivity and enhanced coalbed methane production performance in coal seams. *International Journal of Coal Geology* **77** (2009), 214–221.

[31] Ebigbo, A.; Class, H. & Helmig, R.: CO_2 leakage through an abandoned well: problem-oriented benchmarks. *Computational Geosciences* **11** (2007), 103–115.

[32] Eftekhari, A. A.; Bruining, J.; Wahanik, H. & Marchesin, D.: CO_2 injection in sub-salt water layers at 7000m depth. *Society of Petroleum Engineers-SPE Resevoir SImulation Symposium 2011-2* (2011), 1340–1348.

[33] Ehlers, W.: On thermodynamics of elasto-plastic porous media. *Archives of Mechanics* **41** (1989), 73–93.

[34] Ehlers, W.: *Poröse Medien – ein kontinuumsmechanisches Modell auf der Basis der Mischungstheorie*. Habilitationsschrift, Forschungsberichte aus dem Fachbereich Bauwesen, Heft 47, Universität-GH-Essen 1989.

[35] Ehlers, W.: Constitutive equations for granular materials in geomechanical context. In *Continuum Mechanics in Environmental Sciences and Geophysics*, Hutter, K., ed., Springer-Verlag 1993, CISM Courses and Lecture Notes No. 337, pp. 313–402.

[36] Ehlers, W.: Grundlegende Konzepte in der Theorie Poröser Medien. *Technische Mechanik* **16** (1996), 63–76.

[37] Ehlers, W.: Foundations of multiphasic and porous materials. In *Porous Media: Theory, Experiments and Numerical Applications*, Ehlers, W. & Bluhm, J., eds., Springer-Verlag, Berlin 2002, pp. 3–86.

[38] Ehlers, W.: Challenges of porous media models in geo- and biomechanical engineering including electro-chemically active polymers and gels. *International Journal of Advances in Engineering Sciences and Applied Mathematics* **1** (2009), 1–24.

[39] Ehlers, W.: *Vector and Tensor Calculus: An Introduction*. Lecture notes, Institute of Applied Mechanics (CE), University of Stuttgart 2009, URL `http://www.mechbau.uni-stuttgart.de/ls2/`.

[40] Ehlers, W. & Acartürk, A.: The role of implicit dirichlet boundary conditions for numerically stable computations of swelling phenomena. *Computational Mechanics* **43** (2007), 545–557.

[41] Ehlers, W.; Acartürk, A. & Karajan, N.: Advances in modelling saturated biological soft tissues and chemically active gels. *Archive of Applied Mechanics* **80** (2010), 467–478.

[42] Ehlers, W. & Avci, O.: Stress-dependent hardening and failure surfaces of dry sand. *International Journal for Numerical and Analytical Methods in Geomechanics* (2011), DOI: 10.1002/nag.

[43] Ehlers, W.; Avci, O. & Markert, B.: Computation of large slope movements initiated by rain-induced shear bands. *Vadose Zone Journal* **10** (2011), 512–525.

[44] Ehlers, W. & Ellsiepen, P.: Theoretical and numerical methods in environmental continuum mechanics based on the theory of porous media. In *Enviromental Geomechanics*, Schrefler, B. A., ed., Springer-Verlag, Wien 2001, CISM Courses and Lecture Notes No. 417, pp. 1–81.

[45] Ehlers, W.; Ellsiepen, P.; Blome, P.; Mahnkopf, D. & Markert, B.: *Theoretische und numerische Studien zur Lösung von Rand- und Anfangswertproblemen in der Theorie Poröser Medien*. Forschungsbericht zum DFG-Projekt Eh 107/6-2, Bericht aus den Institut für Mechanik (Bauwesen), Nr. 99-II-1, Universität Stuttgart 1999.

[46] Ehlers, W.; Graf, T. & Ammann, M.: Deformation and localization analysis of partially saturated soil. *Computer Methods in Applied Mechanics and Engineering* **193** (2004), 2885–2910.

[47] Eipper, G.: *Theorie und Numerik finiter elastischer Deformationen in fluidgesättigten porösen Festkörpern*. Dissertation, Bericht Nr. II-1 aus dem Institut für Mechanik (Bauwessen), Universität Stuttgart 1998.

[48] Ellsiepen, P.: *Zeit- und ortsadaptive Verfahren angewandt auf Mehrphasenprobleme poröser Medien*. Dissertation, Bericht Nr. II-3 aus dem Institut für Mechanik (Bauwesen), Universität Stuttgart 1999.

[49] Farajzadeh, R.; Zitha, P. L. J. & Bruining, H.: Enhaced mass transfer of cO_2 into water: experiment and modeling. *Industrial and Engineering Chemistry Research* **48** (2009), 6423–6431.

[50] van Genuchten, M. T.: A closed-form equation for predicting the hydraulic conductivity of unsaturated soils. *Soil Science Society of America Journal* **44** (1980), 892–898.

[51] Ghadiani, S. R.: *A Multiphasic Continuum Mechanical Model for Design Inversigations of an Effusion-Cooled Rocket Thrust Chamber*. Dissertation, Bericht Nr.II-13 aus dem Institut für Mechanik (Bauwessen), Universität Stuttgart 2005.

[52] Gmehling, J. & Kolbe, B.: *Thermodynamik*. VCH, Weinheim 1992.

[53] Graf, T.: *Multiphasic Flow Processes in Deformable Porous Media under Consideration of Fluid Phase Transitions*. Dissertation, Bericht Nr.II-17 aus dem Institut für Mechanik (Bauwessen), Universität Stuttgart 2008.

[54] Green, A. E. & Naghdi, P. M.: A theory of mixtures. *Archive for Rational Mechanics and Analysis* **24** (1967), 243–263.

[55] Gunter, W. D.; Bachu, S. & Benson, S.: The role of hydrogeological and geochemical trapping in sedimentary basins for secure geological storage of carbon dioxide. In *Geological Storage of Carbon Dioxide*, Baines, S. J. & Worden, R. H., eds., The Geological Society, London 2004, pp. 129–145.

[56] Harstad, K. G.; Miller, R. S. & Bellan, J.: Efficient high-pressure state equations. *AIChE Journal* **43 (6)** (1997), 1605–1610.

[57] Helmig, R.: *Multiphase Flow and Transport Processes in the Subsurface*. Spinger 1997.

[58] Holm, R.; Kaufmann, R.; Dale, E. I.; Aanonsen, S.; Fladmark, G. E.; Espedal, M. & Skauge, A.: Constructing three-phase capillary pressure functions by paramters matching using a modified ensemble Kalman filter. *Communications in Computational Physics* **6** (2009), 24–48.

[59] Hughes, T. J. R.: *The Finite Element Method: Linear Static and Dynamic Finite Element Analysis*. Dover Publications 2000.

[60] Karajan, N.: *An Extended Biphasic Description of the Inhomogeneous and Anisotropic Intervertebral Disc*. Dissertation, Bericht Nr. II-19 aus dem Institut für Mechanik (Bauwessen), Universität Stuttgart 2009.

[61] Kopp, A.; Class, H. & Helmig, R.: Investigations on CO_2 storage capacity in saline aquifers - Part 2: Estimation of storage capacity coefficients. *Greenhouse Gas Control* **3** (2009), 277–287.

[62] Kowalski, S. J.: Toward a thermodynamics and mechanics of drying processes. *Chemical Engineering Science* **55** (2000), 1289–1304.

[63] Kreyszig, E.: *Advanced Engineering Mathematics*. John Wiley & Sons 2006, 9th edn.

[64] Kruschwitz, J. & Bluhm, J.: Modeling of ice formation in porous solids with regard to the description of frost damage. *Computational Materials Science* **32** (2005), 407–417.

[65] Larsen, J. W.: The effects of dissolved CO_2 on coal structure and properties. *International Journal of Coal Geology* **57** (2004), 63–70.

[66] Lewis, G. N. & Randall, M.: *Thermodynamics*. McGraw-Hill Book Company, New York 1961.

[67] Li, H.; Ji, X. & Yan, J.: A new modification on RK EOS for gaseous CO_2 and gaseous mixtures of CO_2 and H_2O. *International Journal of Energy Research* **30** (2006), 135–148.

[68] Li, H. & Yan, J.: Evaluating cubic equations of state for calculation of vapor-liquid equilibrium of CO_2 and CO_2-mixtures for CO_2 capture and storage processes. *Applied Energy* **86** (2009), 826–836.

[69] Markert, B.: A constitutive approach to 3-d nonlinear fluid flow through finite deformable porous continua with application to a high-porosity polyurethane foam. *Transport in Porous Media* **70** (2007), 427–450.

[70] Marle, C. M.: On macroscopic equations governing multiphase flow with diffusion and chemical reactions in porous media. *International Journal of Engineering Science* **20 (5)** (1982), 643–662.

[71] McPherson, B. J. O. L.; Han, W. S. & Cole, B. S.: Two equations of state assembled for basic analysis of multiphase CO_2 flow and in deep sedimentary basin conditions. *Computers and Geosciences* **34** (2008), 427–444.

[72] van der Meer, L. G. H.: The conditions limiting CO_2 storage in aquifers. *Energy Conversion and Management* **34** (1993), 959–966.

[73] Metz, B.; Davidson, O.; de Coninck, H.; Loos, M. & Meyer, L. (eds.): *Carbon Dioxide Capture and Storage*. Cambrige University Press 2005.

[74] Michael, K.; Arnot, M.; Cook, P.; Ennis-King, J.; Funnel, R.; Kaldi, J.; Kirste, D. & Paterson, L.: CO_2 storage in saline aquifers I - Current state of scientific knowledge. *Energy Procedia* **1** (2009), 3197–3204.

[75] Müllerschön, H.: *Spannungs-Verformungsverhalten granularer Materialien am Beispiel von Berliner Sand*. Dissertation, Bericht Nr. II-6 aus dem Institut für Mechanik (Bauwessen), Universität Stuttgart 2000.

[76] Niessner, J. & Hassanizadeh, S. M.: Modeling kinetic interphase mass transfer for two-phase flow in porous media including fluid-fluid interfacial area. *Transport in Porous Media* **80** (2009), 329–344.

[77] Nordbotten, J. M.; Celia, M. A. & Bachu, S.: Injection and storage of CO_2 in deep saline aquifers: analytical solution for CO_2 plume evolution during injection. *Transport in Porous Media* **58** (2005), 339–360.

[78] Ott, J. B. & Boerio-Goates, J.: *Chemical Thermodynamics: Principles and Applications*. Elsevier Academic Press 2000.

[79] PANDAS: *A coupled FEM solver*. URL `http://www.get-pandas.com`.

[80] Pappa, G. D.; Perakis, C.; Tsimpanogiannis, I. N. & Voutsas, E. C.: Thermodynamic modeling of the vapor-liquid equlibrium of the CO_2/H_2O mixtures. *Fluid Phase Equilibria* **284** (2009), 56–63.

[81] Peng, D. Y. & Robinson, D. B.: A new two-constant equation of state. *Industrial and Engineering Chemistry Fundamentals* **15 (1)** (1976), 59–64.

[82] Plug, W. J. & Bruining, J.: Capillary pressure for the sand-CO_2-water system under various pressure conditions. application to CO_2 sequestration. *Advances in Water Resources* **30** (2007), 2339–2353.

[83] Poling, B. E.; Prausnitz, J. M. & O'Connell, J. P.: *The Properties of Gases and Liquids*. McGraw-Hill 2001, 5th edn.

[84] Pop, I. S.; van Duijn, C. J.; Niessner, J. & Hassanizadeh, S. M.: Horizontal redistribution of fluids in a porous medium: The role of interfacial area in modeling hysteresis. *Advances in Water Resources* **32** (2009), 383–390.

[85] Potter, M. C. & Somerton, C. W.: *Schaum's Outline of Thermodynamics for Engineers*. McGraw-Hill, New-York 1993.

[86] Pruess, K. & García, J.: Multiphase flow dynamics during CO_2 disposal into saline aquifers. *Environmental Geology* **42** (2002), 282–295.

[87] Pruess, K.; Tsang, C. F.; Law, D. & Oldenburg, C.: Intercomparison of simulation models for CO_2 disposal in underground storage reservoirs (2001), URL `http://esd.lbl.gov/GEOSEQ/`.

[88] Redlich, O. & Kwong, J. N. S.: On the thermodynamics of solutions. V. An equation of state. Fugacities of gaseous solutions. *Chemical Reviews* **44** (1949), 233–244.

[89] Ricken, T.; Schwarz, A. & Bluhm, J.: A triphasic model of transversely isotropic biological tissue with applications to stress and biologically induced growth. *Computational Materials Science* **39** (2007), 124–136.

[90] Ricken, T. & Ustohalova, V.: Modeling of thermal mass transfer in porous media with applications to the organic phase transition in landfills. *Computational Materials Science* **32** (2005), 498–508.

[91] Sasaki, K.; Fujii, T.; Niibori, Y.; Ito, T. & Nashida, T.: Numerical simulation of supercritical CO_2 injection into subsurface rock masses. *Energy Conversion and Management* **49** (2008), 54–61.

[92] Scholz, B.: *Application of a Micropolar Model to the Localization Phenomena in Granular Materials*. Dissertation, Bericht Nr.II-15 aus dem Institut für Mechanik (Bauwessen), Universität Stuttgart 2007.

[93] Segerlind, L. J.: *Applied Finite Element Analysis*. John Wiley & Sons 1984, 2nd edn.

[94] Span, R. & Wagner, W.: A new equation of state for carbon dioxide covering the fluid region from the triple-point temperature to 1100 K at pressures up to 800 MPa. *Journal of Physical and Chemical Reference Data* **25 (6)** (1996), 1509–1596.

[95] Span, R.; Wagner, W.; Lemmon, E. W. & Jacobsen, R. T.: Multiparameter equations of state - recent trends and future challenges. *Fluid Phase Equilibria* **183-184** (2001), 1–20.

[96] Spycher, N.; Pruess, K. & Ennis-King, J.: CO_2-H_2O mixtures in the geological sequestration of CO_2. I. Assessment and calculation of mutual solubilities from 12 to 100 °C and up to 600 bar. *Geochimica at Cosmochimica Acta* **67** (2003), 3015–3031.

[97] Stanley, H. E.: *Introduction to Phase Transitions and Critical Phenomena*. Oxford Univeristy Press 1971.

[98] Steeb, H.; Diebels, S. & Vardoulakis, I.: Theory and numerics of erosion processes in fluid-saturated porous media. In *Modelling of Cohesive-Frictional Materials*, Vermeer, P. A.; Ehlers, W.; Herrmann, H. J. & Ramm, E., eds., Taylor & Francis Group, London 2004, pp. 307–319.

[99] Sterner, S. M. & Pitzer, K. S.: An equation of state for carbon dioxide valid from zero to extreme pressures. *Contributions to Mineralogy and Petrology* **117** (1994), 362–374.

[100] Truesdell, C.: Thermodynamics of diffusion. In *Rational Thermodynamics*, Truesdell, C., ed., Springer-Verlag, New York 1984, 2nd edn., pp. 219–236.

[101] Truesdell, C. & Noll, W.: *The Nonlinear Field Theories of Mechanics*. Band III/3., Springer-Verlag, Berlin 1965.

[102] Truesdell, C. & Toupin, R. A.: The classical field theories. In *Handbuch der Physik*, Flügge, S., ed., Springer-Verlag, Berlin 1960, vol. III/1, pp. 226–902.

[103] Wieners, C.; Ehlers, W.; Ammann, M.; Karajan, N. & Markert, B.: Parallel solution methods for porous media models in biomechanics. *PAMM* **5** (2005), 35–38.

[104] Zhilin, P. A.: *Vectors and Second-Rank tensors in Three-Dimensional Space*. Nestor, St-Petersburg (in Russian) 2001.

[105] Zienkiewicz, O. C.; Qu, S.; Taylor, R. L. & Nakazawa, S.: The patch test for mixed formulations. *International Journal for Numerical Methods in Engineering* **23** (1986), 1873–1883.

[106] Zienkiewicz, O. C. & Taylor, R. L.: *The Finite Element Method. The Basis, Vol. 1.* Butterworth Heinemann, Oxford 2000, 5th edn.

Curriculum Vitae

Personal Data:

Name:	Irina Komarova
Date of Birth:	25th February 1983
Place of Birth:	Leningrad, Russia
Nationality:	Russian

Education:

09/1990 – 06/2000
School: Saint-Petersburg, Russia

09/2000 – 07/2004
Saint-Petersburg State Politechnical University
Degree: Bachelor of Applied Mechanics

07/2004 – 08/2004
University of Jyväskylä, Finland
Summer school

09/2004 – 06/2006
Saint-Petersburg State Politechnical University
Degree: Master of Applied Mechanics

Professional Occupation:

09/2005 – 08/2006
Working Student
Max-Plank-Institute for Plasma Physics (IPP), Germany

09/2006 – 05/2007
Research Assistant
University of Innsbruck, Austria

06/2007 – 08/2010
Doctoral Candidate
Institute of Applied Mechanics (Civil Engineering)
University of Stuttgart, Germany

11/2008
Exchange program
TU Delft, Holland

Released Report Series

II-1 Gernot Eipper: *Theorie und Numerik finiter elastischer Deformationen in fluidgesättigten porösen Festkörpern*, 1998.

II-2 Wolfram Volk: *Untersuchung des Lokalisierungsverhaltens mikropolarer poröser Medien mit Hilfe der Cosserat-Theorie*, 1999.

II-3 Peter Ellsiepen: *Zeit- und ortsadaptive Verfahren angewandt auf Mehrphasenprobleme poröser Medien*, 1999.

II-4 Stefan Diebels: *Mikropolare Zweiphasenmodelle: Formulierung auf der Basis der Theorie Poröser Medien*, 2000.

II-5 Dirk Mahnkopf: *Lokalisierung fluidgesättigter poröser Festkörper bei finiten elastoplastischen Deformationen*, 2000.

II-6 Heiner Müllerschön: *Spannungs-Verformungsverhalten granularer Materialien am Beispiel von Berliner Sand*, 2000.

II-7 Stefan Diebels (Ed.): *Zur Beschreibung komplexen Materialverhaltens: Beiträge anläßlich des 50. Geburtstages von Herrn Prof. Dr.-Ing. Wolfgang Ehlers*, 2001.

II-8 Jack Widjajakusuma: *Quantitative Prediction of Effective Material Parameters of Heterogeneous Materials*, 2002.

II-9 Alexander Droste: *Beschreibung und Anwendung eines elastisch-plastischen Materialmodells mit Schädigung für hochporöse Metallsch äume*, 2002.

II-10 Peter Blome: *Ein Mehrphasen-Stoffmodell für Böden mit Übergang auf Interface-Gesetze*, 2003.

II-11 Martin Ammann: *Parallel Finite Element Simulations of Localization Phenomena in Porous Media*, 2005.

II-12 Bernd Markert: *Porous Media Viscoelasticity with Application to Polymeric Foams*, 2005.

II-13 Saeed Reza Ghadiani: *A Multiphasic Continuum Mechanical Model for Design Investigations of an Effusion-Cooled Rocket Thrust Chamber*, 2005.

II-14 Wolfgang Ehlers & Bernd Markert (Eds.): *Proceedings of the 1st GAMM Seminar on Continuum Biomechanics*, 2005.

II-15 Bernd Scholz: *Application of a Micropolar Model to the Localization Phenomena in Granular Materials: General Model, Sensitivity Analysis and Parameter Optimization*, 2007.

II-16 Wolfgang Ehlers & Nils Karajan (Eds.): *Proceedings of the 2nd GAMM Seminar on Continuum Biomechanics*, 2007.

II-17 Tobias Graf: *Multiphasic Flow Processes in Deformable Porous Media under Consideration of Fluid Phase Transitions*, 2008.

II-18 Ayhan Acartürk: *Simulation of Charged Hydrated Porous Materials*, 2009.

II-19 Nils Karajan: *An Extended Biphasic Description of the Inhomogeneous and Anisotropic Intervertebral Disc*, 2009.

II-20 Bernd Markert: *Weak or Strong – On Coupled Problems In Continuum Mechanics*, 2010.

II-21 Wolfgang Ehlers & Bernd Markert (Eds.): *Proceedings of the 3rd GAMM Seminar on Continuum Biomechanics*, 2012.

II-22 Wolfgang Ehlers: *Poröse Medien – ein kontinuumsmechanisches Modell auf der Basis der Mischungstheorie*, 2012. Nachdruck der Habilitationsschrift aus dem Jahr 1989 (Forschungsberichte aus dem Fachbereich Bauwesen der Universität-GH-Essen **47**, Essen 1989).

II-23 Hans-Uwe Rempler: *Damage in multi-phasic Materials Computed with the Extended Finite-Element Method*, 2012.

II-24 Irina Komarova: *Carbon-Dioxide Storage in the Subsurface: A Fully Coupled Analysis of Transport Phenomena and Solid Deformation*, 2012.